

POLITECNICO DI TORINO

Master of Science in Energy and Nuclear Engineering

Master Degree Thesis

Power generation alternatives for small scale concentrated solar power plants with energy storage based on Calcium-Looping



Supervisors

prof. Vittorio Verda

prof. Elisa Guelpa

Candidate

Umberto Tesio

December 2018

Summary

Introduction.....	1
SOCRATCES project: an essential overview	3
Calcium Looping.....	3
CSP integration and components description	11
Calciner	12
Storages.....	13
Carbonator	15
Solid compounds conveying	16
Heat exchangers.....	17
SOCRATCES goals to achieve	19
Calcium-Looping integration alternatives.....	21
Direct integration	26
Modelling and optimization structure.....	27
Results, comments and comparisons	39
Indirect integration	47
Power cycle optimization structure (first step).....	48
CaL components modelling	49
Carbonator side optimization structure (second step)	49
ORC indirect integration	57
Subcritical cycles	60
Counter-pressure cycle	60
Condensation cycle	65
Supercritical cycles.....	70
Counter-pressure cycle	70
Condensation cycle	75
Comments and comparisons	79
SRC indirect integration.....	82
Basic power block layout.....	84
Single bleeding power block layout	84
Single reheat power block layout.....	85

Regeneration and reheat power block layout	87
Results, comments and comparisons	88
SCO ₂ indirect integration	94
Single intercooling power block layout	95
Recompression power block layout	97
Results, comments and comparisons	99
Final comparison	105
Conclusions.....	107
References.....	109

Introduction

Climate changes due to human activities represent one of the main topic discussed nowadays not just in the scientific community, but also in people's everyday life. During the last decades all the biggest contributors to global warming gas emissions met in many summits in order to establish efficient strategies and policies to reduce the impact caused by fossil fuels utilisation on the atmosphere.

In this context renewable energy sources (RES) play an important role because, despite some of their drawbacks as discontinuity and low density on the territory, they are everywhere present and abundant. That's why at the state of the art they represent the most suitable opportunity to satisfy the growing global energy demand in a sustainable way.

As just mentioned, one of the main issue related to the renewable energy sources is that they are affected by an intrinsic intermittence (both on short and long period). To overcome that problem it's necessary to integrate an energy storage into the power production plants. One of the most important applications in which this solution had been studied it's the concentrated solar power (CSP). In fact, since this technology involves a thermal cycle, it's very important that the operating conditions are maintained as close as possible to the nominal condition and for as long as possible, in order to ensure that all the plant components work at the best of their performances.

From all these considerations born the European project SOCRATCES (SOLar Calcium-looping integRAtion for Thermo-Chemical Energy Storage). This project aims to demonstrate the feasibility of the integration of a Thermo-Chemical Energy Storage (TCES) in a central tower CSP plant starting from a prototype scale, up to a commercial size. In this case the TCES consists in a chemical loop based on the reversible exothermic reaction of carbonation of CaO with CO₂ to give CaCO₃ and the reverse endothermic reaction named calcination; the entire process is called Calcium Looping (CaL).

There are many hopeful aspects related to this plant configuration, the most interesting between them is the fact that the storage is at ambient temperature, making thermal losses equal to zero and the fact that CaCO₃ can be obtained by limestone, which is a very abundant,

non-toxic and cheap material. Furthermore, the expected operating conditions do not present particular criticalities, fact that allows to use components already developed and available both in the field of CSP and in the field of traditional power plant.

The purpose of this thesis is to analyse and compare the different thermodynamic cycles to be integrated in a pilot plant of the SOCRATCES project with a net power output equal to 1 MWe, in order to choose the most suitable and convenient alternative.

SOCRATCES project: an essential overview

Before starting the exposition it's important to specify that this is only a brief treatment of the complex topic concerning the CaL plant, with the aim of provide a basic explanation of the system operation in order to understand the context in which the power unit works, which is the core of this discussion.

Calcium Looping

As previously mentioned in the introduction, the energy storage is a key point in the field of renewable energy sources, especially for those that involves a thermodynamic cycle. One of the most relevant example consists in the CSP technology, the whom, strictly speaking, exploit the direct component of the solar radiation collected by suitable mirrors. Therefore, the main discontinuity factors in this case are represented by the alternation of the seasons, by the alternation of day and night and by the daily weather variation due to the presence of clouds.

Therefore, to exploit the highest amount of the energy collected from the solar radiation, to avoid a design oversizing of the plant and to guarantee a power production as continuous as possible, it's requested a thermal energy storage.

There are three main categories of thermal energy storage:

- Sensible heat storage
- Latent heat storage
- Chemical heat storage

The first group doesn't involve phase change or chemical reaction, so the heat is stored increasing the temperature of a suitable material. The equation governing the phenomena is the following:

$$Q = m \cdot \bar{c}_p \cdot \Delta T$$

Where Q is the thermal energy [J], m is the mass of the storage [kg], \bar{c}_p is the average specific heat [J/(kg*K)] and ΔT is the temperature variation [K].

This methodology will be therefore affected by relevant thermal losses and an appropriate insulation of the storage installation must be adopted to guarantee adequate performances. Molten salts are the most common in this field, but they are characterised by a relevant issue since they must be kept above their solidification temperature, which is usually about 200°C.

The second group involves a phase change of the material used for the thermal storage, so heat will be exchanged approximately at a constant temperature, making possible to use smaller amount of material with respect to the previous case. The equation governing the phenomena is the following:

$$Q = m \cdot \lambda$$

Here λ is the latent heat related to the phase change [J/kg].

Anyway, also this typology is affected by thermal losses, because, to provide a higher as possible quality heat, the phase change temperature must be sufficiently high.

The third group involves endothermic and exothermic chemical reactions, where the recombination of different substances determines an absorption/release of heat. Here are provided the equation governing the phenomena and a simple schematic to explain the concept:

$$Q = n_r \cdot \Delta \bar{H}_r$$

Where n_r stands for the number of moles of the reactant to the whom it's referred $\Delta \bar{H}_r$, the molar heat of reaction [J/mol].

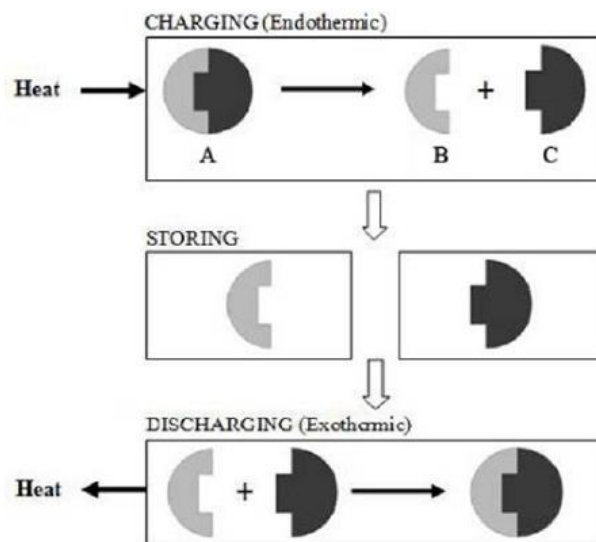


Figure 1.1 – Schematic representation of the reversible chemical reaction at the base of the TCES [3]

In this case, both reactants and products can be kept at ambient temperature, avoiding in this way any heat power loss related to the storage and making possible to collect energy in the long term (weeks or months). Furthermore, chemical reactions are characterised by higher energy density compared to phase change transformations, therefore in terms of mass and volume of the storage it usually represents the best option.

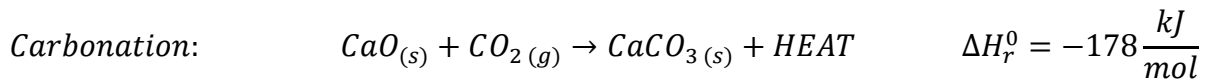
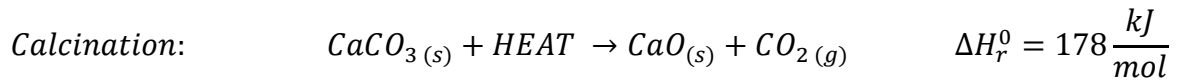
Thermal energy storage methods	Operating temp (°C)	Energy density (MJ/m ³)
<i>Sensible heat</i>		
Silicone oil	300–400 °C	189
Nitrite salts	250–450 °C	548
Nitrate salts	265–565 °C	898
Carbonate salts	450–850 °C	1512
Liquid sodium	270–530 °C	287
<i>Latent heat – high temp molten salts</i>		
	Phase change temp	
Sodium nitrite NaNO ₂	270 °C	373
Sodium nitrate NaNO ₃	307 °C	389
Potassium nitrate KNO ₃	333 °C	561
Sodium carbonate Na ₂ CO ₃	854 °C	701
<i>Thermochemical</i>		
Iron carbonate FeCO ₃ – FeO + CO ₂	180 °C	2600
Calcium hydroxide, Ca(OH) ₂ –CaO + H ₂ O	500 °C	3000
Calcium carbonate, CaCO ₃ –CaO + CO ₂	800–900 °C	4400

Table 1.1 - Thermal energy storages comparison for both the operating temperature and the energy density [29]

From the last table it's possible to observe that the calcium carbonate is one of the most interesting alternatives both in terms of operating temperature and energy density; furthermore, since the energy density can be expressed as the energy stored per unit of volume, it's important to evaluate properly the storage conditions, especially if gaseous compounds are involved.

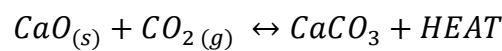
The storage chosen for the SOCRATCES project belongs to the third group and it's based on a calcium looping. In fact, from more than 30 years CaO has been recognised to be one of the most interesting materials for TCES applied to central tower CSP plants; however, up to nowadays, CaL has been studied only in the field of post combustion capture of CO₂, where showed some important issues, and its effectiveness in the CSP sector has still to be proven.

Calcium looping is based on two steps: the first one is called calcination and it's an endothermic reaction, while the second one is called carbonation and it's an exothermic reaction. Calcination takes place in a chemical reactor named calciner while the carbonator is the component in which carbonation occurs.



The calcium oxide (CaO) and calcium carbonate (CaCO₃) take part in the reaction at the solid state; in order to guarantee an adequate rate of reaction (maximization of reactants' contact surface) and allow their transport, the solid phases are reduced into powders.

To make some considerations about the different operating conditions of the two reactors it's important to analyse the equilibrium state of the reversible reaction:



The thermodynamic parameters (T and P) at the equilibrium are described by the following equation [1]:

$$P_{CO_2,eq} = 4.137 \cdot 10^7 \exp\left(-\frac{20474}{T_{eq}}\right)$$

where $P_{CO_2,eq}$ is the partial pressure of the CO₂ (expressed in bar), while T is its temperature (expressed in K).

Therefore, in accordance with Le Chatelier's principle of equilibrium, the reaction of carbonation is enhanced by high CO₂ partial pressure and low temperature, while the opposite happens for the reaction of calcination, which is enhanced by high temperature and low CO₂ partial pressure. This concept is clearly showed in the following graph (notice that the CO₂ pressure axis it's in logarithmic form):

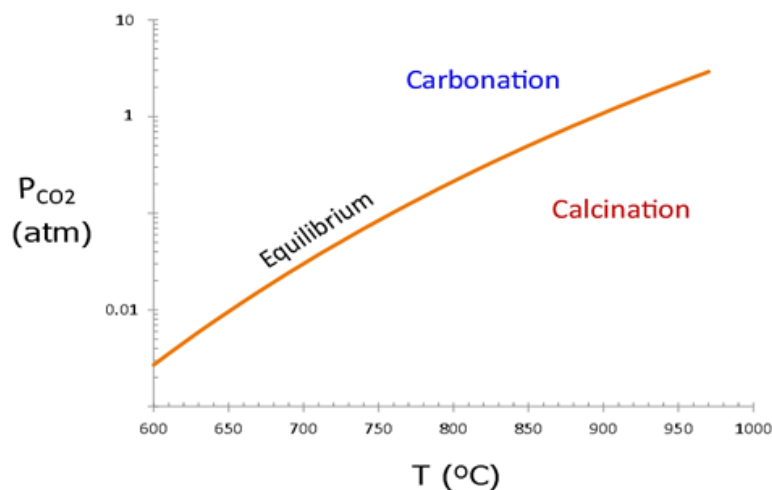


Figure 1.2 – Equilibrium pressure as a function of the reaction temperature [2]

The main issue related to the CaL is that the reaction involved is not perfectly reversible: in fact, the capability of the calcium oxide to react with the carbon dioxide inside the carbonator decreases with the rising of number of cycles performed, leading to a corresponding increase of inactive CaO that acts as an inert substance. This phenomenon is due to two mechanisms:

- Concerning the first one, the active surface and the useful number of pores of the calcium oxide grains are decreased (during the reaction) by the formation of a layer of calcium carbonate, which has a higher molar volume compared to the CaO. This fact can determine a drop of the reaction rate, since when the active surface is completely covered, only the diffusion of CO_3^{2-} and O^{2-} mobile ions is able to continue the reaction. Therefore, the carbonation reaction takes place in two consecutive stages: one is the fast carbonation and the other is the slow carbonation.
- The second deactivation mechanism consists in sintering, since, in presence of high temperatures (about one half of the melting temperature expressed in K) and long residence time in the calciner, the dimensions of pores and grains start to increase because of a coalescence phenomenon. Furthermore, as will be explained further on, this kind of mechanism can be enhanced by the presence of steam or carbon dioxide with high partial pressure, acting as catalyst for the sintering effect.

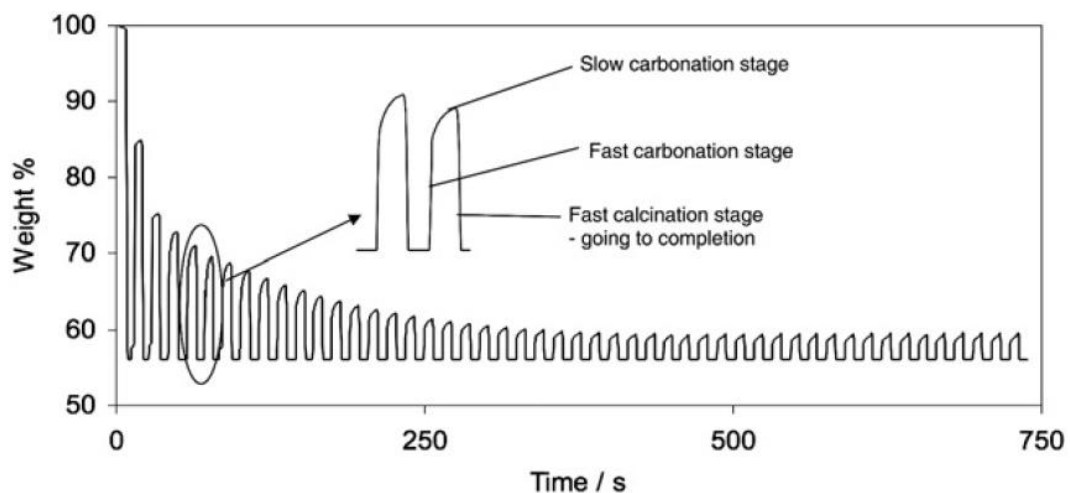


Figure 1.3 – Percentage weight variation during carbonation/calcination cycles [3]

The graph above is the result of the Calcium-Looping applied to a sample of CaCO_3 : the weight reported in the y-axis is the weight of the solid phase of reactants and products expressed as a percentage of the initial amount of calcium carbonate. Clearly, the calcination leads to a decrease of this quantity because of the formation of gaseous CO_2 and complete conversion

in CaO, while the carbonation reaction determines a recovery of the solid phase weight but in an asymptotically decreasing way, proofing the incapability of the calcium oxide to completely react with the carbon dioxide.

To sum up, as just observed, during a single carbonation the decrease of the weight variation speed of the solid phase is due to the passage between the fast and slow carbonation stage; the calcination is indeed very fast compared to the previous reaction and goes always to completion, while the progressive decrease of maximum weight recovered at the end of carbonation is due to the progressive worsening of the microstructure of the particles of calcium oxide, leading to smaller amounts of active reactant.

Previously has been said that steam in the calciner acts as a catalyst for the sintering process, but, surprisingly, the overall effect of steam is instead opposite in terms of CaO reactivity. This happens for two reasons: for the first one, the water steam helps to keep a low value of the partial pressure of the CO₂, so it's possible to work at lower temperature (as shown in figure 1.2) and therefore reduce the contribution that temperature itself gives to sintering.

The second mechanism's dynamics are not clear yet but, according to the last researches, it's supposed that water sintering permits to open pore structures less sensible to pore blockage by calcium carbonate [3].

Another substance that has been considered to reach optimal operating conditions in the calciner is helium. Basically, it has the same function already discussed for the steam, since its presence in the reactor atmosphere decreases the CO₂ partial pressure, allowing to operate at lower temperature and therefore causing a reduction of the sintering effect.

Furthermore, using it instead of water decreases also the required heat exchange outside of the calciner since there isn't any evaporation and condensation stages and moreover it is able to accelerate the calcination reaction thanks to its high thermal conductivity.

Finally, it's important to notice that both in case of steam or helium presence in the reactor atmosphere, these two inert substances can be easily separated from carbon dioxide: in case of H₂O it's just required a condensation step, while in case of He it's necessary a selective membrane.

As seen up to now, CaO reactivity (or activity) is an important and non-constant parameter, defined as:

$$X = \frac{\text{moles CaO reacted}}{\text{moles CaO stoichiometric}}$$

It is the ratio between the moles of calcium oxide that effectively take part to the carbonation reaction and the moles of CaO provided with the corresponding stoichiometric amount of CO₂. As will be possible to see, it is a very important parameter because changing the amount of the inert compound in the two reactions has a direct impact on the plant performances.

Regarding the calcium carbonate precursor, many alternatives have been taken into account; the most interesting is represented by limestone, a natural compound mainly composed by calcium and magnesium carbonates (although it's a common practice to talk about limestone referring only to CaCO₃). It shows some interesting advantages because it's inexpensive (<10\$/ton), widely available, non-toxic, non-corrosive and allows the opportunity of working in synergy with the lime industry, since the spent calcium oxide can still be useful for commercial purposes.

Moreover, others synthetic materials have been developed to obtain better performances in terms of CaO activity, but their price can be up to 1000 times higher than natural limestone; so, the convenience of their usage must be properly evaluated.

As previously mentioned, the main reason why the CaL technology couldn't enter the market was due to the strong deactivation of the calcium oxide, which reach a value of reactivity lower than 0,1 just after some tens of cycles.

However, this is the behaviour reported by the carbon capture applications, the main field in which this process has been studied. In fact, in this context, the carbonator is fed with CaO and a stream of flue gases (coming from a traditional power plant) with low CO₂ partial pressure; carbon dioxide is therefore captured and a stream of CaCO₃ is sent to the calciner. In this application, the heat needed by the reactor is provided by an oxy-combustion, in order to avoid the presence of nitrogen in the products; as a result, the CO₂ partial pressure in the reactor atmosphere is quite high, making necessary to reach high temperatures. Finally, after having removed water steam (oxy-combustion product) with condensation, a stream of pure carbon dioxide is obtained, while the solid flow of CaO is recirculated in the carbonator.

In other words, the carbonator works with low CO_2 partial pressure although the carbonation reaction is enhanced by high P_{CO_2} and vice versa for the calciner; as a result, in order to take place, the calcination reaction must reach high temperature, causing relevant CaO sintering and therefore reducing its activity.

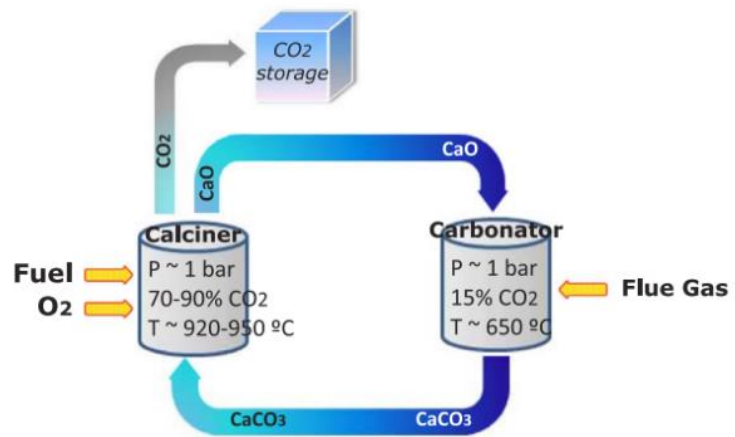


Figure 1.4 – CaL schematic to perform CCS in a traditional power plant [30]

Things are different for the SOCRATCES plant configuration, which, as will be better explained later, presents optimised operating conditions for the calcium looping, reaching therefore higher performances. This new plant configuration is constituted by the ENDEX cycle (patented by CALIX), which is entirely adopted by the SOCRATCES project.

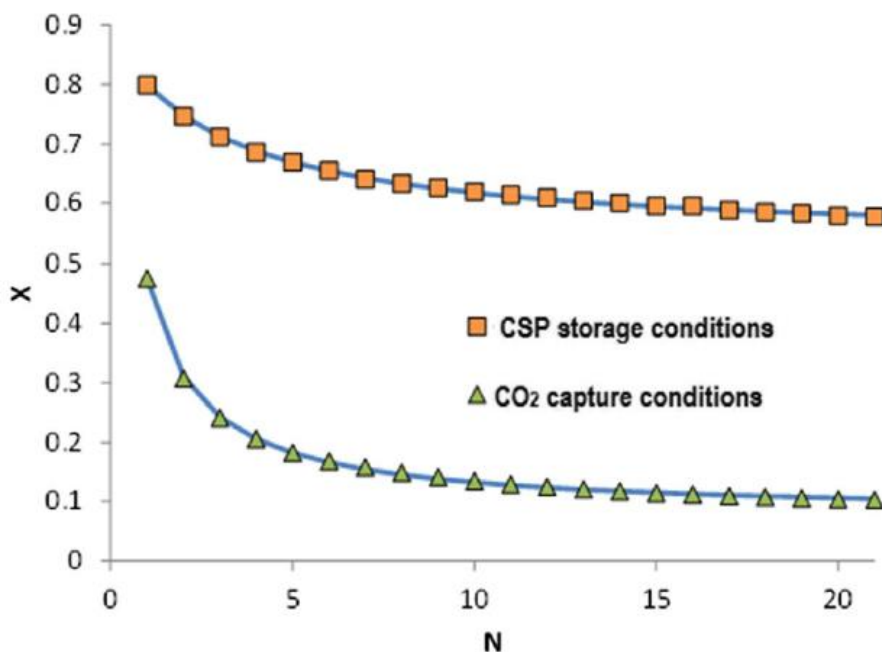


Figure 1.5 – CaO activity variation for the increasing of cycles performed [4]

The comparison between the two configurations (Concentrated Solar Power and Carbon Capture and Sequestration) showed above in terms of calcium oxide reactivity as a function

of the number of cycles performed demonstrate an evident difference, making calcium looping a very promising technology when integrated in the concentration solar power plant.

Finally, being the calcium looping constituted by chemical reactions, an important aspect to study should be the kinetic of these reactions, which is strictly related to the solid particles size, the nature of the sorbent and the CO_2 partial pressure.

Anyway, this aspect won't be analysed in this work because of the following reasons: first, it's a complex problem that would require a deep treatment on an object that it's not the main topic of this analysis; second, since the plant simulations are performed at the steady state, it's possible to avoid to consider the residence time of the reactants inside the chemical reactors; third: assuming values of the parameters coherently with respect to the scientific literature, the obtained results should be consistent.

CSP integration and components description

Once that the essential functioning of the CaL technology has been presented, it's possible to discuss how it can be integrated inside a central tower CSP plant.

Being endothermic, the calcination will take place in the receiver of the central tower, so that the required heat is provided at an adequate temperature by the concentrated solar radiation. The exothermic carbonation reaction instead will provide high quality heat to a suitable power cycle.

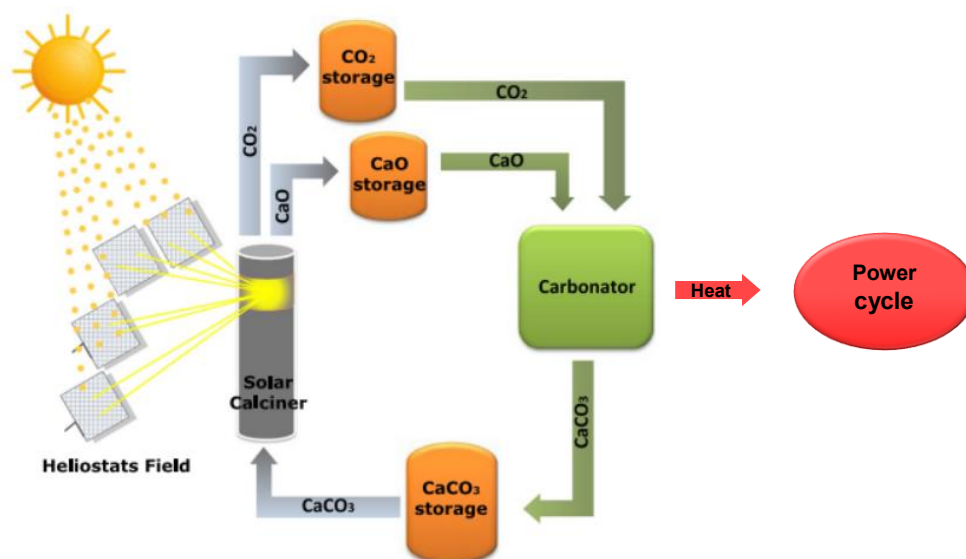


Figure 2.1 – Calcium-Looping integration in CSP plant [5]

As will be discussed further on, it can be very useful to make a conceptual division of the SOCRATCES plant layout into two main blocks: the calciner side and the carbonator side. For fixed physical conditions of the storages, these two blocks can be actually considered as independent. In fact, while the calciner side will operate only in case of an adequate solar radiation income, the carbonator side should theoretically work without interruptions to provide a continuous power generation at its rated power (and therefore at its maximum efficiency). As a consequence, the instantaneous mass flow of reactants and products circulating in the calciner side will be higher with respect to the carbonator side but, of course, their integrals on a time period will be equal.

Calciner

As previously discussed, the lower is the calciner temperature the better are the performances in terms of CaO activity, so, in accordance to the chemical equilibrium, it's necessary to operate at low CO₂ partial pressure. At the state of the art, the most interesting way to reach this low partial pressure in the calciner is to work at ambient pressure with the addition of a gaseous substance having high molar fraction.

For this component, the SOCRATCES project utilizes the mature Fast Calcining Technology (or Catalytic Flash Calcination, CFC, patented by CALIX) based on an entrained flow reactor under superheated steam. The following image shows the essential design of the reactor:

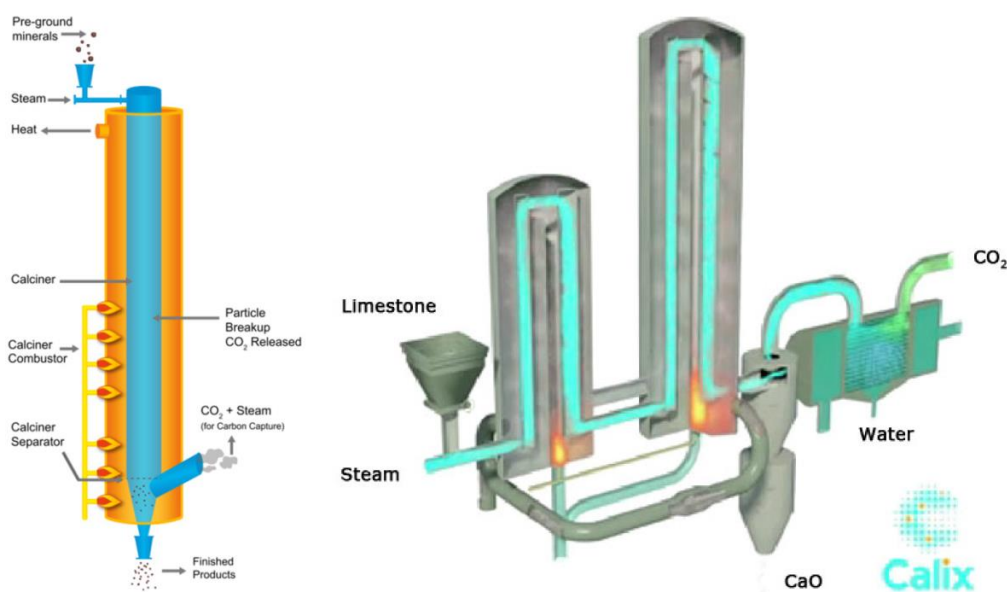


Figure 2.2 – Calciner reactor patented by CALIX (notice that in this figure it operates in the CCS configuration [6])

The solid particles are fluidized in a steam bed, which has actually many different functions: it acts as a reactant carrier, as a heat transfer medium and moreover (as previously explained) it enhances the calcium oxide reactivity. In this way it's possible to reach full calcination with a residence time of the order of the seconds. The products are then easily separated by the use of a cyclone (for the calcium oxide powder) and a condenser (for the two gaseous compounds: water and carbon dioxide). Of course, for the CSP application all the combustors present in the figure won't be present since the thermal power is provided by the solar radiation collected by the receiver absorber.

The expected operating temperatures are below 700°C and this aspect has others beneficial effects in addition to the ones already seen: first, allows to use already developed, reliable and not particularly expensive central receivers since the materials involved haven't got to sustain extremely high temperatures. Second, the convective and radiative losses will be less consistent in comparison to the others CSP plants, where the actual trend is to reach temperatures the highest as possible.

Since the calcium carbonate entering the calciner is extracted from its storage vessel (where we can assume that it is kept at ambient temperature) and the two outlet streams exit at the same temperature at which the calcination reaction occurs, it's fundamental to perform a heat recovery. This allows to store the CO₂ and the CaO at adequate temperatures and increase the reaction efficiency, because a smaller amount of solar energy is requested to heat the reactant up to the operating temperature and therefore the fraction of solar energy available for the endothermic reaction is higher.

Storages

Being both at the solid state, the CaCO₃ and the CaO storage conditions coincide with the external environment state: 1 bar and 20°C. This temperature represents a realistic approximation of the yearly average temperature in Seville, the location where the SOCRATCES plant is expected to be realized.

Anyway, since the heat recovery between products and reactants may be insufficient to completely cool down the solid products coming from the calciner or carbonator, they can be sent to their storages with a higher temperature.

In this way it's possible to store an amount of sensible heat that is exploited by the following carbonation/calcination reaction, since the reactants will be available at higher temperature and therefore will be requested a lower preheating; of course, in this case the tanks containing the solids must be properly insulated to avoid heat losses.

The choice of the storage condition for the CO₂ is instead more complex and critical. Obviously, being a gas, the volume occupied by a unit mass of carbon dioxide is much higher than the other two solid substances, fact that risks to nullify the advantage of the calcium carbonate TCES on its competitors in terms of energy density; it's therefore necessary to keep CO₂ at high pressures and low temperatures.

Taking into account these consideration, in order to have an adequate storage system both in terms of performances, volume and costs, there are two main alternatives: a vessel at 75 bar and 25°C (approximately ambient temperature) or, reaching cryogenic temperatures, a tank at less than 20 bar [1].

At the state of the art, the most interesting choice seems to be the first one, with the carbon dioxide kept at supercritical conditions and in absence of thermal losses. Of course, a suitable compression and expansion system must be installed, eventually provided of inter-cooling/heating stages.

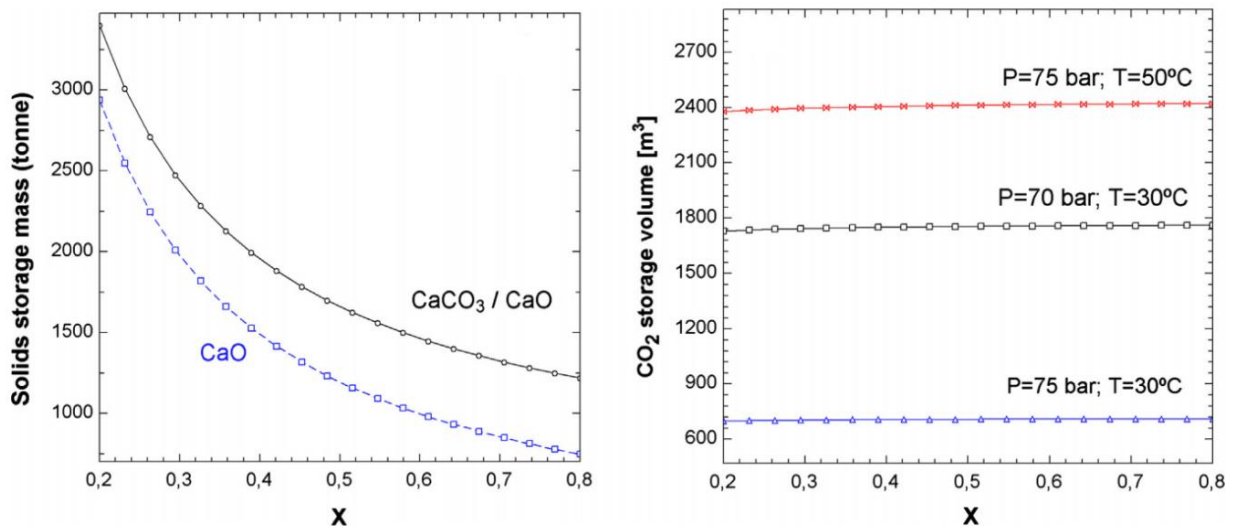


Figure 2.3 - An example of the storages size dependence on the three main thermo-physical parameters: CaO activity, CO₂ temperature and pressure [1]

From the last two graphs it's important to notice that the solids storage is only influenced by the calcium oxide reactivity, while the CO₂ storage is nearly totally independent from this parameter and only its temperature and pressure can make relevant differences.

Carbonator

Concerning the carbonator reactor, the SOCRATCES project adopts a fluidized bed reactor (FBR), which has the advantage of being a mature and widely diffused technology, fact that helps to limit the plant investment cost and guarantees a good reliability.

To sum up its functioning, the solid particles of calcium oxide are conveyed by a gaseous flow made of pure carbon dioxide or, in alternative, CO₂ with another suitable compound (usually helium). Once that the exothermic reaction takes place, the different outlet phases are separated with a cyclone, obtaining the carbon dioxide in excess and a stream of solid grains made of two different compounds: calcium carbonate on the external layer and calcium oxide in the inner core.

This, as already discussed, is due to the fact that the carbonation reaction doesn't manage to reach the completion and therefore a part of the solid reactant will actually act as an inert compound. Instead, concerning the inlet CO₂, it is provided in excess for two main reasons: first, to control the carbonator temperature and second to guarantee the fluidization of the outlet solids.

Furthermore, this parameter is strictly related to many other factors, such as the mass flowrate of the solids, the calcium oxide activity, the residence time and the gas speed [3].

Regarding the reaction rate of the fast carbonation (the first of the two reaction phases), an increase of the CO₂ molar fraction in the reactor atmosphere (at constant total pressure) leads to an enhancement of the kinetic, and, in accordance to the Le Chatelier principle in case of exothermic reaction, the same result can be obtained by lowering the operating temperature. However, one of the main target of the SOCRATCES project is to reach the highest as possible carbonator temperature, in order to provide a very high-quality heat to the power cycle and therefore increase its efficiency, although the benefit on the total plant efficiency must be proven.

Finally, for a constant CO₂ molar fraction in the reactor atmosphere, both the reaction rate and the solid-state diffusion (prevailing in the slow carbonation phase) are improved for higher carbonator pressures, but with a maximum limit equal to 5.3 bar [7].

Solid compounds conveying

Since the CaL process involves solid phases at the state of powders, a suitable conveying system must be developed in order to guarantee an adequate transport of reactants and products; it must be able to sustain high temperatures and to ensure good efficiency.

The operating conditions of the plant are such that the best choice between the solids transport techniques seems to be the pneumatic conveying, a mature, diffused and reliable technology. It is a fluidization technique already seen for the calciner and carbonator: a stream of powder is provided to a gas flow (promoted by fans or compressors), which carries it along a pipe up to a reactor or a phase separator (usually cyclones).

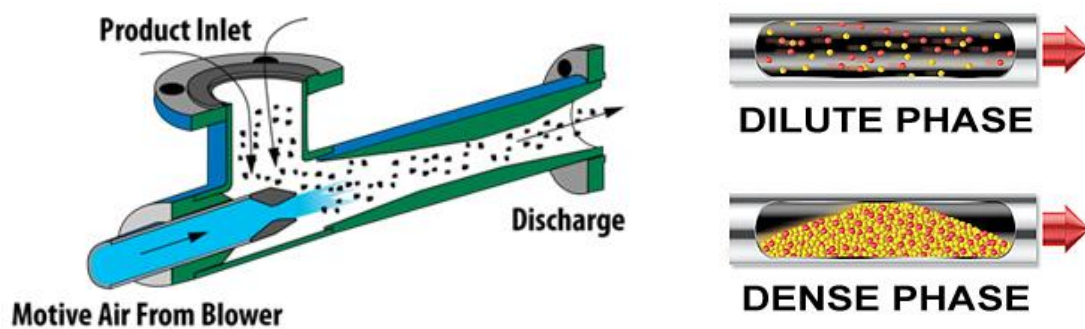


Figure 2.4 – Pneumatic conveying device and solid particles transportation phases [8] [9]

This kind of conveying is interesting for the CaL application for many reasons: first, it provides a fast transportation; second, the restriction on the particles size is compatible with the dimensions expected to have in the SOCRATCES project; third, can be useful in terms of gas-solids heat exchange during the preheating steps.

Very briefly, there are two recognised kinds of pneumatic conveying: the first one is dilute phase conveying and the second one is dense phase conveying.

In the first type, the amount of powder transported by the gas flow it's such that it stays in suspension in the gas itself; the main requirement in this case it's a high gas velocity to allow the particles suspension and this is also the main reason for the sustained energy consumption of this technique.

In the second type, the particles are not suspended in the gas flow because of the low speed of the gas itself; in fact, the powder is transported in dunes or plugs, which leads to a lower power absorption with respect to the previous case, but with an important drawback, since

this type of conveying is not applicable for every kind of material. Furthermore, it is usually necessary to pressurize the gas in order to overcome the pressure drop, phenomenon that is directly dependent on the ratio between the solid flow and the gas flow.

Therefore, considering all these aspects, the most interesting choice for the SOCRATCES project seems to be the pneumatic-dense phase conveying, at the condition that suitable strategies to avoid the particles cohesion (such as sonoprocessing techniques) will be employed, otherwise the CaL efficiency would suffer a non-negligible decrease.

Heat exchangers

As already explained, preheating of reactants is a very important aspect for the CaL plant, therefore a suitable heat exchangers system must be designed. According to the phases involved in the SOCRATCES project, the different types of heat exchangers will be:

- Gas-gas heat exchangers:

Obviously, for this kind of exchangers is only possible the closed configuration, otherwise the two streams would mix together. The main designs are: shell and tube, plate, plate and shell, primary surface and spiral plate. All these configurations have been already fully developed and are commercially available.

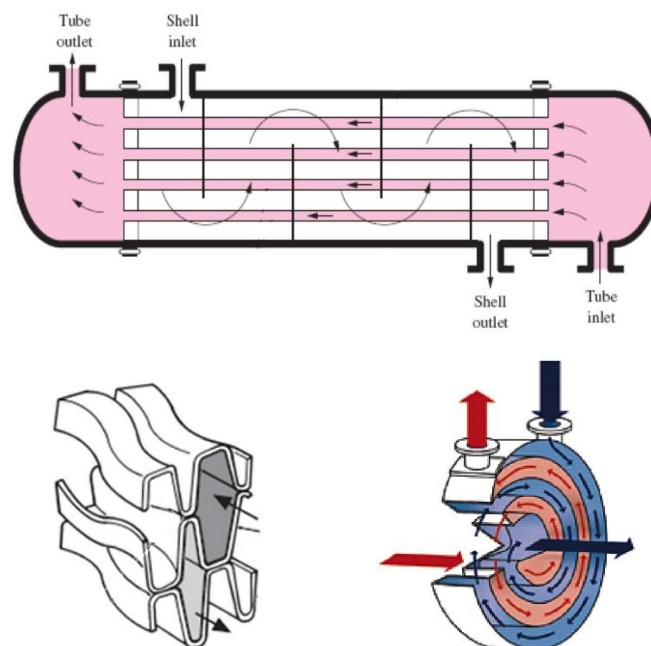


Figure 2.5 – Possible solutions for the gas-gas heat exchange in the SOCRATCES project [10] [11] [12]

- Gas-solid heat exchangers:

In this case both the open and closed thermal exchange are possible, because the two streams are easily separable.

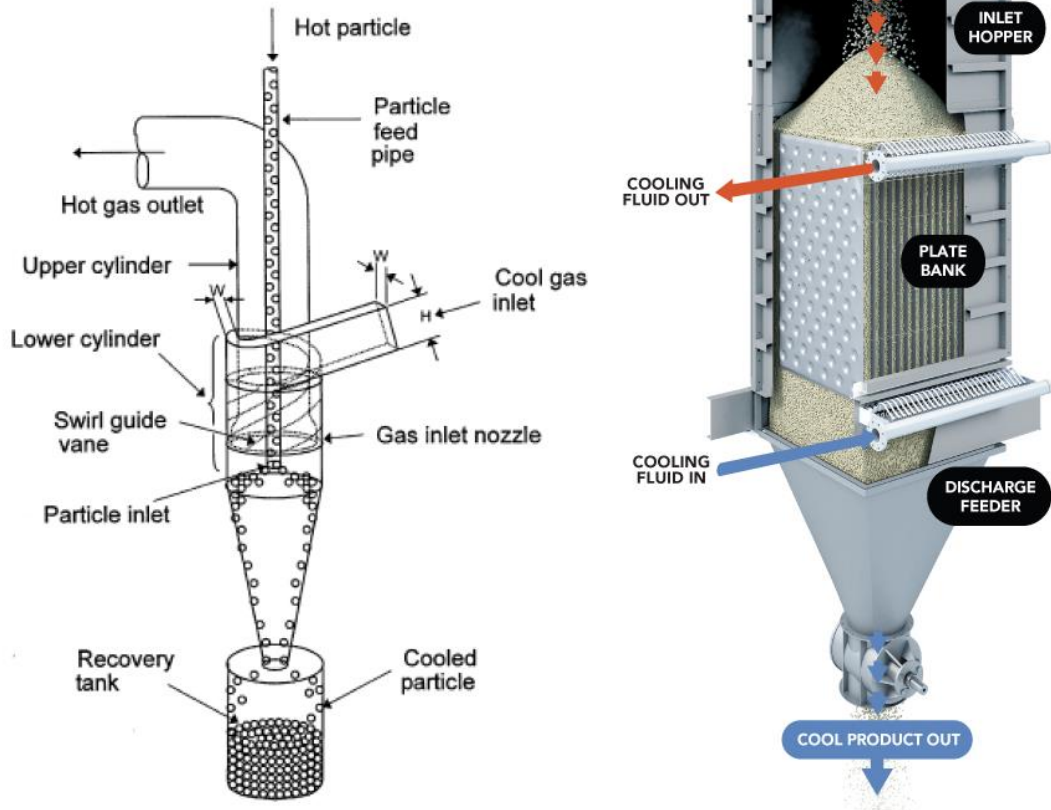


Figure 2.6 – Gas-solid heat exchangers respectively in case of direct and indirect heat exchange [13] [14]

Concerning the indirect type, an interesting option is represented by the device patented by Solex Thermal Science, whose design is very similar to a pillow plate heat exchanger and its functioning consists in heating or cooling a solid flow descending by gravity with a fluid stream passing between the plates in counter current configuration.

For the direct type there are two possibilities: the first one (which has been previously exposed) is a consequence of the pneumatic conveying technique, where heat exchange and solid particles transportation happen contemporary; the second one involves the use of cyclones and is able to guarantee good performances.

Its functioning consists in both inserting and extracting the gas stream from the upper side, creating a swirl and exchanging heat with the solid powder falling downward.

Remarkable advantages of this technology are the fact that there isn't any kind of contamination between the streams, both abrasion and degradation of the device are reduced because of the slow powder velocity, it requests low and easy maintenance, and, last but not least, it's able to sustain very high working temperatures (according to the manufacturer, up to 2000°C).

- Solid-solid heat exchangers:

At the state of the art, the best way to execute the solid-solid heat exchange seems to be the adoption of two gas-solids heat exchangers in a configuration where the fluid stream is recirculated between the exchangers and therefore the thermal power absorbed from the hot solid is given to the cold one; this heat transfer medium must have good thermal properties in order to minimize the electrical absorption for the fluid flow promotion, so its choice should be made carefully.

In any case the design of the exchanger will be chosen between the alternatives evaluating many different aspects, such as achievable operating pressure and temperature, exchanger efficiency, auxiliaries' consumption and investment cost.

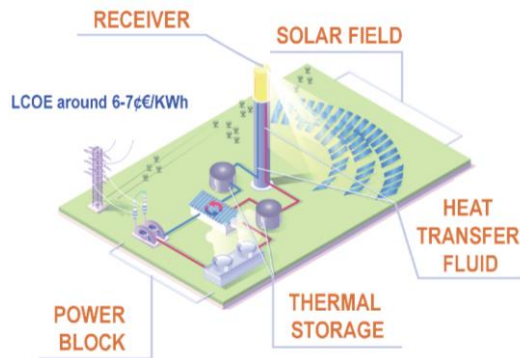
SOCRATCES goals to achieve

In the light of all the considerations seen up to now it's possible to say that, with this new plant configuration, higher performances will be reached in the CSP technology.

The realisation of the project is divided into three main steps: for first, a 10 kW prototype will be implemented to identify and solve the criticalities; then a 1 MW pilot plant will be built to analyse in detail and optimise its working conditions and finally, the first commercial-size plant will be realised for demonstrating purposes.

Every step is expected to take about three years so, roughly, the full development of this technology will take 10 years; during this period all the compounds and components involved in the project will be exhaustively studied in order to obtain a reliable and performing power plant.

The goals to achieve with the SOCRATCES project are summarized in the following table.



GOALS	SUNSHOT program of the DOE (USA)	SOCRATCES PROJECT
SOLAR FIELD	Optimal Error ≤ 3 mrad Wind Speed ≥ 30 yrs Cost $\leq \$75/m^2$	
RECEIVER	HTF Exit Temp $\geq 720^\circ\text{C}$ Thermal Eff. $\geq 90\%$ Lifetime $\geq 10,000$ cycles Cost $\leq \$150/kW_{th}$	HTF Exit Temp $< 700^\circ\text{C}$ Thermal Eff. $\geq 90\%$ Lifetime $\geq 10,000$ cycles Cost $\leq 132\text{€}/kW_{th}$
HEAT TRANSFER FLUID	Thermal Stab. $\geq 800^\circ\text{C}$ Melting Pt. $\leq 250^\circ\text{C}$ Cost $\leq \$1/\text{kg}$	Thermal Stab. $\geq 900^\circ\text{C}$ Activity after 1000 cycles > 0.5 Cost $< 0.01 \text{€}/\text{kg}$
THERMAL STORAGE	Power Cycle Inlet Temp $\geq 720^\circ\text{C}$ Exergetic Eff. $\geq 95\%$ Cost $\leq \$15/kW_{th}$	No Energy Losses Storage at ambient Temp. Exergetic Eff. $\geq 95\%$ Higher Storage Capacity Cost $< 12\text{€}/kW_{th}$
POWER BLOCK	Net Cycle Eff. $\geq 50\%$ Cost $\leq \$900/kW_{he}$	Net Cycle Eff. $\geq 50\%$ T power block $> 850^\circ\text{C}$ Cost $\leq \$900/kW_{he}$

Figure 2.7 - SOCRATCES techno-economic targets compared with the SUNSHOT project, a very advanced CSP plant but with a PCM storage; CaL benefits are highlighted in orange [2]

Calcium-Looping integration alternatives

As already said, calcium looping integration in CSP plant is made in order to obtain a more performing energy storage (both in thermodynamic and economic terms), which exploit a reversible endothermic/exothermic reaction. Anyway, this process is only able to absorb thermal power and release it again in form of heat flux in a following moment. To convert it into electricity it's therefore necessary a thermodynamic cycle.

According to the CaL operation conditions, there are many suitable alternatives to take into account and they can be distinguished in two different categories.

Direct integration

In the direct cycle configuration the power fluid coincide with one of the reactants/products of the reversible reaction, which obviously is the CO_2 (since the others are solids); so, the power block and the chemical reactors will be directly connected each other.

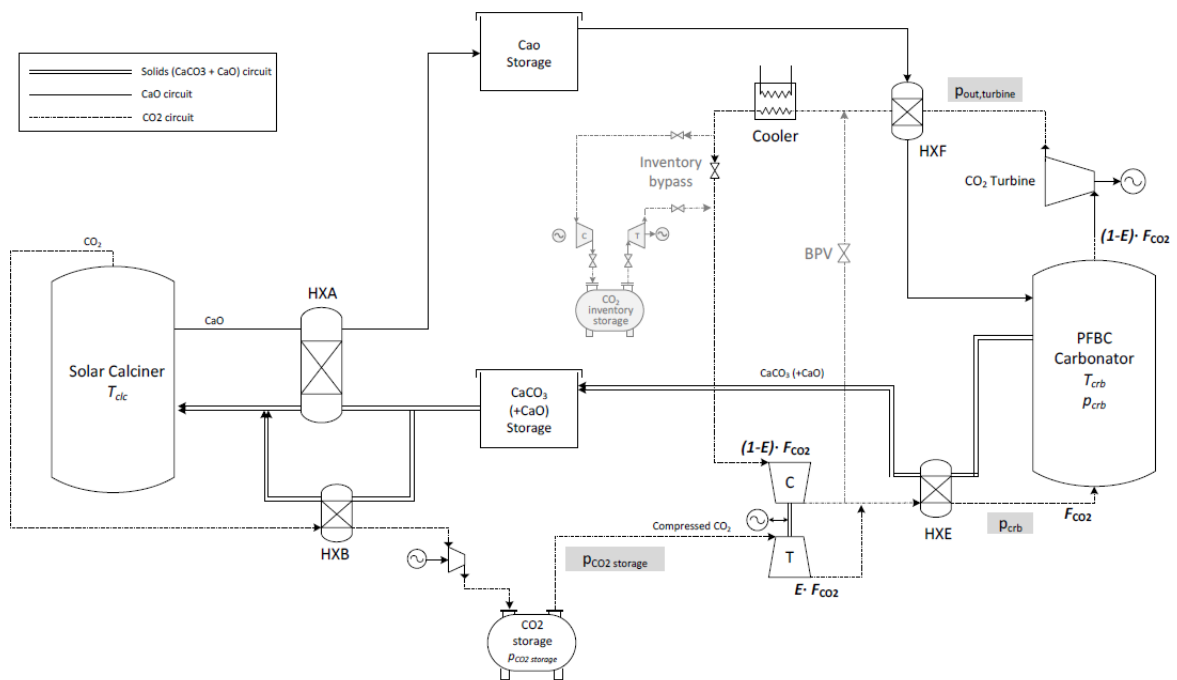


Figure 3.1 - Calcium looping CSP integration with a direct cycle configuration [3]

Concerning the carbonator side, the CO₂ is extracted from its storage to be heated up and expanded until the carbonator pressure is reached and it usually takes from five to seven intermediate steps, although in the figure it's represented a single turbine to simplify the schematic.

The reason of a multistage expansion is due to the fact that the temperature decrease (in consequence to the pressure decrease) can result as not convenient or even problematic and therefore some inter-heating steps are needed.

Subsequently it is mixed with the recirculating carbon dioxide and preheated to enter the reactor; at the same time, the other reactant, the calcium oxide, is also preheated by the reaction products. Once that the carbonation occurs, the CO₂ in excess (provided to control the reactor temperature) is expanded to produce electric power and then, after being cooled, it can be recirculated.

At this point, after having performed a heat recovery, the calcium carbonate (with the unreacted calcium oxide) is sent to its storage.

Things are easier for the calciner side, where it's only necessary to perform a preheating of the solid reactants and a multi-stage intercooled compression of the carbon dioxide; anyway, as already explained in the previous chapter, to obtain an optimised configuration it should be evaluated to operate with the presence of steam or helium in the reactor atmosphere and therefore a suitable separation unit must be installed in order to obtain pure CO₂.

Finally, this functioning mode implies two alternatives: in one case the carbonator operates at ambient pressure and the carbon dioxide reaches vacuum conditions after the turbine expansion or, in the other case, it's used a pressurised fluidised bed carbonator to exploit higher pressure drops.

A variant of this configuration is the air/CO₂ open cycle, whose layout is showed in the following figure.

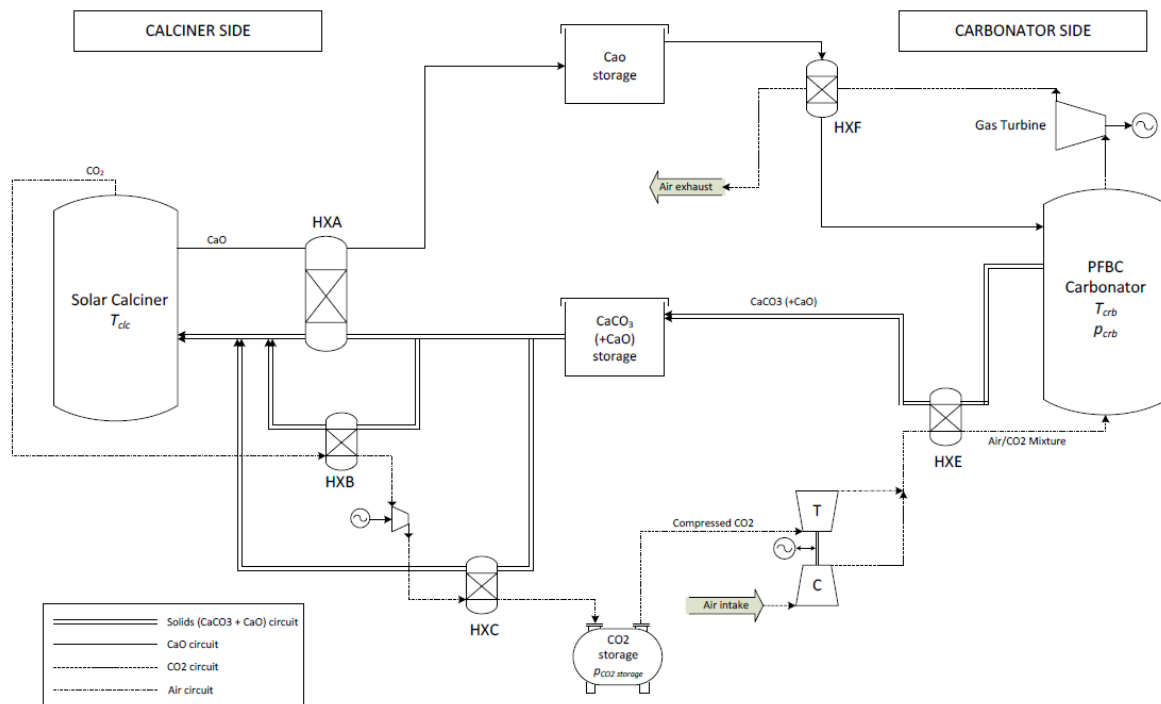


Figure 3.2 - Calcium looping CSP integration with an air/CO₂ open cycle configuration [3]

The difference with respect to the base case consists in the fact that the power fluid is not anymore the carbon dioxide. In fact a stream of ambient air is compressed and mixed with the stoichiometric amount of CO₂ in order to obtain at the carbonator outlet only solids and air (which acts as an inert) at high temperature. Then, after the turbine expansion and a heat recovery, it can be rejected to the environment.

Furthermore, there are some important aspects related to this plant design: first, the carbonator must be necessary pressurized to allow the exhausted air expulsion; second, carbon dioxide in the reactor atmosphere will have a molar fraction smaller than one, with possible consequences on the carbonator temperature and the reaction equilibrium, and third, it's important to achieve the complete carbonation or part of the CO₂ extracted from the storage will be vented in the environment.

According to literature results, this configuration seems to be actually less interesting than the previous one, both because of lower performance and the increase of complexity for the use of a carbonator atmosphere composed by other elements in addition to the CO₂. For this reason it won't be analysed further on.

Indirect integration

In the indirect cycle, the power block and the carbonator side are not anymore in direct communication since they only exchange thermal power through a heat exchanger, exactly as a heat recovery made for the reactants preheating.

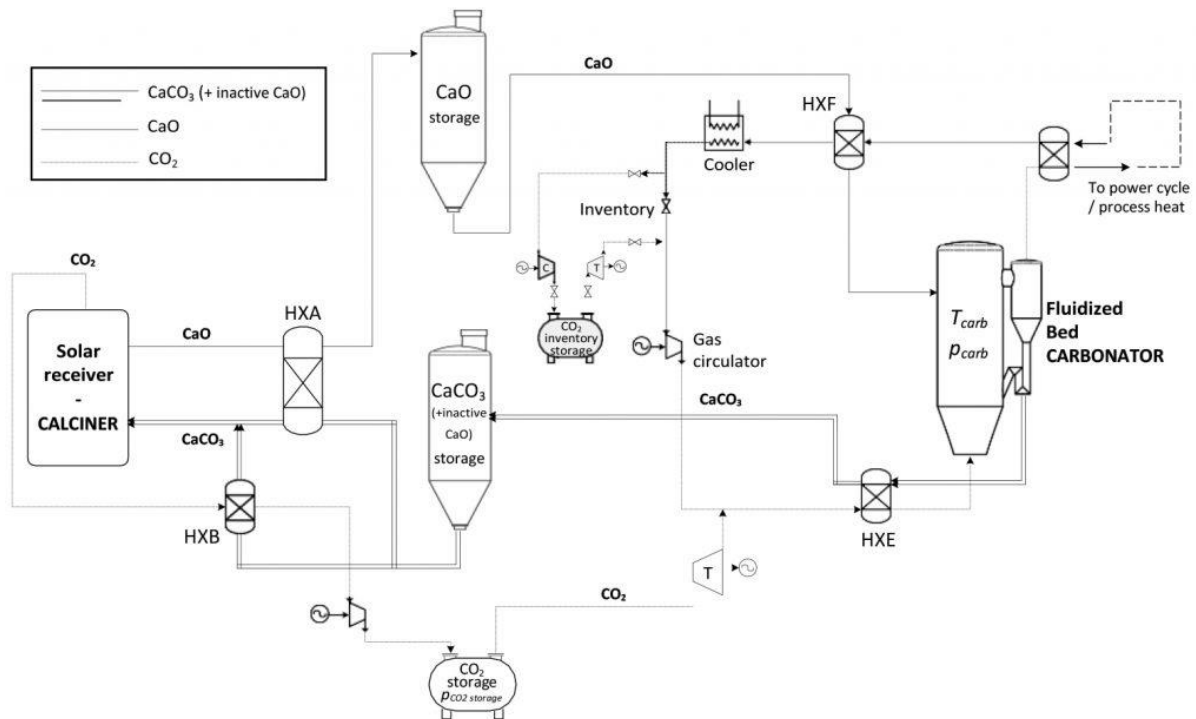


Figure 3.3 – Calcium looping integration with an indirect cycle configuration [3]

For this layout there is more freedom in the choice of the carbonator operating conditions and, according to most of the present literature on CaL integration in CSP, it's suggested the use of a reactor working at ambient pressure and with an atmosphere made of pure CO₂.

Another consequence is that the power block is free to adopt any thermodynamic cycle in accordance to the disposable amount of heat and its range of temperatures.

Some suitable power cycles are represented by: steam Rankine cycle, organic Rankine cycle, Brayton-Joule cycle, Stirling cycle, combined cycles and Kalina cycle. Obviously, being these alternatives very different between them, it is necessary to study in deep every configuration in order to establish the most convenient choice.

Furthermore, there are still two important aspects to point out about the direct and indirect CaL integration.

The first one is that, except for the air/CO₂ variant (the only case where it isn't needed a CO₂ recirculation), the plant design must include a carbon dioxide inventory storage with its relative compressor and turbine. This is due to the fact that, in the transients happening during its functioning, the carbonator will need to change the amount of recirculated flow, and the best way to obtain this result, instead of vary the stream extracted by the main CO₂ storage, is to install a small system able to increase or decrease rapidly the backflow by the injection or withdraw of a suitable amount of gas. Anyway, since all the simulations have been performed assuming the plant in steady-state conditions, it has been possible to avoid considering it.

The second interesting aspect to notice is that, in first approximation, the calciner side layout isn't influenced by the power cycle integration (both for the direct and indirect case). This confirm the correctness of the previous conceptual plant subdivision in correspondence of the three storages; in fact, once that the carbonation reactants are produced by the calciner and sent to their vessels, the way in which they will be subsequently used doesn't influence the previous process. This is why, concerning the simulations performed in the following chapters, for equal storage conditions it's sufficient to simulate only the carbonator side to make a comparison between the thermodynamic cycles.

Finally, as will be discussed later, the optimization strategy for both the direct and indirect integration is based on the pinch analysis but the differences between the two integration alternatives make necessary to develop two different optimization processes, which will be separately exposed at the beginning of their respective paragraph.

All the simulations have been developed on two software: Aspen Plus V8.8 and MATLAB R2017b.

heat up the stream, otherwise the temperatures reached at the end of the expansion will be too low. In many works found in literature ([3], [15], [1]) it's adopted a multistage expansion with about seven inter-heatings fed by a traditional thermal power source; anyway, taking into account the relatively small plant size, it has been decided to perform a single heating before the turbine inlet, in order to simplify both the simulation and the final plant layout.

Furthermore, the required thermal power will be internally provided performing a heat recovery. In this way the obtained configuration will be only fed by the solar radiation and therefore its functioning won't release global warming gases in the atmosphere, coherently with the renewable and sustainable principles at the base of the international policies that started up the SOCRATCES project.

Leaving the turbine, the CO₂ is mixed with another stream of carbon dioxide and the resulting flow exchange heat to reach the carbonator inlet temperature. At the meantime, the calcium oxide is preheated from its storage conditions (1 bar, 20°C) and enters the reactor.

At the reactor outlet are present the carbon dioxide in excess, the calcium carbonate (product of carbonation) and the unreacted calcium oxide; all these compounds are at the carbonation temperature and it's important to notice that the two solids are intrinsically related, because, as explained in the first chapter, they are both constituting the same solid grains.

Therefore, these solids will be subjected to the same temperature variations and for the simulation purposes it's convenient to consider them with an equivalent stream having equal bulk properties.

Anyway, the carbonator outlet is sent to a cyclone with the aim of divide the carbon dioxide from the solids, then, the CaCO₃ and the unreacted CaO are cooled down and directly sent to their storage (1 bar, 20°C), while the CO₂ in excess is expanded in order to produce electrical power, then it's performed a heat recovery and finally it's compressed and recirculated.

Modelling and optimization structure

To find the optimal operating conditions it has been used (on Matlab) the genetic algorithm method, the whom, for a set of independent variables, evaluates iteratively the objective

function (i.e. the plant performance) until it finds the optimal solution which guarantees (through the pinch analysis) that any thermophysical constraint provided is respected.

The (partial) integration efficiency has been expressed as the ratio between the outlet electric net power and the consumption of primary energy, which, analysing only the carbonator side layout, is represented by the amount of reactants extracted by the respective storages and, consequently, their energetic content in chemical form.

Anyway, in order to run the plant simulation is necessary to model all the different components included in the layout. This isn't particularly difficult for the compressor and turbines, since it's just necessary to provide the respective values of isentropic efficiencies, pressure variations and inlet temperatures, but it's a little more complex for the chemical reactor.

The carbonator functioning has been simulated at constant temperature and solid reactivity, varying both the reactants inlet temperature and the operating pressure, with a fixed thermal power loss equal to the 1% of the reaction heat power developed [15]. In this way is possible to obtain the ratio between the carbon dioxide and the calcium oxide streams or the CO₂ excess (these are two equivalent alternatives, since they both allow to completely determine the reactor functioning).

For completeness, the carbon dioxide excess index is defined as the ratio between the CO₂ stream effectively provided and the stoichiometric CO₂ flow.

$$Excess\ index = n = \frac{\dot{m}_{CO_2\,eff}}{\dot{m}_{CO_2\,stoich}}$$

Obviously, the carbon dioxide excess is independent form the amount of reactants provided to the reactor inlet and this is why (as will be later discussed) these mass flows have been assumed as variables in the optimization.

A simplified way to understand the carbonator functioning consists in imagine the reactor operation as divided in two steps: in the first one, the reactants are heated up to the carbonator temperature with the thermal power provided by the exothermic reaction, while, in the second step, the reaction itself takes place. Now, increasing the temperature of the inlet streams reduces the amount of heat required to heat up the reactants, but, assuming as constant the calcium oxide mass flow and the operating temperature, the only way to

guarantee the functioning is to adequately increase the excess of carbon dioxide; that's why, as will be observed further on, higher reactants inlet temperature cause higher values of the excess index.

Another important thing to point out is that there may be cases where the thermal power provided by the exothermic reaction it's insufficient to heat the reactants up to the carbonator temperature, even if the carbon dioxide flow is minimized (i.e. stoichiometric), making impossible the reactor functioning. The parameters that can cause this phenomenon are two: of course the first one is the inlet streams temperature, while the second is the solid reactivity, because, when it decreases, the corresponding amount of inert matter involved by the reaction increase, requiring a higher thermal power for its heat up.

This concept is shown in the following graph, which makes possible to observe that a decrease of the carbonation temperature or an increase of the solid reactivity brings to a less stringent configuration, so that in some cases the pareto curve disappears, which means that (in first approximation) there aren't any thermal constraints for the reaction.

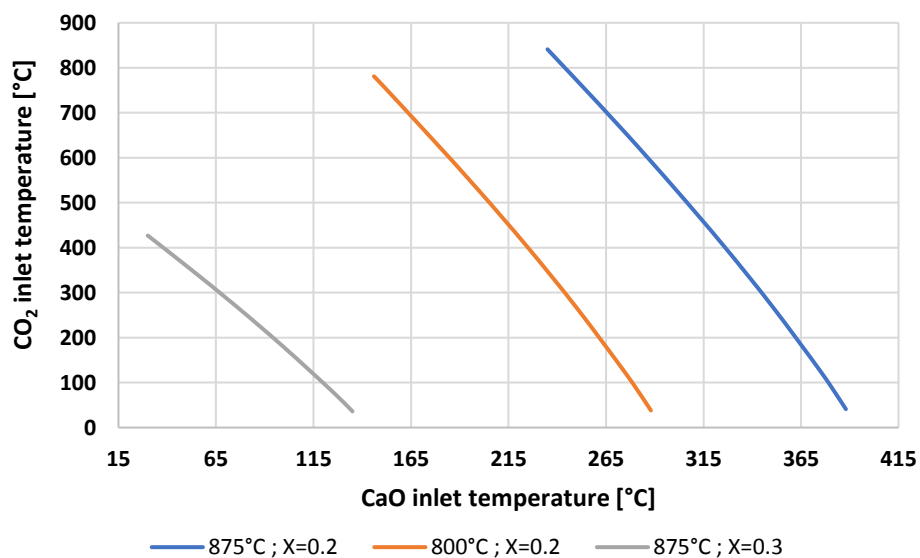


Figure 4.2 - Pareto curves for the carbonator inlet streams temperature for different CaO activity and reactor temperature.

Anyway, although on a thermodynamic point of view the carbonation reaction can occur even at low inlet reactants temperatures, it should be considered that a cold flow entering the vessel can create a local temperature decrease (with respect to the operating target). This can cause a strong slowdown of the reaction kinetic, determining excessively long residence times which are actually unsustainable for the practical purposes of this kind of technology.

So, this is why it's necessary to evaluate the possibility of insert a lower bound for these two parameters. Now, concerning the carbon dioxide, no particular temperature limits were found and therefore the minimum has been set to 35°C ($T_{amb} + \Delta T_{min}$). Things are different regarding the calcium oxide temperature, for the which the carbonation reaction kinetic seems to be more sensible, so in this case it has been set a minimum inlet temperature equal to 310°C, which is the minimum value found in the scientific literature [1].

The carbonator simulation has been performed on Aspen using a RStoic reactor modelled with the UNIFAC method. For first, all the constant parameters are inserted (X , P_{carb} , T_{carb} , $T_{CO_2,in}$, $T_{CaO,in}$), then it's necessary to establish an arbitrary CaO mass flow such that a design-spec will find the amount of CO_2 that makes possible to operate at the specified carbonator temperature. In this way the carbon dioxide excess is determined.

From the figures on the side it's possible to see the excess index behaviour in case of variable carbonation temperature or CaO activity, in addition to the inlet streams temperature. Roughly speaking, there is a linear dependence between n and the CaO feed temperature, while the CO_2 temperature determines a much more exponential variation, with a consistent increase in correspondence of higher temperatures; otherwise, the provided carbon dioxide is nearly stoichiometric.

Furthermore, increasing the reactor operating temperature basically determines a shift of the surface towards higher values of the carbon

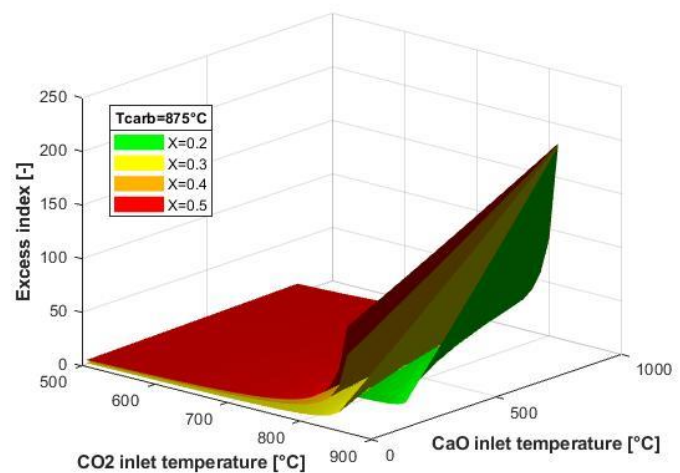
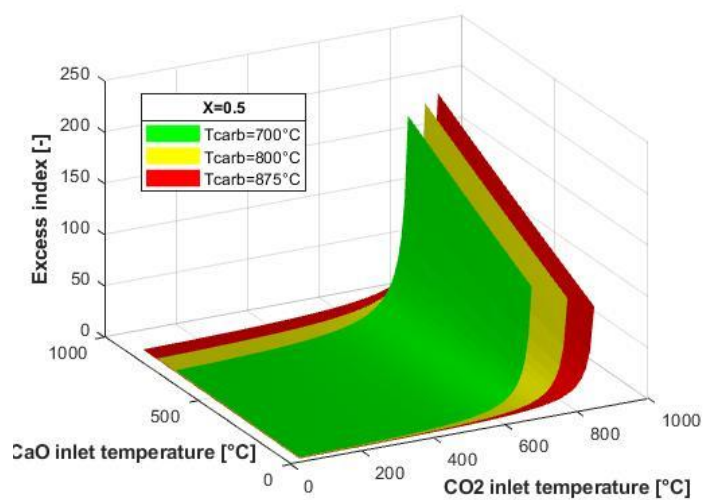


Figure 4.3 - Excess index for the carbonation reaction in case of fixed reactivity and in case of fixed reactor temperature ($P_{carb}=1bar$)

dioxide temperature, while an increase of the calcium oxide reactivity causes an increase of the excess index, which is more consistent for lower CaO temperatures and for higher CO₂ temperatures.

Once that all the single components have been modelled, is possible to develop the complete simulation of the carbonator side. It's therefore necessary to distinguish between the constant and variable parameters and, for these last ones, between the dependent and independent variables. As already mentioned, the value of these independent variables is investigated by the genetic algorithm in order to maximize the plant efficiency. At the same time, through the pinch analysis is calculated the external heating needed and, if different from zero, the result is discarded because unacceptable (the plant must avoid the use of fossil fuels) and the algorithm continues the research until both the convergence tolerance and the constraints are satisfied.

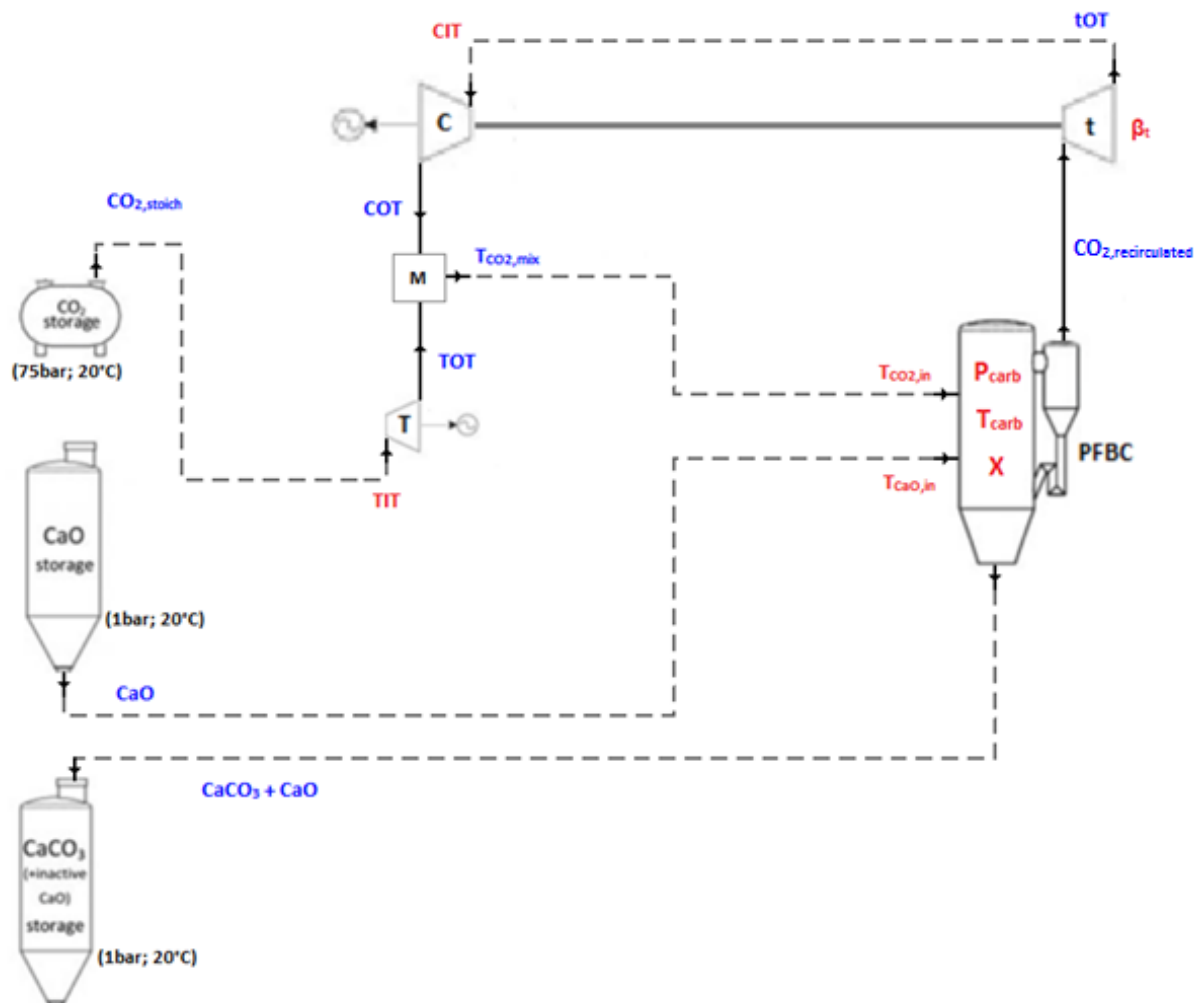


Figure 4.4 – Plant layout with streams data for the pinch analysis reported in correspondence of their actual plant location. The fixed parameters are the ones in black, the independent variables in red and the dependent variables in blue

As shown in the image above, the storages thermophysical states are considered as fixed, while the parameters assumed as independent variables are: the CaO activity, the carbonator operating pressure and temperature, the carbonator feed streams temperatures, the main turbine pressure ratio, the compressor inlet temperature and the CO₂ storage turbine inlet temperature. Any other pressure, temperature or flowrate is directly calculated from these parameters.

Furthermore, all the data assumed for the components functioning are listed in the table below.

ASSUMPTIONS		REFERENCE
$\eta_{is,T}$	0,75	[15]*
$\eta_{is,t}$	0,9	[15]
$\eta_{is,C}$	0,87	
η_{el}	0,97	
$PL_{\%,CO2,stoic}$	1%	[1]
$PL_{\%,HP}$	6%	[1] + [15]
$PL_{\%,LP}$	4%	
Conveying consumptions	10 MJ/(ton*100m)	[16]
Storages-carbonator distance	100 m	
Auxiliaries consumptions	0,8% rejected heat	[15]
$\Delta T_{min,pinch}$	15°C	
$T_{ambient}$	20°C	[16]

Table 4.1 - Data assumptions for the direct integration simulation (*adapted for the analyzed size)

Regarding these assumptions it's necessary to make some clarifications: both the pressure losses between the main turbine outlet and the compressor inlet (low pressure side, $PL_{\%,LP}$) and between the compressor outlet and the main turbine inlet (high pressure side, $PL_{\%,HP}$) are dependent on the number of heat exchangers that the streams have to cross. Anyway, since this is an information that is available only at the end of the optimization, they have been obtained as a first approximation considering both the physical assumptions made in [15] and the heat exchangers layout presented in [1].

Furthermore, in order to reduce wherever as possible the internal electricity consumption, when the solids stream exiting from the carbonator ends to exchanging thermal power to heat up the cold fluids, it is directly sent to its storage even if it has not reached the target

temperature of 20°C (as found in [16]). In fact, cooling down completely this stream is not actually strictly necessary and, on the other hand, it would just determine an increase in the auxiliaries consumptions to feed the dry-coolers.

To allow an easier comprehension of the optimization process, all the different parameters analysed are summed up in the following tables.

CONSTANT PARAMETERS

Storage vessel	Pressure	Temperature
CO ₂	75 bar	20°C
CaO	1 bar	20°C
CaCO ₃	1 bar	20°C

INDEPENDENT VARIABLES

Name and acronym	Lower bound	Upper bound	TREATED AS
CaO activity: X	0,2	0,5	Discrete
Carbonator temperature: T_{carb}	775°C	875°C	Discrete
Carbonator pressure: P_{carb}	1,5 bar	15 bar	Continuous
Main turbine pressure ratio: β_t	1,2	15	Continuous
CO ₂ inlet stream temperature: T_{CO₂,in}	T _{amb} + ΔT _{pinch}	T _{carb} - ΔT _{pinch}	Continuous
CaO inlet stream temperature: T_{CaO,in}	310°C	T _{carb} - ΔT _{pinch}	Continuous
Compressor inlet temperature: CIT	T _{amb} + ΔT _{pinch}	250°C	Continuous
Turbine inlet temperature: TIT	250°C	650°C	Continuous

DEPENDENT VARIABLES

CaO from storage mass flow: \dot{m}_{CaO}	Mixed CO ₂ flow temperature: T_{CO₂,mix}
CO ₂ mass flow from storage: $\dot{m}_{CO_2,stoich}$	Main turbine outlet temperature: tOT
CaCO ₃ mass flow: \dot{m}_{CaCO_3}	Compressor outlet temperature: COT
Unreacted CaO mass flow: $\dot{m}_{CaO_{unr}}$	Storage turbine outlet temperature: TOT
Recirculated CO ₂ mass flow: $\dot{m}_{CO_2,rec}$	All the inlet/outlet unknown pressures

Tables 4.2, 4.3, 4.4 - Three tables to sum up the different parameters and, eventually, their variation ranges

Concerning the two independent variables treated as discrete (the CaO activity and the carbonator temperature), it's necessary to make an important clarification; in fact, during a

single generic optimization run, both these parameters are actually handled as constants and, in order to vary their value, it's necessary to perform another different run.

This choice was made because of two reasons: for the solid reactivity there was a precise intention to perform different simulation runs and consequently obtain the respective results in order to make some considerations regarding the plant efficiency dependence on this parameter. For the carbonator temperature the motivation was instead due to the expected monotonic behaviour and therefore the possibility of adopt a coarser definition for the parameter's value.

Now, to completely determine the plant thermophysical parameters, it's still necessary to apply some requirements and constraints, such that the results obtained will be consistent. Notice that the value imposed for the net electrical power production is only related to the main turbine and compressor (t and C), while the storage turbine (T) doesn't have any size constraint.

CONSTRAINTS

CIT_{min} and $T_{CO2,in,min}$	35°C
$P_{CO2,min}$	1 bar
$\dot{Q}_{heat,need}$	0 MW
$P_{el(t+c),net}$	1 MW

Table 4.5 - Direct integration optimization constraints

Furthermore, the minimum pressure achievable by the recirculated carbon dioxide is set to 1 bar because in this way, as explained in [15], the heat exchangers utilized at the main turbine outlet will operate under no particularly demanding conditions (pipelines and turbomachinery high dimensions), in accordance to the efforts already justified to avoid, whenever as possible, any not essential complication. Making this assumption leads at the meantime to another benefit, because is consequently eliminated any eventual air infiltration, which could bring negative drawbacks on the efficiency, since the carbonator wouldn't operate with an atmosphere only composed by carbon dioxide.

At this point, starting from the independent variables, the constant parameters and the other assumptions, it's possible to determine all the remaining unknowns (i.e. the dependent parameters) applying the equations listed below.

$\left. \begin{matrix} T_{CO_2,in} \\ T_{CaO,in} \\ P_{carb} \end{matrix} \right\}$ Excess index (EI) obtained from the carbonator simulation with Aspen

MAIN TURBINE: $tOP = \frac{P_{carb}}{\beta_t}$ $\left. \begin{matrix} T_{carb} \\ P_{carb} \\ tOP \\ \eta_{is,t} \end{matrix} \right\}$ tOT and $\dot{w}_{s,t}$

COMPRESSOR: $CIP = tOP \cdot (1 - PL_{\%LP})$ $COP = \frac{P_{carb}}{PL_{\%HP}}$

$\left. \begin{matrix} CIT \\ CIP \\ COP \\ \eta_{is,c} \end{matrix} \right\}$ COT and $\dot{w}_{s,c}$

STORAGE TURBINE: $TOP = \frac{P_{carb}}{PL_{\%HP}}$ $\left. \begin{matrix} TIT \\ TIP \\ TOP \\ \eta_{is,T} \end{matrix} \right\}$ TOT and $\dot{w}_{s,T}$

In order to calculate the flowrates it may be helpful to draw a simple balance of a control volume that includes the carbonator side without the three storages. In this way it's easy to observe that the single outlet mass flow is composed by calcium carbonate and calcium oxide (because the CaO reactivity is smaller than one), but the carbon dioxide is absent; this means that the entering CO₂ is provided in its stoichiometric amount, and therefore it will completely react during the carbonation. Anyway, the first flowrate calculated is the recirculated carbon dioxide, because (being also the power fluid) it must guarantee a net electrical production equal to the imposed value. Any other stream is consequently obtained applying the following equations.

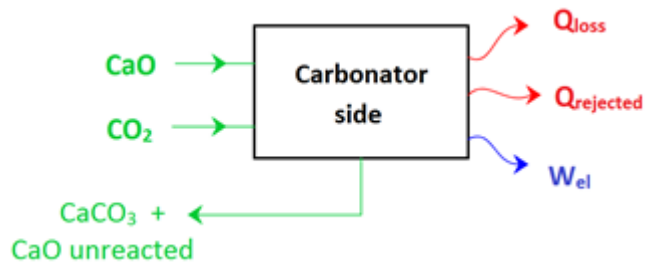


Figure 4.5 - Mass and energy balance of the analyzed system

MASS FLOWS: $\dot{m}_{CO_2,rec} = \frac{1 \text{ MW}}{\eta_{el} \cdot (\dot{w}_{s,t} - \dot{w}_{s,c})}$

$\dot{m}_{CO_2,stoich} = \frac{\dot{m}_{CO_2,rec}}{EI - 1}$

$$\dot{m}_{CO_2,carb,in} = \dot{m}_{CO_2,stoich} + \dot{m}_{CO_2,rec}$$

$$\dot{m}_{CaO,carb,in} = \frac{\dot{m}_{CO_2,stoich}}{X \cdot MM_{CO_2}}$$

$$\dot{m}_{CaCO_3} = X \cdot \frac{MM_{CaCO_3}}{MM_{CaO}} \cdot \dot{m}_{CaO,carb,in}$$

$$\dot{m}_{CaO,unreac} = (1 - X) \cdot \dot{m}_{CaO,carb,in}$$

MIXER:

$$T_{CO_2,mix} = \frac{\dot{m}_{CO_2,recirc} \cdot \overline{c_{p,recirc}} \cdot COT + \dot{m}_{CO_2,stoich} \cdot \overline{c_{p,stoich}} \cdot TOT}{\dot{m}_{CO_2,recirc} \cdot \overline{c_{p,recirc}} + \dot{m}_{CO_2,stoich} \cdot \overline{c_{p,stoich}}}$$

$$\cong \frac{\dot{m}_{CO_2,recirc} \cdot COT + \dot{m}_{CO_2,stoich} \cdot TOT}{\dot{m}_{CO_2,carb,in}} \leftrightarrow \text{Hypothesis: } \overline{c_{p,recirc}} \cong \overline{c_{p,stoich}}$$

SOLIDS CARBONATOR OUTLET:

$$c_{p(CaO_{unreac}+CaCO_3)} = \frac{(1 - X) \cdot MM_{CaO} \cdot c_{p,CaO} + X \cdot MM_{CaCO_3} \cdot c_{p,CaCO_3}}{(1 - X) \cdot MM_{CaO} + X \cdot MM_{CaCO_3}}$$

When all the fluids parameters are calculated, it's possible to execute the pinch analysis in order to determine if the plant needs an external heat source for its functioning.

COLD FLUIDS

Flowrate	Inlet temperature	Outlet temperature
$\dot{m}_{CO_2,stoich}$	20°C	TIT
$\dot{m}_{CO_2,carb,in}$	$T_{CO_2,mix}$	$T_{CO_2,in}$
$\dot{m}_{CaO,carb,in}$	20°C	$T_{CaO,in}$

HOT FLUIDS

Flowrate	Inlet temperature	Outlet temperature
$\dot{m}_{CO_2,recirc}$	tOT	CIT
$\dot{m}_{CaCO_3} + \dot{m}_{CaO,unreac}$	T_{carb}	20°C

Tables 4.7, 4.8 - Hot and cold fluids for the pinch analysis with their respective temperature ranges; notice that in some cases the CO₂ entering the carbonator may be colder than the mixed CO₂, moving the stream between the hot fluids

The streams specific heat capacity has been provided to the pinch analysis algorithm in different ways, according to the particular case. For the calcium oxide and the calcium carbonate have been used three mathematical correlations [3], whose temperature range of validity is compatible with the values assumed during the simulation, while for the carbon dioxide it has been provided by the CoolProp data library.

As already explained, if the pinch analysis results provide a heating requirement different from zero the configuration is considered as unacceptable and therefore the set of values assumed for the independent variables is discarded. The optimization algorithm continues its research on this pathway until it converges to an optimal and acceptable solution.

Obviously, the objective function evaluated by the genetic algorithm is the carbonator side efficiency, which is calculated as the ratio between the net electrical power output and the heat flux developed by the exothermic reaction, as reported by the following formula.

$$\eta_{carbonator\ side} = \frac{\dot{W}_{net,el}}{\dot{Q}_{carb}} = \frac{\dot{W}_{net,el}}{\dot{m}_{CaO} \cdot X \cdot \Delta h_r^0}$$

The term Δh_r^0 stands for the standard enthalpy of reaction per unit of mass of calcium oxide (3178,6 kJ/kg).

Of course, it could be argued that the two reactants extracted from their storages aren't in standard conditions since both are at 20°C and the carbon dioxide has a pressure of 75bar, so they do not only make available a thermal power during the chemical reaction, but the CO₂ provides also the possibility of an expansion from which an electrical power is obtained.

The fact that the energy previously consumed to compress this stream is not considered in the definition of the carbonator side efficiency but, on the contrary, the power received by its expansion is taken into account (inside the net electrical power) must not mislead: as already explained, this parameter is referred to only a portion of the complete CaL plant.

The most important thing is that all the simulations performed (direct and indirect integrations) start from the same storages conditions, which is sufficient to get consistent results.

To sum up the optimization process structure is reported below an essential flow chart that illustrates all the main steps performed by the algorithm to reach the optimized configuration.

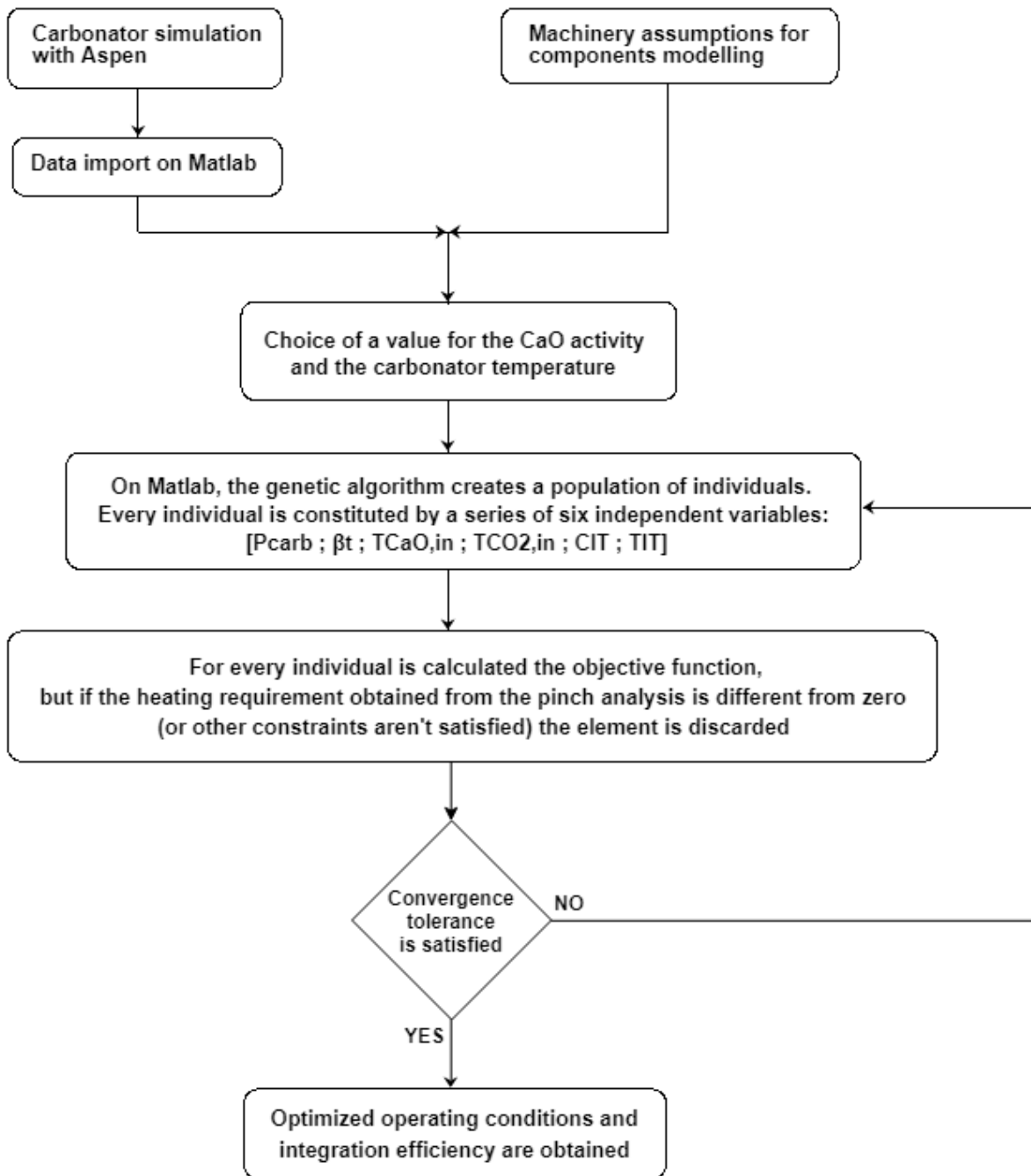


Figure 4.6 - Simple flow chart to sum up the optimization structure for the direct integration

Results, comments and comparisons

In this paragraph are reported the optimization results, compared each other according to their efficiency in order to make possible the evaluation of the most suitable alternative.

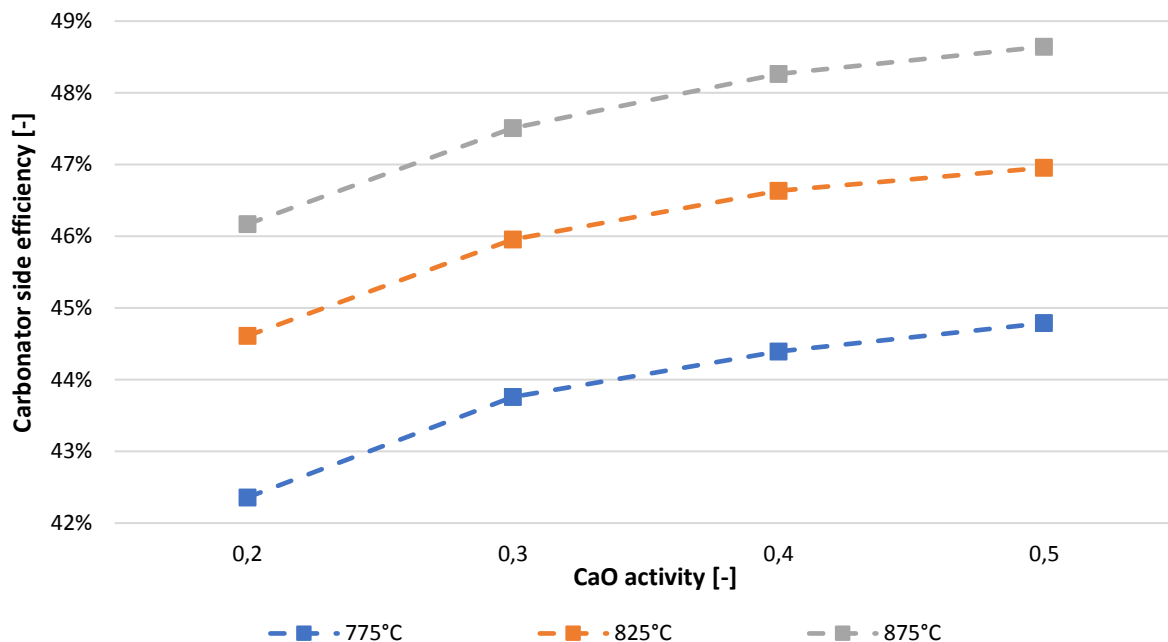


Figure 4.7 - Direct integration optimization results

As could be imagined, the higher is the reactor temperature, the higher is the carbonator side efficiency and the same happens for the calcium oxide reactivity, where a smaller amount of inert CaO brings benefits to the integration performance, although the trend seems to have an asymptote.

In the tables below are reported the results obtained from the optimization process for the most important plant parameters (notice that the turbomachinery powers are expressed in terms of shaft powers, not electricity).

So, at this point is possible to make some interesting considerations. In fact, for every investigated value of carbonator temperature and CaO reactivity, the algorithm converges to values of carbonator pressure and pressure ratio such that the recirculated carbon dioxide reaches its minimum acceptable pressure, equal to 1 bar, in correspondence of the compressor inlet.

Moreover, operating at lower reaction temperatures makes necessary (in order to satisfy the constraint on the power production) higher flowrates of the recirculated carbon dioxide,

which determines an increase of both the compressor and main turbine size, while the storage turbine size, which is mainly dependent on its inlet operating temperature, doesn't show a precise trend.

As could be expected, the compressor inlet temperature always reaches its lower value, in order to minimize the compression power requirement, and, obviously, the calcium oxide flowrate decreases with the increasing of the solid reactivity, although the amount of reactant that participates actively to the chemical reaction has an opposite variation, in accordance to the results obtained for the efficiency.

As a consequence of that, the conveying power decrease with the increase of the calcium oxide activity, while the rejection power is relatively small and its variations are actually negligible (if considered in absolute terms). So, the total auxiliaries consumption (which is the sum of these two components) becomes smaller both for higher values of the carbonator temperature and CaO reactivity.

	X [-]	Main turbine power [kW _s]	Compressor power [kW _s]	Storage turbine power [kW _s]	Conveying power [kWe]	Rejection power [kWe]	Total auxiliaries consumption [kWe]	Total plant net power [kWe]
T_{carb} = 775°C	0,2	2087	1056	122	82,5	6,7	89,1	1029
	0,3	2087	1056	112	56,0	7,1	63,1	1046
	0,4	2087	1056	114	43,5	7,4	50,9	1060
	0,5	2087	1056	111	35,8	7,6	43,4	1065
T_{carb} = 825°C	0,2	1981	950	115	78,2	6,0	84,2	1027
	0,3	1981	950	114	53,6	6,5	60,1	1051
	0,4	1981	950	112	41,4	6,7	48,1	1061
	0,5	1981	950	117	34,4	6,9	41,3	1072
T_{carb} = 875°C	0,2	1931	900	108	75,3	5,3	80,6	1024
	0,3	1931	900	111	51,8	5,8	57,6	1050
	0,4	1931	900	106	39,9	6,0	45,9	1057
	0,5	1931	900	105	32,9	6,2	39,1	1063

Table 4.9 - Shaft and electrical powers obtained from the direct integration optimization process

At this point it's necessary to make an important clarification. In fact, as is possible to see in the following table, unluckily not all the parameters show a particular trend, which is not a very cheering fact.

There can be two main feasible justifications for this phenomenon: first one is the non-linearity of the problem and therefore the consistent complexity of the objective function,

which make some variables to converge to values with a non-predictable trend. The second one can be related to the heuristic nature of the genetic algorithm and therefore the intrinsic impossibility of obtain exact outcomes for the optimization problem.

Anyway, these two drawbacks are not enough crucial to compromise the entire process, since the achieved results are actually reasonable and coherent with the ones found in literature [4] (taking into account that the configuration here analysed presents some differences with respect to the one investigated in the scientific article).

	INDEPENDENT VARIABLES							DEPENDENT VARIABLES AND RESULTS					FLOWRATES					
	X [-]	P _{carb} [bar]	β _t [-]	T _{CaO,in} [°C]	T _{CO₂,in} [°C]	TIT [°C]	CIT [°C]	Excess index [-]	tOT [°C]	COT [°C]	TOT [°C]	T _{CO₂,mix} [°C]	\dot{m}_{CaO} [kg/s]	$\dot{m}_{CO_2,stoic}$ [kg/s]	$\dot{m}_{CO_2,rec}$ [kg/s]	$\dot{m}_{CaO,unr}$ [kg/s]	\dot{m}_{CaCO_3} [kg/s]	η _{carb} [%]
T _{carb} = 775°C	0,2	3,10	2,98	746	625	348	35,1	20,36	629	136	137	136	3,82	0,601	11,63	3,06	1,37	42,36
	0,3	3,10	2,98	688	635	315	35,1	20,69	629	136	110	135	2,51	0,591	11,63	1,75	1,34	43,76
	0,4	3,10	2,98	737	626	322	35,1	20,74	629	136	116	135	1,88	0,590	11,65	1,13	1,34	44,39
	0,5	3,10	2,98	682	631	313	35,1	20,81	629	136	108	135	1,50	0,588	11,64	0,75	1,34	44,79
T _{carb} = 825°C	0,2	2,92	2,81	807	676	338	35,1	20,51	681	131	125	131	3,62	0,569	11,11	2,90	1,29	44,61
	0,3	2,92	2,81	728	689	337	35,1	20,65	681	131	125	131	2,40	0,565	11,11	1,68	1,28	45,96
	0,4	2,92	2,81	706	688	332	35,1	20,75	681	131	121	130	1,79	0,562	11,11	1,07	1,28	46,63
	0,5	2,92	2,81	763	679	349	35,1	20,68	681	131	134	131	1,44	0,564	11,11	0,72	1,28	46,96
T _{carb} = 875°C	0,2	3,43	3,30	842	708	345	35,1	17,52	704	146	139	145	3,49	0,548	9,06	2,79	1,25	46,17
	0,3	3,43	3,30	839	706	359	35,1	17,59	704	146	150	146	2,32	0,546	9,06	1,62	1,24	47,51
	0,4	3,43	3,30	837	706	340	35,1	17,74	704	146	135	145	1,72	0,541	9,06	1,03	1,23	48,26
	0,5	3,43	3,30	822	707	339	35,1	17,77	704	146	134	145	1,38	0,540	9,06	0,69	1,23	48,64

Table 4.10 - Temperatures, pressures and flowrates obtained from the direct integration optimization process

Finally, it can be interesting to observe both the grand composite curve and the hot and cold fluids composite curves for the case (between the ones analysed) with the highest efficiency value, that is when the calcium oxide activity is equal to 0,5 and the carbonator temperature reaches 875°C.

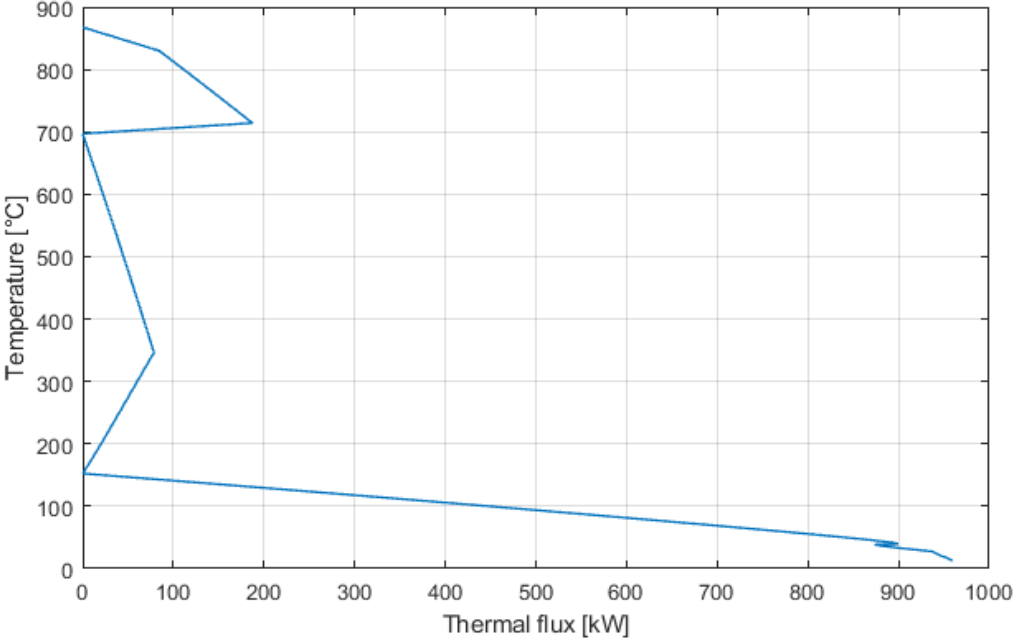


Figure 4.8 - Grand composite curve for the direct integration layout ($T_{carb}=875^{\circ}C$; $X=0,5$)

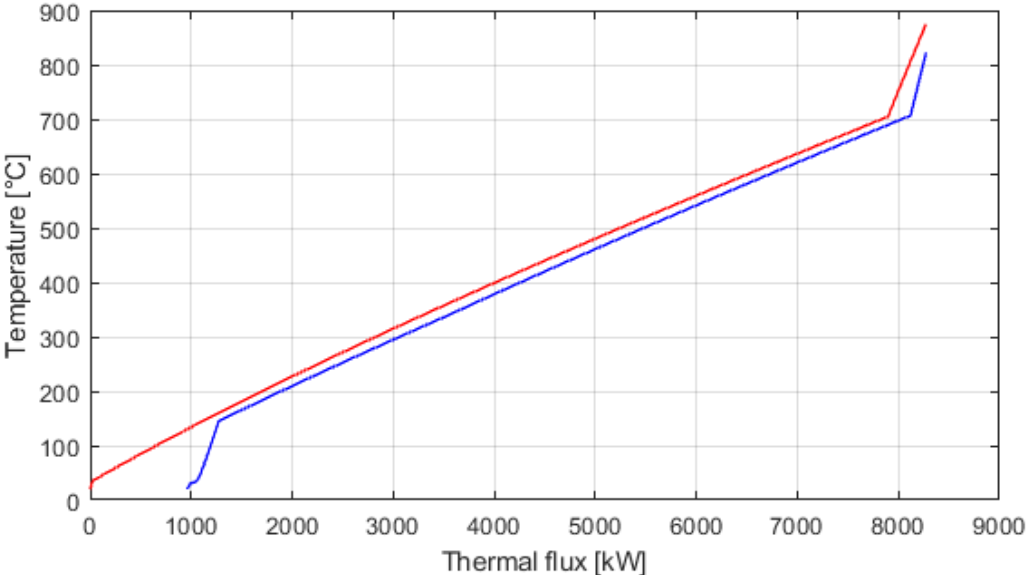


Figure 2.9 - Hot and cold composite curves for the direct integration layout ($T_{carb}=875^{\circ}C$; $X=0,5$)

It is worth to comment these last two graphs. Concerning the grand composite curve, it reaches a null thermal flux in correspondence of three different temperatures: in the case of the highest value it simply means that the external heat requirement is equal to zero, as

imposed to the pinch analysis outcomes; instead, in the case of the mid and lower value it means that the hot and cold fluids reach the minimum temperature difference and therefore the final layout will have two different pinch points.

Concerning the hot and cold composites graph, the two curves are very close each other, except when the thermal flux is either at its minimum or maximum. In particular, the change of slope at high temperatures for the hot composite curve is due to the fact that only the CaCO_3 (and the relative unreacted CaO) stream is available at the carbonator temperature, while the CO_2 exiting from the reactor, being sent to the main turbine, undergoes a decrease in temperature. So, in order to exploit this characteristic as well as possible, the algorithm converges to an optimal solution in which the CaO entering the carbonator is heated more than the inlet CO_2 : in this way also the cold composite curve shows a similar change in its slope for high temperatures.

The other change of slope for the cold composite happens for low temperatures, when the carbon dioxide extracted from the storage is the only fluid to be heated up; however, in this case it's not convenient for the hot curve to follow this trend because it would mean to have an higher compressor inlet temperature and, as a consequence, an higher power consumption for the compression of the recirculated CO_2 .

In conclusion of this chapter it's exposed the heat exchanger network for the configuration that, as will be proven in the final comparisons, seems to be the most interesting between the ones analysed (according to its performance and functioning complexity). This layout is constituted by the direct integration with a carbonator operating temperature set to 875°C and a calcium oxide activity equal to 0,5 and it is actually the same case for the whom has been previously showed the composite curves.

Now, as is possible to find in [16], there are two advices regarding the heat exchanger network design that, if followed, help to obtain a relatively easier to manage plant configuration: the first one is that splitting a solid stream should be avoided because, in practical terms, it is much more complex with respect to the split of a fluid stream. The second one is that it would be better also to avoid heat exchange between solid streams because, if compared to the case of gas-solid or gas-gas heat exchange, it shows lower performances and adopts a less mature technology.

Now, regarding the first advice, no particular difficulties have been encountered in order to respect it and therefore all the stream splitting appearing in the layout have been only performed on the carbon dioxide. However, it hasn't been possible to satisfy the second advice because prohibiting the coupling between the two solid streams brings to an increment of the external heat requirement, which, as imposed during the optimization process, must be null in order to avoid the use of fossil fuels.

Anyway, this drawback shouldn't constitute a strong disadvantage because, as it's easy to notice looking at the heat exchanger network obtained, there is actually only one heat exchanger performing this kind of thermal recovery and moreover its size is relatively small when compared to the total power involved in the process.

Stream	Flowrate [kg/s]	T _{in} [°C]	T _{out} [°C]	Thermal power [kW _t]
CaCO ₃ + CaO _{un}	1,92	875	20	1764
CO _{2,rec}	9,06	704	35,1	6553
CaO	1,38	20	822	996
CO _{2,mix}	9,60	145	707	6024
CO _{2,stoic}	0,540	20	287	

Table 4.10 - Hot and cold fluids involved in heat recovery

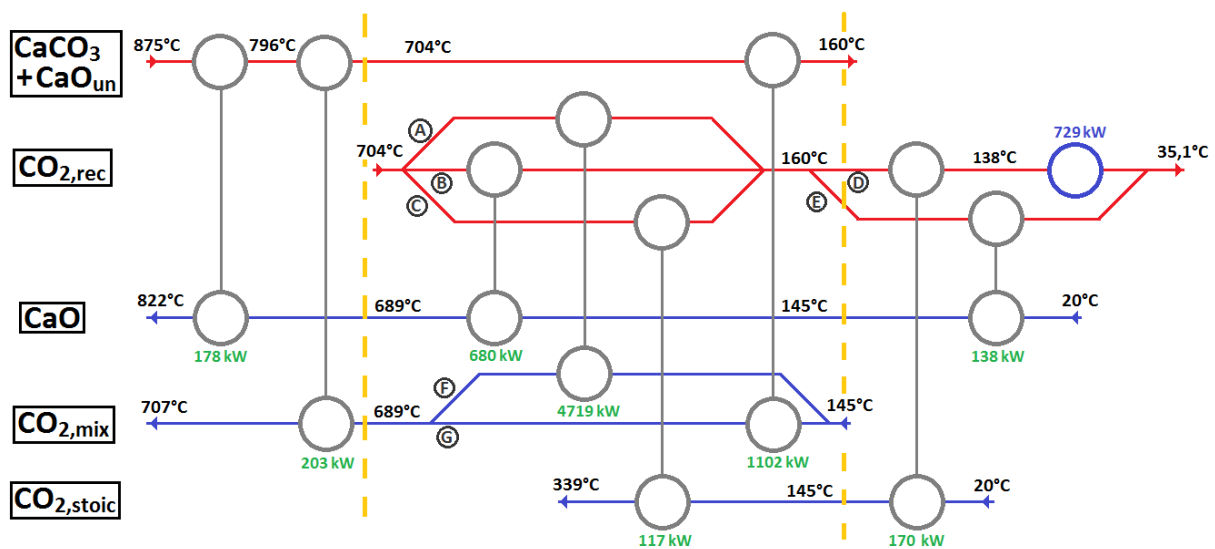


Figure 4.10 - Heat exchanger network for the direct integration optimized configuration (the yellow dashed lines are located in correspondence of the two pinch points)

Branch	%	Branch	%	Branch	%
A	85,5	D	86,8	F	18,9
B	12,4	E	13,2	G	81,1
C	2,1				

Table 2.11 - Flowrates of the splitted branches expressed as a percentage of the total relative stream

In conclusion is left a comment about the heat exchanger network showed above. The most important thing to say is that, differently from what reported in the table with the hot and cold fluids data, the carbonator solid outlet stream isn't completely cooled down, since it doesn't reach the target temperature equal to 20°C.

This happens because, as already discussed, once that all the cold fluids have been heated up, the CaCO₃ stream can be sent directly to its storage, avoiding in this way the electrical consumptions due to the dry-cooling and obtaining a storage with an amount of sensible heat that may be useful in the calcination process. Obviously, this is the same reason why the cooler size is only equal to 729 kW_t but the cooling requirement obtained from the pinch analysis (and showed by the composite curves) was nearly 1000 kW_t.

The last thing to say is that, looking at the three regions identified by the two pinch points and considering them as three parts energetically independent, it's possible to observe the absence of meshes in each of the regions and therefore it seems that the layout obtained has already the minimum number of heat exchangers, making impossible to perform any other simplification.

Indirect integration

The power cycles indirectly integrated in the CaL plant that have been considered in this work belong to three different categories: organic Rankine cycles (ORC), steam Rankine cycles (SRC) and Brayton-Joule cycles (in particular, the supercritical carbon dioxide cycle, SCO₂).

Furthermore, although the Stirling cycle is usually listed among the possible alternatives, its integration hasn't been considered because of its complex design and functioning, besides its relatively immature development state, especially for the analysed power plant size [17].

The aim of this chapter is to expose the thermodynamic cycle optimization and its subsequent integration optimization; even in this case the performance results will be provided as a function of the calcium oxide activity and therefore any consideration made about choice in the chapter dedicated to the direct integration is still valid here.

The main difference from the previously analysed integration type is that, as will be described further on, it has been chosen to divide the optimization process in two parts: in the first one it's optimized only the thermodynamic cycle while in the second one it's optimized the calciner side configuration.

Anyway, the parameter to optimize is always the same: the carbonator side efficiency, calculated in the same way shown in the previous chapter.

Before to explain the optimization process, it may be useful to point out some aspects of the carbonator side functioning in case of indirect integration. Broadly speaking, the operating principle is the same already discussed in the chapter of the direct integration, but there are some fundamental differences: the first one is that both the carbonator outlet streams are now only acting as heat transfer fluids, since the power generation is left to the power block. The second one is that, as a consequence, the carbonator it's not any more pressurized and the carbon dioxide recirculated is affected by small pressure losses (here assumed equal to 10% of the carbonator operating pressure [3]); therefore the compressor size will be much smaller than in the previous case.

Anyway, also for this configuration it has been imposed an external heating requirement equal to zero, in order to avoid any use of fossil fuels.

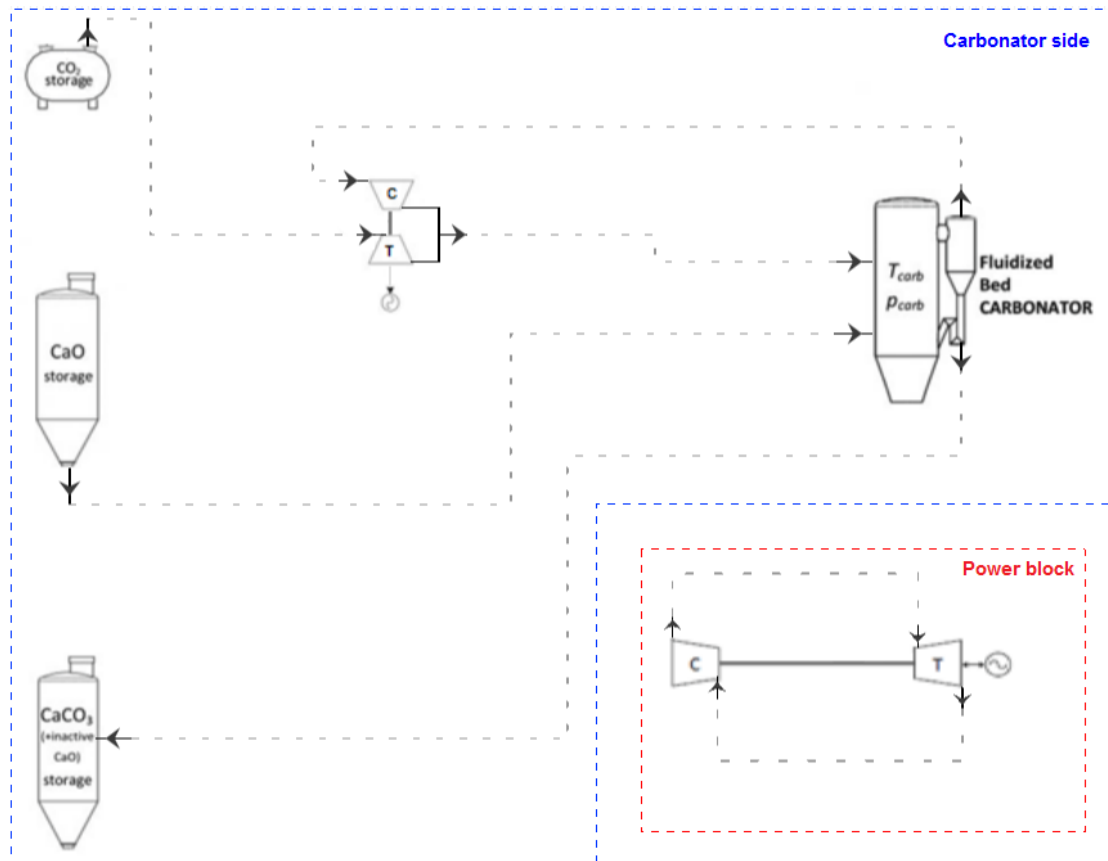


Figure 5.1 - Plant layout for the pinch analysis (the power cycle configuration is only proposed as an example)

Power cycle optimization structure (first step)

Regarding the power block, once that both the design and the power fluid are chosen, it's possible to perform a specific optimization in order to maximise the cycle efficiency in accordance to any technical constraints; all the power block components have been modelled on Aspen with the REFPROP method. The optimization strategies assumed for this step are the quadratic approximation method and the conjugate directions method, respectively in case of a single or double variable problem. In any case, the power unit size must be sufficient to provide a net electrical power output of 1 MW.

Moreover, once that the thermodynamic cycle optimization is terminated, all the data of the two streams passing through the heater/boiler and cooler/condenser are exported and provided to the last step of the optimization procedure, as explained further on.

Finally, it's necessary to make an important specification: on a theoretical point of view, the correct way to optimize the complete plant operation would be to perform a single simulation,

including both the carbonator side and the power cycle, such that the variables of the two blocks could be varied contemporary. Unfortunately, this would introduce a non-negligible complexity in the optimization algorithm and a consequent increase of the computational cost.

This is the reason why it has been decided to split the process into two simpler steps: for first it's optimized the single thermodynamic cycle and then the results obtained are inserted into the second optimization step (for the carbonator side configuration), where they are kept constant. In this way the power block and the CaL parameters have been varied separately.

CaL components modelling

Since the carbon dioxide in the carbonator side is subjected to constant pressure losses (necessary only to guarantee the recirculation), the pressure variations across both the compressor and the storage turbine are known. So their outlet temperature and the specific power depend only on the feed stream temperature and, obviously, on the components isentropic efficiencies (which have been chosen in accordance to literature proposals [15] but with an arbitrary decrease because of the smaller machinery size).

Furthermore, everything that has been said in the direct integration chapter about the carbonator simulation is also valid for this case, with the difference that the reactor will always operate at atmospheric pressure while the operating temperature can vary.

Carbonator side optimization structure (second step)

At this point, as already done for the integration previously investigated, the first distinction to do is between the constant and variable parameters, and then the dependencies between these last ones. Obviously, being all the pressures fixed, only the temperatures and mass flowrates can be varied.

Regarding the involved streams, also in this case the carbon dioxide extracted from its storage will be equal to the required stoichiometric amount but now the calcium oxide flowrate is

assumed as an independent variable (from the whom is possible to calculate any other stream).

For the optimization purposes, the others independent variables assumed are: the carbonator temperature, the CaO reactivity, the temperature of the two streams entering the reactor and finally, the inlet temperature of the compressor and turbine belonging to the carbonator side. Again, the calcium oxide activity cannot vary during a single optimization run and therefore different simulations with a different value of this parameter have been performed. For practical reasons the reactor operating temperature is defined as a discrete variable, which is not an issue if the values assumed are not too coarse; all the other parameters have been treated as continuous.

The following image should clarify the differences and relations between these elements.

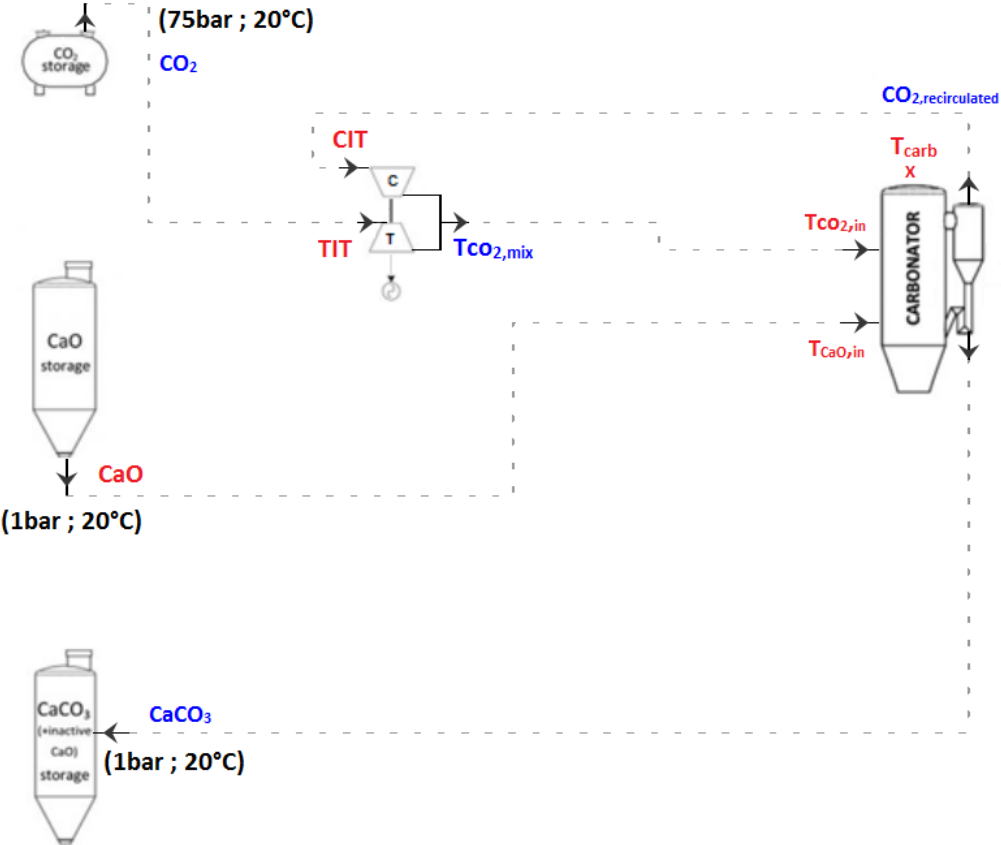


Figure 5.2 - Carbonator side layout with the fixed parameters (in black), the independent variables (in red) and the dependent variables (in blue) reported in correspondence of their actual plant location

CONSTANT PARAMETERS

Storage vessel	Pressure	Temperature
CO ₂	75 bar	20°C
CaO	1 bar	20°C
CaCO ₃	1 bar	20°C

INDEPENDENT VARIABLES

Name and acronym	Lower bound	Upper bound	TREATED AS
Carbonator temperature: T_{carb}	650°C	875°C	Discrete
CaO activity: X	0,2	0,5	Discrete
CO ₂ inlet stream temperature: $T_{CO_2,in}$	$T_{amb} + \Delta T_{pinch}$	$T_{carb} - \Delta T_{pinch}$	Continuous
CaO inlet stream temperature: $T_{CaO,in}$	310°C	$T_{carb} - \Delta T_{pinch}$	Continuous
Compressor inlet temperature: CIT	$T_{amb} + \Delta T_{pinch}$	350°C	Continuous
Turbine inlet temperature: TIT	250°C	650°C	Continuous
CaO molar flow: \dot{n}_{CaO}	-	-	Continuous

DEPENDENT VARIABLES

Mixed CO₂ flow temperature: $T_{CO_2,mix}$

CO₂ molar flow from storage: $\dot{n}_{CO_2,stoich}$

CaCO₃ molar flow: \dot{n}_{CaCO_3}

Unreacted CaO molar flow: $\dot{n}_{CaO_{unr}}$

Recirculated CO₂ molar flow: $\dot{n}_{CO_2,rec}$

Tables 5.1, 5.2, 5.3 - Three tables to sum up the different parameters and, eventually, their variation ranges

So, once that the chemical reactor has been separately simulated and the thermodynamic cycle performance has been maximized, it's possible to perform the second step of the complete process: the optimization of the carbonator side functioning with the power block integration. This part of the procedure is based on two nested optimization techniques: the genetic algorithm method and the bisection method, and both are applied in the field of the pinch analysis.

For first, a value of the CaO reactivity must be fixed and kept constant for all of the remaining steps; if it's requested an evaluation with a different activity value it's necessary to execute by the beginning another simulation. Then, the genetic algorithm creates a population whose

elements are a set of values for five independent variables: the carbonator temperature, the CO₂ inlet temperature, the CaO inlet temperature, the compressor inlet temperature and the turbine inlet temperature. These parameters are the inputs of the objective function, which has the aim of determine, through the pinch analysis and the bisection method, the minimum calcium oxide flow compatible with the given set of temperatures or, in other words, the smaller flowrate that guarantees an external heating requirement equal to zero, in order to obtain a plant whose heating need is completely satisfied by the exothermic carbonation reaction. So, once that are defined two extremes between the whom it's surely located the point of optimum, the CaO stream is iteratively varied according to the pinch analysis results (i.e. the heating needed) with the bisection method, until it converges.

Here are reported the equations and pathways that allows to determine all the parameters necessary to perform the pinch analysis at the base of the objective function (MM stands for molar mass):

$$\left. \begin{array}{l} \text{TOT} \\ \text{COT} \\ \text{Turbine specific power} \\ \text{Compressor specific power} \\ \text{CO}_2 \text{ excess index} \end{array} \right\} \text{obtained from Aspen simulations}$$

$$\dot{m}_{\text{CO}_2, \text{carb}, \text{in}} = \text{excess index} \cdot X \cdot \frac{MM_{\text{CO}_2}}{MM_{\text{CaO}}} \cdot \dot{m}_{\text{CaO}, \text{carb}, \text{in}}$$

$$\dot{m}_{\text{CO}_2, \text{stoich}} = X \cdot \frac{MM_{\text{CO}_2}}{MM_{\text{CaO}}} \cdot \dot{m}_{\text{CaO}, \text{carb}, \text{in}}$$

$$\dot{m}_{\text{CO}_2, \text{recirc}} = \dot{m}_{\text{CO}_2, \text{carb}, \text{in}} - \dot{m}_{\text{CO}_2, \text{stoich}}$$

$$\dot{m}_{\text{CaO}, \text{unreac}} = (1 - X) \cdot \dot{m}_{\text{CaO}, \text{carb}, \text{in}}$$

$$\dot{m}_{\text{CaCO}_3} = X \cdot \frac{MM_{\text{CaCO}_3}}{MM_{\text{CaO}}} \cdot \dot{m}_{\text{CaO}, \text{carb}, \text{in}}$$

$$\begin{aligned} T_{\text{CO}_2, \text{mix}} &= \frac{\dot{m}_{\text{CO}_2, \text{recirc}} \cdot \overline{c_{p, \text{recirc}}} \cdot \text{COT} + \dot{m}_{\text{CO}_2, \text{stoich}} \cdot \overline{c_{p, \text{stoich}}} \cdot \text{TOT}}{\dot{m}_{\text{CO}_2, \text{recirc}} \cdot \overline{c_{p, \text{recirc}}} + \dot{m}_{\text{CO}_2, \text{stoich}} \cdot \overline{c_{p, \text{stoich}}}} \\ &\cong \frac{\dot{m}_{\text{CO}_2, \text{recirc}} \cdot \text{COT} + \dot{m}_{\text{CO}_2, \text{stoich}} \cdot \text{TOT}}{\dot{m}_{\text{CO}_2, \text{carb}, \text{in}}} \leftrightarrow \text{Hypothesis: } \overline{c_{p, \text{recirc}}} \cong \overline{c_{p, \text{stoich}}} \end{aligned}$$

$$c_{p(CaO_{unreact}+CaCO_3)} = \frac{(1 - X) \cdot MM_{CaO} \cdot c_{p,CaO} + X \cdot MM_{CaCO_3} \cdot c_{p,CaCO_3}}{(1 - X) \cdot MM_{CaO} + X \cdot MM_{CaCO_3}}$$

Now that both the independent and dependent variables have been determined, it's possible to provide the hot and cold fluids data to the pinch analysis algorithm, which calculates the heating and cooling requirements and, according to these results, the bisection method modifies its extremes and establish a new attempt value for the calcium oxide flowrate.

This process ends when it's satisfied the tolerance imposed and therefore the objective function gives the value of the parameter to maximize, that is the total net electrical power produced per unit of CaO mass flow.

In other words, the aim of the entire optimization process is to obtain the higher as possible amount of electricity with the lower as possible reactants consumption. The simulation ends when the genetic algorithm converges to a set of temperatures that maximize this ratio.

COLD FLUIDS

Flowrate	Inlet temperature	Outlet temperature
$\dot{m}_{CO_2,stoich}$	20°C	TIT
$\dot{m}_{CO_2,carb,in}$	$T_{CO_2,mix}$	$T_{CO_2,in}$
$\dot{m}_{CaO,carb,in}$	20°C	$T_{CaO,in}$
$\dot{m}_{power,fluid,heat}$	$T_{in,heater}$	$T_{out,heater}$

HOT FLUIDS

Flowrate	Inlet temperature	Outlet temperature
$\dot{m}_{CO_2,recirc}$	T_{carb}	CIT
$\dot{m}_{CaCO_3} + \dot{m}_{CaO,unreact}$	T_{carb}	20°C
$\dot{m}_{power,fluid,cool}$	$T_{in,cooler}$	$T_{out,cooler}$

Tables 5.4, 5.5 - Hot and cold fluids for the pinch analysis with their respective temperature ranges; notice that in some cases the CO₂ entering the carbonator may be colder than the mixed CO₂, moving the stream between the hot fluids

Finally, the streams specific heat capacity has been provided to the pinch analysis algorithm in different ways, according to the particular case. For the calcium oxide, the calcium carbonate and the carbon dioxide (at 1bar) have been used three mathematical correlations [3], whose temperature range of validity is compatible with the values assumed during the

simulation. For all the other fluids have been provided a dataset obtained from Aspen, and the specific heat capacity was calculated performing a linear interpolation.

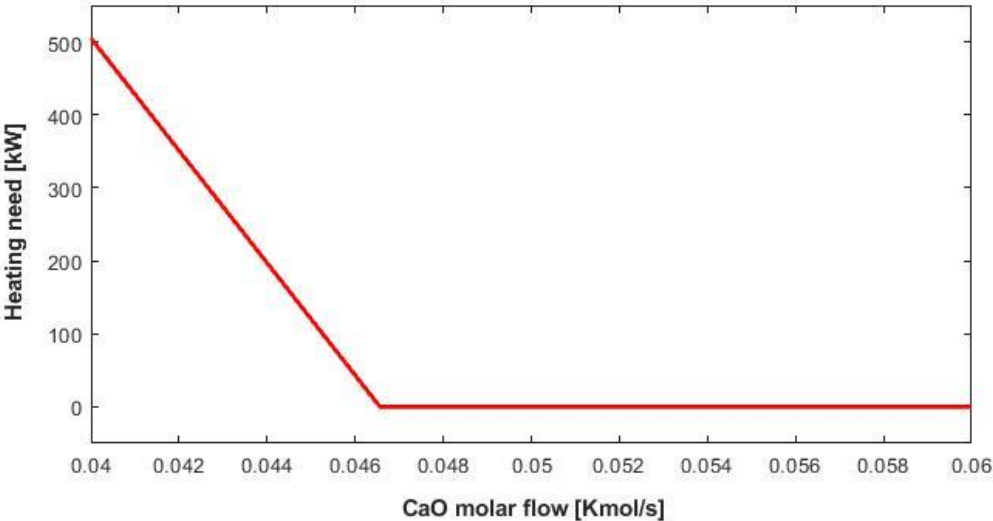


Figure 5.3 - Example of the heating need dependence on the CaO stream

The optimization has the aim to find the point where the curve changes slope, because it's the lower value of CaO flowrate with a null heating need. On equal terms for the other independent variables, a lower amount of the calcium oxide stream brings to a lower thermal power released by the exothermic reaction, which can become insufficient to heat all the cold streams and therefore will determine an heating requirement different from zero.

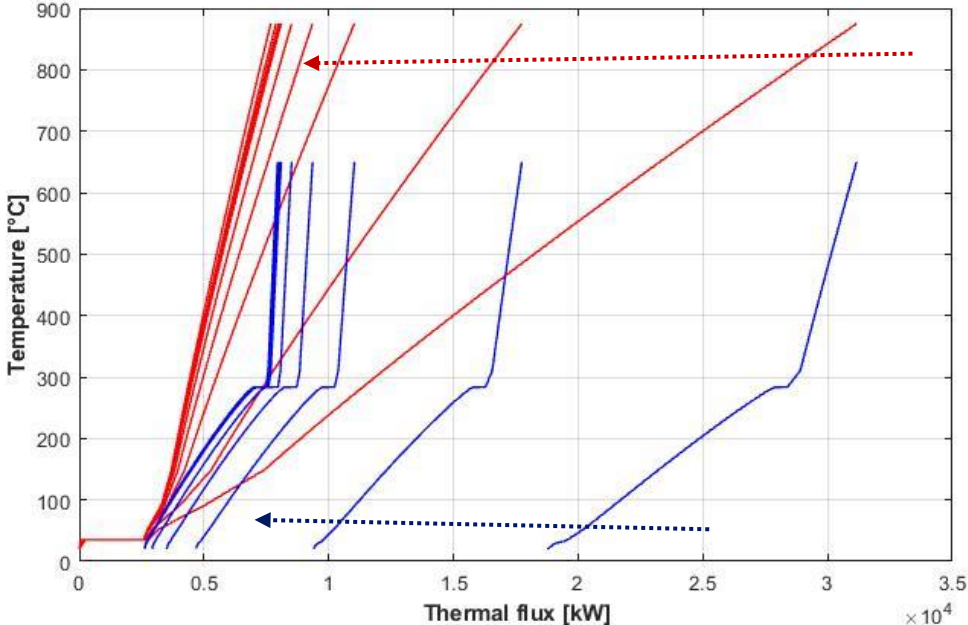


Figure 5.4 - The same concept can be seen with the hot and cold cumulative curves variation during the iterations of the bisection method (again, this graph is just an example)

Three last things to point out: the first one is the fact that the power fluid crossing the cooler or condenser is considered between the hot fluids in the pinch analysis and therefore it may be used as a heat source at relatively low temperature (anyway, it depends case by case).

The second one is the fact that, regarding the cooling need, the atmosphere is assumed as heat sink (dry-cooling), according to the common lack of water in most of the CSP plant locations.

The last thing is that, as already mentioned, it's not strictly necessary to cool down the solid products of the carbonation reaction up to 20°C and therefore, if it's not any more possible to recover heat from this hot stream, it can be sent directly to the storage, avoiding a dry-cooling step and the consequent auxiliaries' electrical consumption.

OTHER ASSUMPTIONS		REFERENCE
$\eta_{is,turbine}$	0,75	[15]*
$\eta_{is,compressor}$	0,65	
η_{el}	0,97	[15]
P_{carb}	1 bar	[1]
ΔP_{comp}	10% P_{carb}	[3]
Conveying consumptions	10 MJ/(ton*100m)	[16]
Storages-carbonator distance	100 m	
Auxiliaries consumptions	0,8% rejected heat	[15]
$\Delta T_{min,pinch}$	15°C	
$T_{ambient}$	20°C	[16]

Table 5.6 - Assumptions for the carbonator side components
(*adapted to the analysed size)

Finally, in order to have an easier comprehension of the complete optimization algorithm, it has been represented graphically with an essential flowchart.

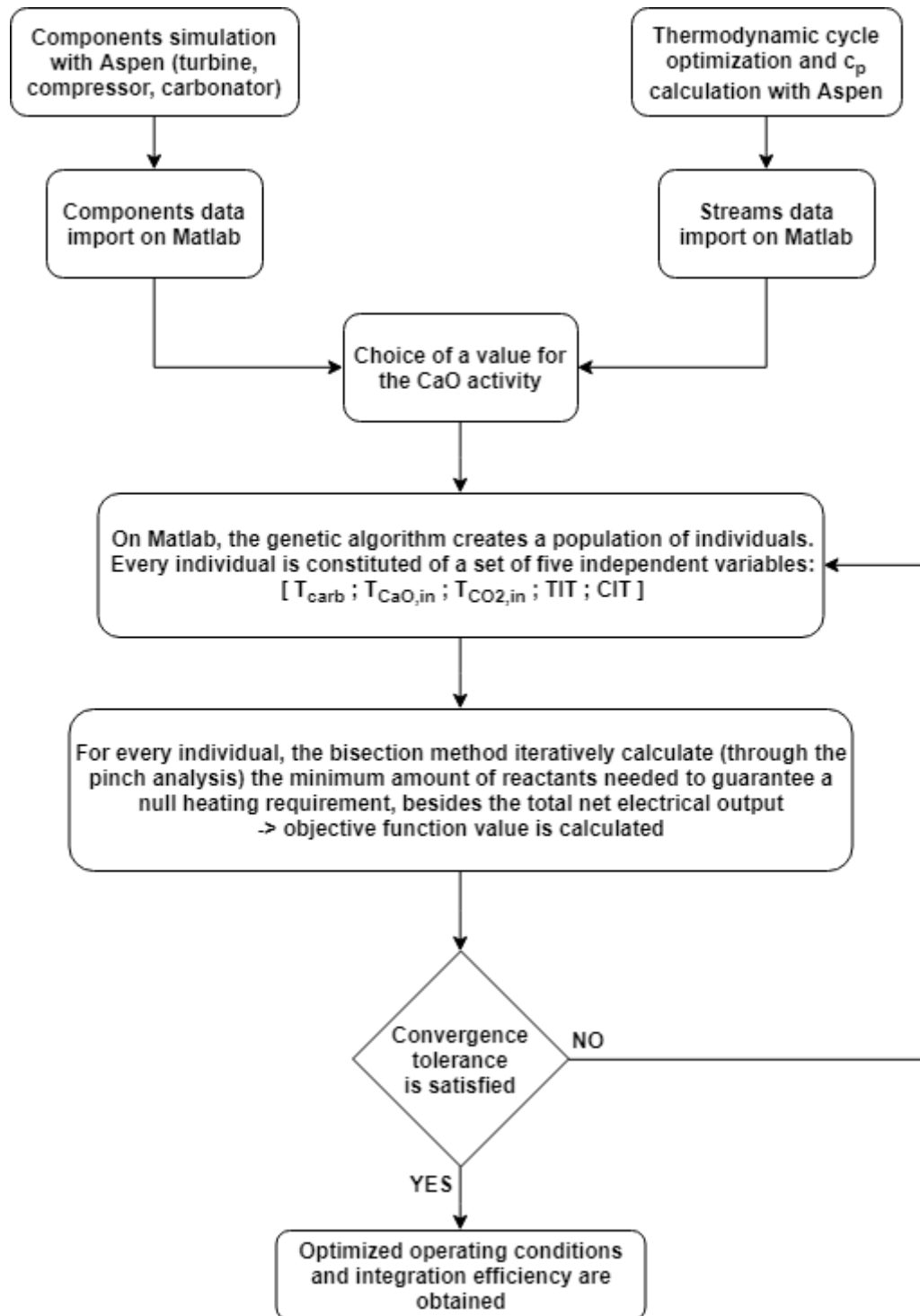


Figure 5.5 - Simple flow chart to sum up the optimization structure for the indirect integration

ORC indirect integration

The organic Rankine cycles are, at the state of the art, one of the best choices in the field of relatively small size power generation with low temperature sources. Therefore, considering the high temperatures reached in the carbonator, the CaL technology represents a quite different case with respect to the common context in which the ORCs operate.

However, it could be interesting to analyse their integration because of the good thermal properties of these fluids and the consistent performance advantages at reduced power loads given by the machineries.

Furthermore, despite most of the constructed power plants operate at subcritical conditions, it has been considered as interesting to perform the integration of supercritical cycles, in order to evaluate the possible benefits for the absence of the evaporation step and its consequent heat exchange at constant temperature, in addition to the higher exploitable pressure drops.

For all the different ORC fluids investigated and for both the subcritical and supercritical operating conditions have been assumed one single power block layout, which is actually the simplest as possible: one turbine and one condenser divided by one heating and one cooling stage. This essential design has been chosen according to the common trend (at least in the ORC field) in searching to avoid any not indispensable complication; therefore, any kind of bleeding or reheating has been omitted.



Figure 5.6 - Thermodynamic cycle layout

Moreover, the regeneration between the turbine and compressor outlets has not been considered, since its possible convenience will be determined by the second step of the optimization process, based on the pinch analysis.

Regarding the simulation assumptions, the turbine data has been arbitrary decreased starting from the nominal condition for the Siemens SST-060 (compatible with ORC), which produce up to 6 MW of electric power, while the turbomachinery's isentropic efficiencies have been taken from literature.

DATA

Parameter		Reference	Parameter		Reference
$P_{1,min}$	1,1bar / 0,1bar	[18], [19]	$\eta_{is,turb}$	0,85	[20]
$P_{3,max}$	110 bar	[19]	$\eta_{is,pump}$	0,75	
$T_{3,max}$	510°C		$\Delta P_{cooling}$	$2\% \cdot P_4$	[21]
η_{el}	0,97	[21]	$\Delta P_{heating}$	$2\% \cdot P_2$	

CONSTRAINTS

Parameter		Parameter		Reference
$T_{1,min}$	$T_{amb} + \Delta T_{pinch} = 35^\circ C$	Minimum vapor fraction during expansion	0,85	[22]
$P_{el,net}$	1 MW			
$\dot{Q}_{heat,need}$	0 MW			

Tables 5.7, 5.8 - Assumptions and constraints relative to the ORC cycles

As is possible to see from the last tables, all the simulations have been performed assuming two different values for the condensing pressure. In fact, since most of the ORC fluids are compounds quite unstable and inflammable, it wouldn't be a bad decision, especially in terms of safety, to avoid pressures lower than the atmospheric value at the condenser, in order to avoid air infiltration [18] and, therefore, obtaining a simpler layout (deaerator is not necessary). However, it's very common to find cases in literature where the condenser works under vacuum conditions, obviously allowing to reach higher thermodynamic efficiencies. So, trying to make an assessment as complete as possible, both the configurations have been considered.

Anyway, the physical lower bound in case of sub-atmospheric condensing pressure is actually double, since it's not possible to have less than 0,1 bar (machinery limit) and contemporary temperatures lower than 35°C are not attainable (thermal exchange limit).

Another thing to point out is the criteria used to choose the suitable ORC fluids, because, to make a reasonable selection, there are many important requirements to satisfy. For first, in order to obtain a plant whose functioning is as sustainable as possible, it has been tried to avoid compounds able to deplete the ozone layer or giving relevant contributions in terms of global warming. Furthermore, regarding the subcritical layout, have been investigated fluids

with relatively high critical pressure, such that the turbine can operate with suitable pressure drops and the thermodynamic cycle manage to reach higher efficiencies.

ORC fluid	Saturation curve type	P_{crit} [bar]	T_{crit} [°C]	T_{max} [°C]
Benzene	Isentropic	48,94	289	452
Cyclohexane	Dry	40,824	280,5	427
Cyclopentane	Isentropic	45,712	238,6	277
Ethanol	Wet	62,68	242	377
Toluene	Dry	41,26	318,6	427

Table 5.9 - ORC fluids physical properties from COOLPROP library

Now, in case of subcritical cycle, the different type of saturation curve is a very important characteristic, because, in case of dry or isentropic ORC fluid the turbine inlet will be set in saturated conditions, because a superheated feed stream would determine an efficiency decrease and, thanks to the curve shape, the vapor expansion won't end in saturated conditions.

Anyway, it's important to notice the fact that even with a dry fluid (and therefore with turbine outlet conditions in the region of superheated vapor) it's possible to have a temporary formation of condensate during the expansion in turbine, at least if the inlet pressure is near to the critical pressure. So, this is because has been set a minimum limit for the vapor fraction achievable during the entire expansion and not only at the turbine outlet.

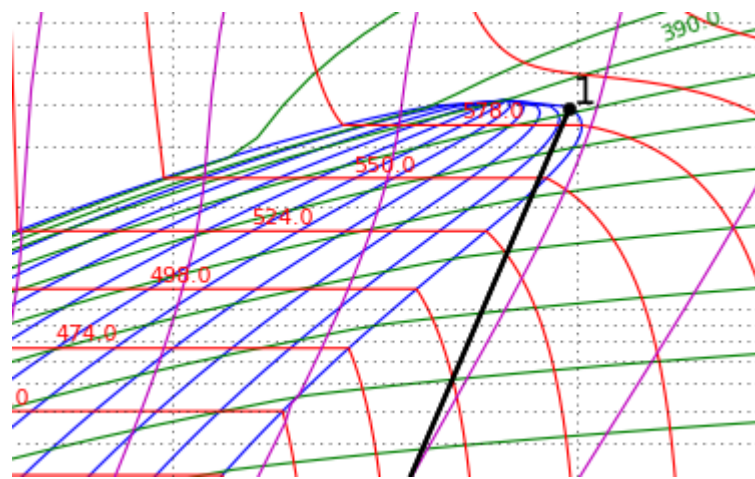


Figure 5.7 - Detail of saturated toluene expansion (in black) represented in a P-h diagram

Finally, the maximum sustainable temperature is another important parameter, since it guarantees the compound chemical stability; it constitutes a simulation limit in case of superheated turbine inlet or supercritical cycle and, to be precautionary, the maximum temperatures used in the simulations have been always set to at least 5°C lower than this value.

Subcritical cycles

In the following pages will be analysed organic Rankine power cycles whose functioning remains in the subcritical state. As previously mentioned, it will be done one main distinction: in one case is assumed a condensation above the ambient pressure and in another case the condenser operates under vacuum conditions.

Counter-pressure cycle

For all the different cycles is set a constant condensation pressure, equal to 1,1 bar. Therefore, regarding the isentropic and dry ORC fluids, the optimization is performed on a single variable: the evaporation pressure. In fact, for these cases, the turbine inlet is assumed at saturated conditions.

Anyway, being the ethanol a wet fluid, its optimization is performed on both the evaporation pressure and the superheating temperature at the turbine inlet.

Thermodynamic cycles optimization (first step):

From the sensitivity analysis on the side it's possible to observe that higher pressures always determine a performance improvement, except for the case of the benzene, which presents a non-monotonic trend. Furthermore, the toluene, cyclopentane and benzene pressures must be limited to avoid excessively low value of vapor fraction at the beginning of the expansion.

It's not very different the case with the double-variable optimization (bottom graph): the ethanol cycle reaches its best operating conditions with high evaporation pressures and superheating temperature as close as possible to its maximum sustainable value.

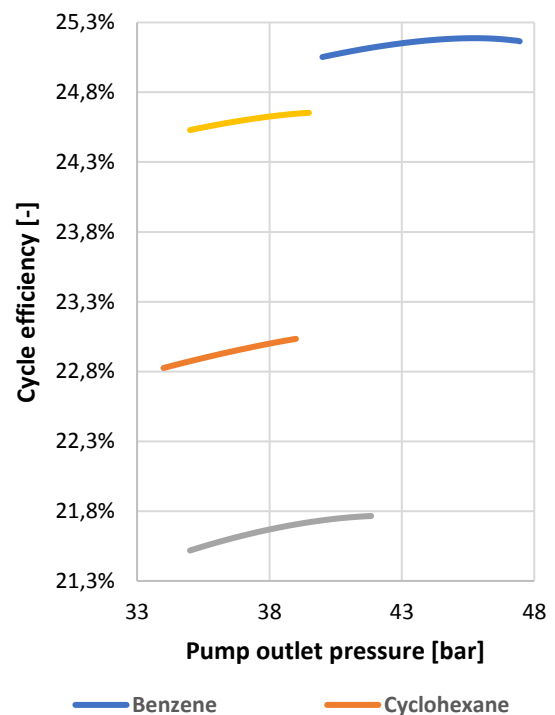


Figure 5.8 - ORC simulation of cycles with wet/isentropic fluids

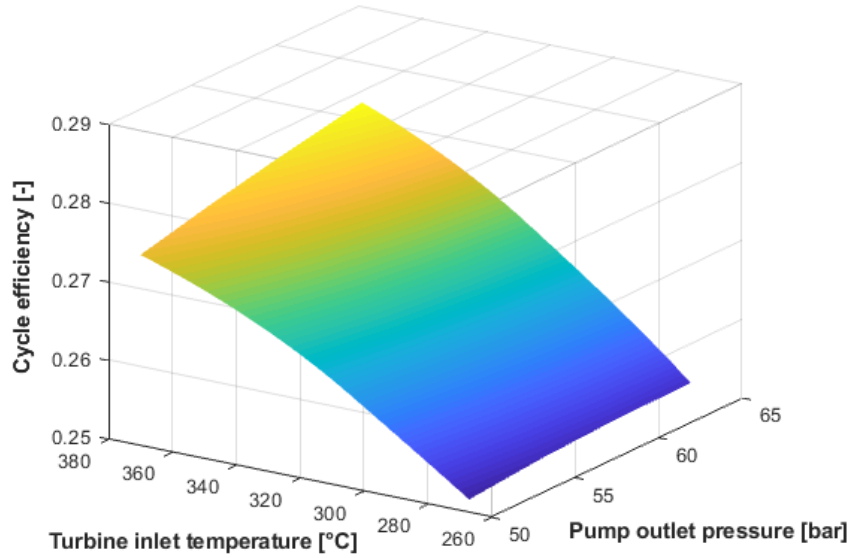


Figure 5.9 - Ethanol cycle sensitivity analysis

In the following table are reported the thermophysical parameters for the different states assumed in the cycle.

	BENZENE		CYCLOHEXANE		CYCLOPENTANE		ETHANOL		TOLUENE	
	P [bar]	T [°C]								
1	1,1	82,8	1,1	83,5	1,1	51,8	1,1	80,5	1,1	113,5
2	46,75	85,2	39,8	85,6	41,84	54,1	62,24	82,8	37,72	115,5
3	45,82	283,4	39	276,9	41	230,6	61	370	36,96	309,7
4	1,12	133,1	1,12	168,6	1,12	93,8	1,12	203,2	1,12	189,3
\dot{m}_{ORC}	8,785 [kg/s]		9,200 [kg/s]		9,056 [kg/s]		3,368 [kg/s]		9,918 [kg/s]	
η_{cycle}	19,63%		17,58%		19,64%		21,49%		17,11%	
$\dot{W}_{s,turb}$	1097 [kW]		1097 [kW]		1100 [kW]		1068 [kW]		1093 [kW]	
$\dot{W}_{s,pump}$	65,9 [kW]		66,2 [kW]		69,0 [kW]		37,4 [kW]		62,4 [kW]	

Table 5.10 - Thermodynamic cycles optimization results

Indirect integration optimization (second step):

These results are then provided as part of the input for the following step. The successive diagram shows the value of the objective function (the ratio of net power output and CaO extracted from storage) assumed for the optimized plant configurations, including both the power block and the carbonator side.

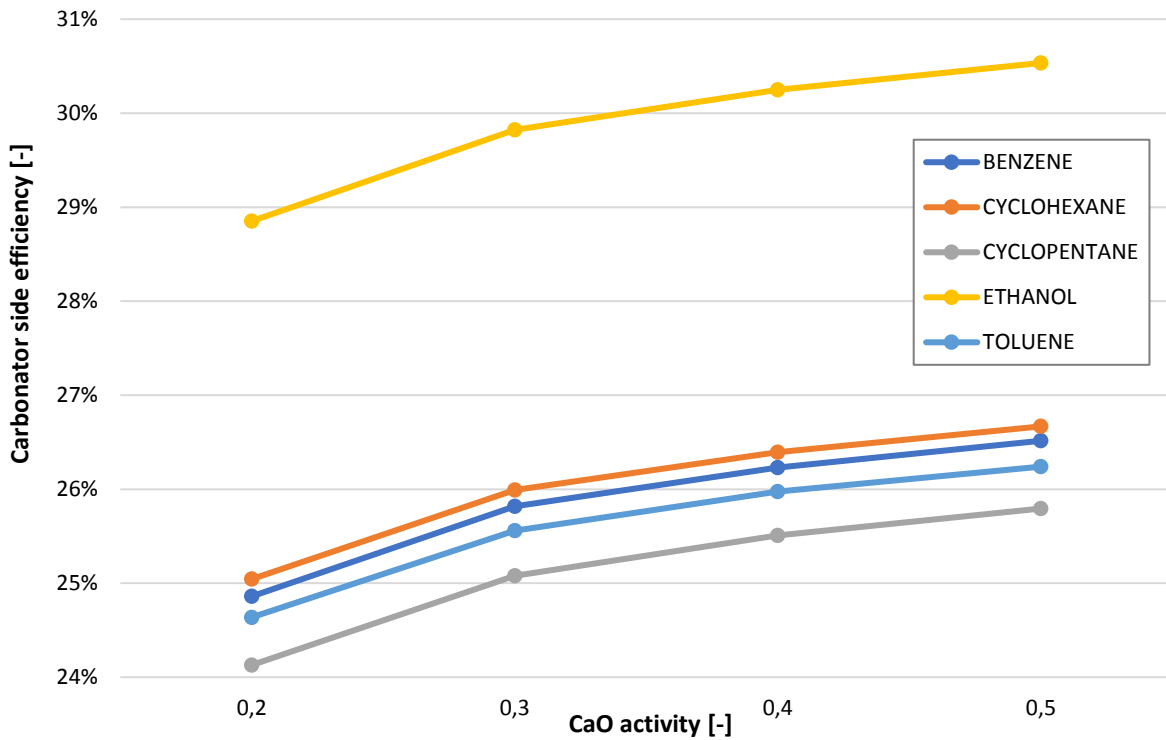


Figure 5.10 - Performance of the optimized ORC integrated in the CaL plant

As it's easy to notice, the best alternative is constituted by the ethanol, thanks to the high pressures and temperatures achieved in the thermodynamic cycle.

Finally, the complete results (independent variables, dependent variables and other parameters) are summed up in the next tables. Any comment regarding these outcomes is left to the paragraph at the end of this chapter and the same is done for all the others ORC configurations analysed, in order to make any comparison easier.

	X [-]	Storage turbine power [kW _s]	Compressor power [kW _s]	Conveying power [kW _e]	Rejection power [kW _e]	Total auxiliaries consumption [kW _e]	Total plant net power [kW _e]
BENZENE	0,2	519	0,26	178	24,4	202	1301
	0,3	515	12,53	122	25,5	147	1340
	0,4	514	21,72	94	26,0	120	1357
	0,5	511	27,81	77	26,8	104	1364
CYCLOHEXANE	0,2	514	0,2	176	23,8	200	1299
	0,3	511	12,29	121	24,7	145	1338
	0,4	509	21,68	94	24,6	118	1355
	0,5	506	29,65	77	25,0	102	1360
CYCLOPENTANE	0,2	538	0,16	184	27,9	212	1310
	0,3	535	10,93	127	27,9	154	1354
	0,4	534	19,63	98	28,0	126	1373
	0,5	531	25,11	81	27,9	109	1382
ETHANOL	0,2	429	0,68	147	19,9	167	1249
	0,3	426	10,14	101	20,7	121	1282
	0,4	424	19,2	78	21,0	99	1294
	0,5	422	25,39	64	21,5	86	1299
TOLUENE	0,2	526	0,3	180	23,7	204	1306
	0,3	521	14,49	123	25,2	148	1343
	0,4	519	25,87	95	26,4	122	1357
	0,5	516	33	78	26,2	105	1364

Table 5.11 - Shaft and electrical powers obtained from the indirect integration optimization process of subcritical ORCs with counterpressure condensation

	INDEPENDENT VARIABLES						DEPENDENT VARIABLES				FLOWRATES					
	X [-]	T _{carb} [°C]	T _{CaO,in} [°C]	T _{CO₂,in} [°C]	TIT [°C]	CIT [°C]	COT [°C]	TOT [°C]	T _{CO₂,mix} [°C]	Excess index [-]	\dot{m}_{CaO} [kg/s]	$\dot{m}_{CO_2,stoic}$ [kg/s]	$\dot{m}_{CO_2,rec}$ [kg/s]	$\dot{m}_{CaO,unr}$ [kg/s]	\dot{m}_{CaCO_3} [kg/s]	η_{carb} [%]
BENZENE	0,2	875	368	178	650	163	177	294	292	1,015	8,23	1,29	0,019	6,59	2,94	24,86
	0,3	875	311	101	650	106	118	294	214	1,834	5,44	1,28	1,071	3,81	2,92	25,82
	0,4	875	312	102	650	100	113	294	186	2,470	4,07	1,28	1,883	2,44	2,91	26,23
	0,5	875	311	106	650	104	116	294	178	2,877	3,24	1,27	2,389	1,62	2,89	26,52
CYCLOHEXANE	0,2	875	368	179	650	128	141	294	292	1,012	8,16	1,28	0,016	6,53	2,91	25,04
	0,3	875	310	101	650	103	116	294	213	1,831	5,40	1,27	1,057	3,78	2,89	25,99
	0,4	875	311	105	650	102	115	294	187	2,473	4,04	1,27	1,871	2,42	2,89	26,40
	0,5	875	323	112	650	122	135	294	189	2,928	3,21	1,26	2,431	1,60	2,86	26,67
CYCLOPENTANE	0,2	875	368	177	650	118	131	294	292	1,010	8,54	1,34	0,013	6,83	3,05	24,13
	0,3	875	311	70	650	69	81	294	201	1,775	5,66	1,33	1,034	3,96	3,03	25,08
	0,4	875	312	69	650	71	82	294	171	2,389	4,23	1,33	1,850	2,54	3,03	25,51
	0,5	875	313	72	650	71	83	294	159	2,783	3,37	1,32	2,360	1,69	3,01	25,79
ETHANOL	0,2	875	368	206	650	156	170	294	288	1,048	6,81	1,07	0,051	5,45	2,43	28,85
	0,3	875	310	98	650	101	113	293	212	1,826	4,51	1,06	0,877	3,15	2,41	29,82
	0,4	875	310	99	649	130	143	293	204	2,458	3,37	1,06	1,544	2,02	2,41	30,25
	0,5	875	318	100	650	143	156	294	204	2,879	2,68	1,05	1,976	1,34	2,39	30,53
TOLUENE	0,2	875	368	179	650	132	145	294	291	1,018	8,34	1,31	0,024	6,67	2,98	24,64
	0,3	875	311	131	650	131	144	294	223	1,894	5,51	1,30	1,162	3,86	2,95	25,56
	0,4	875	310	133	650	144	158	294	211	2,549	4,12	1,29	2,006	2,47	2,94	25,98
	0,5	875	310	156	650	134	147	294	195	3,042	3,28	1,28	2,627	1,64	2,92	26,24

Table 5.12 - Temperatures, pressures and flowrates obtained from the indirect integration optimization process of subcritical ORCs with counterpressure condensation

Condensation cycle

The following investigated cycles operate with sub-atmospheric condensation pressures, so their efficiencies will be surely higher than the previous cases. Anyway, it will be assessed if this benefit is still visible when the power blocks are integrated in the carbonator side, which is not easy to say without performing a simulation.

The thermodynamic cycles optimization strategy is actually equal to the one adopted for the subcritical counter-pressure case, therefore it won't be repeated.

Finally, it is worth to remember that the condensing limit may be given by either the pressure (0,1 bar) or the temperature (35°C), as already justified.

Thermodynamic cycles optimization (first step):

Also concerning the cycles sensitivity analysis, the results obtained are practically identical to the previous ones, making actually unnecessary to show them. Therefore will be directly showed the optimized cycles operating conditions.

	BENZENE		CYCLOHEXANE		CYCLOPENTANE		ETHANOL		TOLUENE	
	P [bar]	T [°C]								
1	0,198	35	0,201	35	0,619	35	0,138	35	0,1	45,25
2	46,71	37,2	39	36,9	41,84	37,3	62,2	37,1	37,72	47
3	45,78	283,3	38,22	275,3	41,00	230,6	61	370	36,96	309,7
4	0,202	91,4	0,205	138	0,631	79,9	0,140	134,4	0,102	141
\dot{m}_{ORC}	5,944 [kg/s]		6,034 [kg/s]		7,732 [kg/s]		2,372 [kg/s]		5,653 [kg/s]	
η_{cycle}	25,18%		23,03%		21,77%		27,99%		24,62%	
$\dot{W}_{s,turb}$	1074 [kW]		1072 [kW]		1089 [kW]		1056 [kW]		1065 [kW]	
$\dot{W}_{s,pump}$	42,7 [kW]		40,8 [kW]		58,2 [kW]		25,3 [kW]		33,6 [kW]	
Gain %	28,27%		31,00%		10,85%		30,25%		43,89%	

Table 5.13 - Thermodynamic cycles optimization results

The only fluid that reaches a pressure of 0,1 bar at the condenser is the toluene, all the others have a higher saturation pressure in correspondence of the thermal exchange limit, especially the cyclopentane.

As expected, in every case it's observed a performance improvement, which is very similar for the benzene, cyclohexane and ethanol, while is quite poor for the cyclopentane. The toluene

is the fluid that takes the greatest advantage from the sub-atmospheric condensation, reaching a relative improvement higher than the 40%, but anyway, the ethanol still reaches the highest efficiency.

Indirect integration optimization (second step):

As for the previous case, the resulting efficiencies are exposed in a graph.

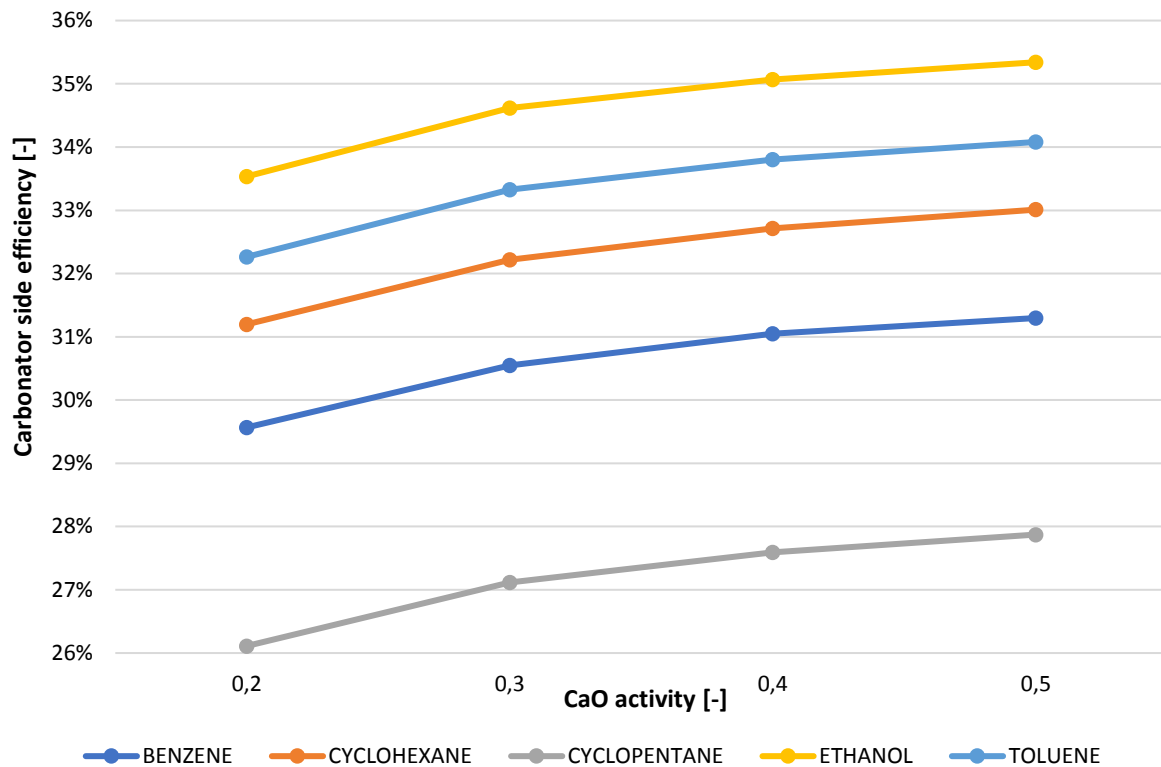


Figure 5.11 - Performance of the optimized ORC integrated in the CaL plant

With the following diagram it's easy to notice that the indirect integration performances show a close correlation with the thermodynamic cycles results; in fact, the final relative improvement follows the order already observed for the only thermodynamic cycles, except for the benzene and ethanol, which are inverted.

Furthermore, these last results confirm the fact that the toluene takes a consistent benefit from a condensation under vacuum conditions, while is interesting to observe the fact that, although its lower cycle efficiency, the cyclohexane reaches higher performances with respect to the benzene when the power block is integrated in the carbonator side.

Finally it's observed that the relative improvement is slightly higher for lower values of the calcium oxide activity, although this doesn't change the fact that the carbonator side efficiency has an opposite trend.

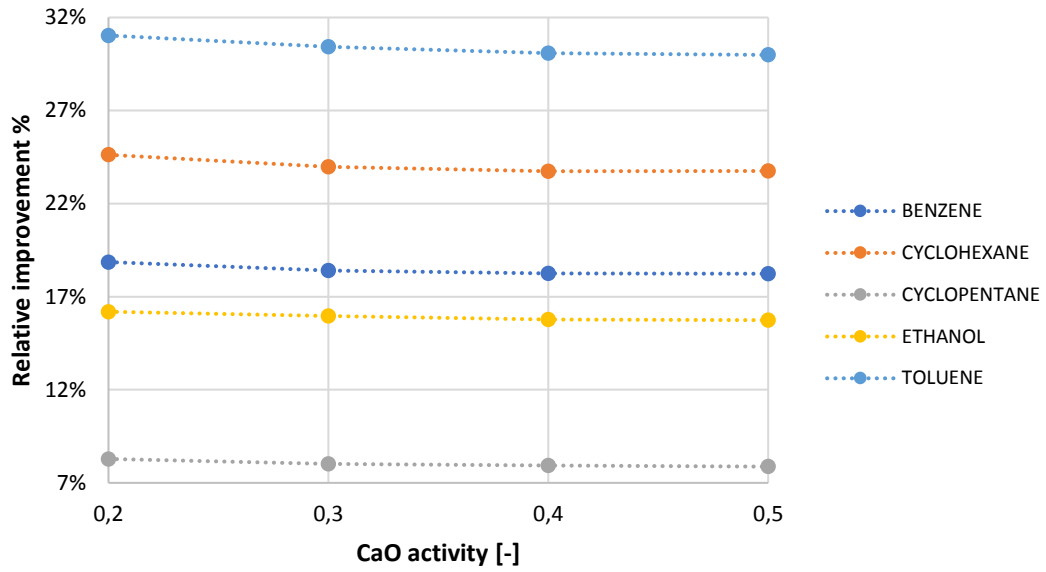


Figure 5.12 - ORC relative improvement for the passage from a counter-pressure cycle to a condensation cycle

Of course it must be considered that these improvements are affected by an increased functioning complexity and therefore their feasibility must be carefully evaluated, especially regarding the fluid stability in presence of air infiltrations and its necessary removal. The other outcomes of the optimization process are reported in the two tables below.

	X [-]	Storage turbine power [kW _s]	Compressor power [kW _s]	Conveying power [kW _e]	Rejection power [kW _e]	Total auxiliaries consumption [kW _e]	Total plant net power [kW _e]
BENZENE	0,2	416	0,23	142	20,2	163	1241
	0,3	414	8,57	98	21,0	119	1274
	0,4	413	14,53	76	20,7	97	1290
	0,5	411	17,71	62	21,0	83	1298
CYCLOHEXANE	0,2	389	0,17	133	19,2	152	1225
	0,3	387	8,83	91	18,9	110	1256
	0,4	386	13,89	71	19,3	90	1271
	0,5	384	17,77	58	18,9	77	1278
CYCLOPENTANE	0,2	486	0,26	166	24,8	191	1280
	0,3	483	9,99	114	25,4	139	1319
	0,4	482	16,37	89	25,4	114	1338
	0,5	480	20,91	73	25,0	98	1347
ETHANOL	0,2	357	0,22	122	16,9	139	1207
	0,3	353	9,56	84	16,9	100	1233
	0,4	354	12,97	65	17,7	83	1248
	0,5	352	16,53	53	16,9	70	1255
TOLUENE	0,2	378	1,3	129	6,8	136	1229
	0,3	375	8,86	89	6,5	95	1260
	0,4	375	13,95	69	6,5	75	1275
	0,5	373	18,44	57	7,1	64	1280

Table 5.14 - Shaft and electrical powers obtained from the indirect integration optimization process of subcritical ORCs with vacuum condensation

	INDEPENDENT VARIABLES						DEPENDENT VARIABLES				FLOWRATES					
	X [-]	T _{carb} [°C]	T _{CaO,in} [°C]	T _{CO₂,in} [°C]	TIT [°C]	CIT [°C]	COT [°C]	TOT [°C]	T _{co₂,mix} [°C]	Excess index [-]	\dot{m}_{CaO} [kg/s]	$\dot{m}_{CO_2,stoic}$ [kg/s]	$\dot{m}_{CO_2,rec}$ [kg/s]	$\dot{m}_{CaO,unr}$ [kg/s]	\dot{m}_{CaCO_3} [kg/s]	η_{carb} [%]
BENZENE	0,2	875	339	343	650	144	157	294	291	1,017	6,60	1,04	0,018	5,28	2,36	29,57
	0,3	875	310	51	650	90	102	294	212	1,742	4,37	1,03	0,765	3,06	2,34	30,55
	0,4	875	311	51	650	66	78	294	170	2,346	3,28	1,03	1,386	1,97	2,34	31,05
	0,5	875	310	52	650	52	63	294	148	2,722	2,61	1,03	1,764	1,30	2,33	31,30
CYCLOHEXANE	0,2	875	368	179	650	168	182	294	292	1,012	6,18	0,97	0,012	4,94	2,21	31,20
	0,3	875	313	51	650	121	134	294	225	1,753	4,09	0,96	0,726	2,86	2,19	32,22
	0,4	875	315	49	650	72	84	294	173	2,353	3,06	0,96	1,303	1,84	2,19	32,71
	0,5	875	312	51	650	75	87	294	163	2,725	2,44	0,96	1,651	1,22	2,18	33,01
CYCLOPENTANE	0,2	875	339	343	650	135	148	294	291	1,017	7,71	1,21	0,021	6,17	2,75	26,11
	0,3	875	312	49	650	88	100	294	211	1,745	5,10	1,20	0,896	3,57	2,73	27,11
	0,4	875	312	51	650	54	66	294	163	2,346	3,82	1,20	1,619	2,30	2,73	27,59
	0,5	875	312	54	650	54	66	294	149	2,732	3,04	1,20	2,070	1,52	2,72	27,87
ETHANOL	0,2	875	368	184	650	138	151	294	291	1,019	5,66	0,89	0,017	4,53	2,02	33,54
	0,3	875	313	53	650	190	204	294	255	1,758	3,74	0,88	0,668	2,62	2,00	34,62
	0,4	875	315	47	650	80	92	294	178	2,348	2,81	0,88	1,189	1,69	2,00	35,07
	0,5	875	313	52	650	80	92	294	166	2,728	2,23	0,88	1,515	1,11	1,99	35,34
TOLUENE	0,2	875	399	69	650	172	186	294	284	1,100	5,99	0,94	0,095	4,79	2,14	32,26
	0,3	875	311	63	650	129	142	294	228	1,764	3,96	0,93	0,714	2,78	2,12	33,33
	0,4	875	310	62	650	80	92	294	177	2,368	2,97	0,93	1,279	1,79	2,12	33,80
	0,5	875	310	75	650	87	99	294	169	2,785	2,36	0,93	1,658	1,18	2,11	34,08

Table 5.15 - Pressures, temperatures and flowrates obtained from the indirect integration optimization process of subcritical ORCs with vacuum condensation

Supercritical cycles

Another investigated ORC configuration is constituted by the supercritical plants. These cycles have some consistent advantages that makes interesting to perform an evaluation to demonstrate their possible benefits when integrated with the carbonator side.

The layout assumed is equal to the subcritical cases (one pump, one turbine and two steps for the heat exchange), as for the all the simulation assumptions (isentropic efficiencies, temperature limits, etc.).

Finally, for the condenser pressure there are again two alternatives: counter-pressure condensation and vacuum condensation, which have been both analysed.

Counter-pressure cycle

As for the subcritical counter-pressure cycles, the condensation pressure is set to 1,1 bar for all the ORC fluids.

Thermodynamic cycles optimization (first step):

The variables to optimize in the present layout are two: the turbine inlet temperature and the evaporation pressure; their lower limits are the values assumed by the critical point, while their upper limits are respectively the maximum pressure sustainable by the turbine and the maximum temperature achievable by the fluid without compromise its chemical stability.

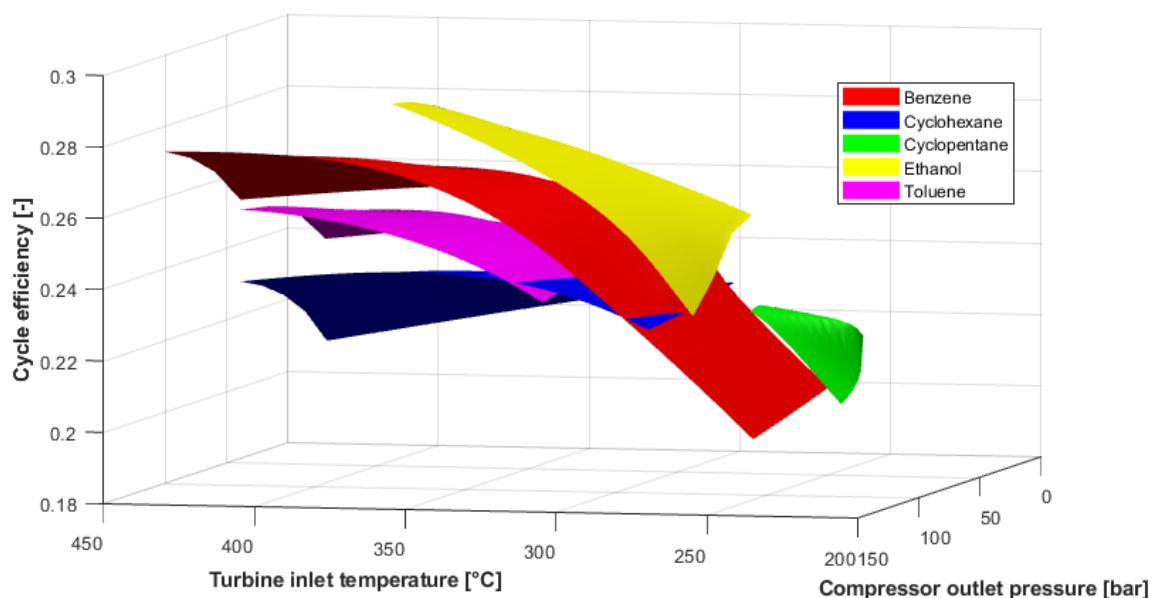


Figure 5.13 - Supercritical counter-pressure cycles sensitivity analysis

From the cycles simulations it's possible to observe that higher values of pressure bring to higher efficiencies, except for the case of the cyclopentane, which presents a non-monotonic behaviour. The performances dependence on the turbine inlet temperature is instead a little bit more complex, since its trend changes with the evaporation pressure; anyway, the benzene and the toluene assume intermediate values, while the other fluids reach the upper limit given by the maximum available temperature. These results are summed up in the following table.

	BENZENE		CYCLOHEXANE		CYCLOPENTANE		ETHANOL		TOLUENE	
	P [bar]	T [°C]	P [bar]	T [°C]	P [bar]	T [°C]	P [bar]	T [°C]	P [bar]	T [°C]
1	1,1	82,76	1,1	83,47	1,1	51,78	1,1	80,52	1,1	113,5
2	112,25	88,6	112,25	89,42	57	55	112,25	84,62	112,25	119,4
3	110	420	110	370	55,86	270	110	370	110	420
4	1,12	256,1	1,12	239,9	1,12	134,4	1,12	165,2	1,12	264,8
\dot{m}_{ORC}	5,297 [kg/s]		6,516 [kg/s]		7,384 [kg/s]		3,293 [kg/s]		6,864 [kg/s]	
η_{cycle}	21,82%		18,8%		20,67%		23,12%		17,78%	
$\dot{W}_{s,turb}$	1128		1166		1108		1097		1162	
$\dot{W}_{s,pump}$	96,8		134,7		77,2		66,5		131,0	
Gain %	11,16%		6,94%		5,24%		7,58%		3,92%	

Table 5.16 - Cycle optimization results (the relative gain is referred to the analogous subcritical case)

Reaching supercritical conditions is convenient for every ORC fluid, although the relative improvement is not always particularly consistent. The second optimization step will determine if the higher temperature reached in the cycle and the absence of the isothermal heat exchange (due to evaporation) can bring to better integration performances.

Indirect integration optimization (second step):

The results obtained from the indirect integration optimization are very interesting because they unequivocally show an important concept related to the power block integration in the carbonator side: a higher thermodynamic efficiency of the power cycle doesn't mean a higher integration efficiency. In fact, although the toluene and the cyclohexane could seem not very interesting because of their relatively poor cycle performance, they are actually between the best alternatives once that the complete optimization process is executed.

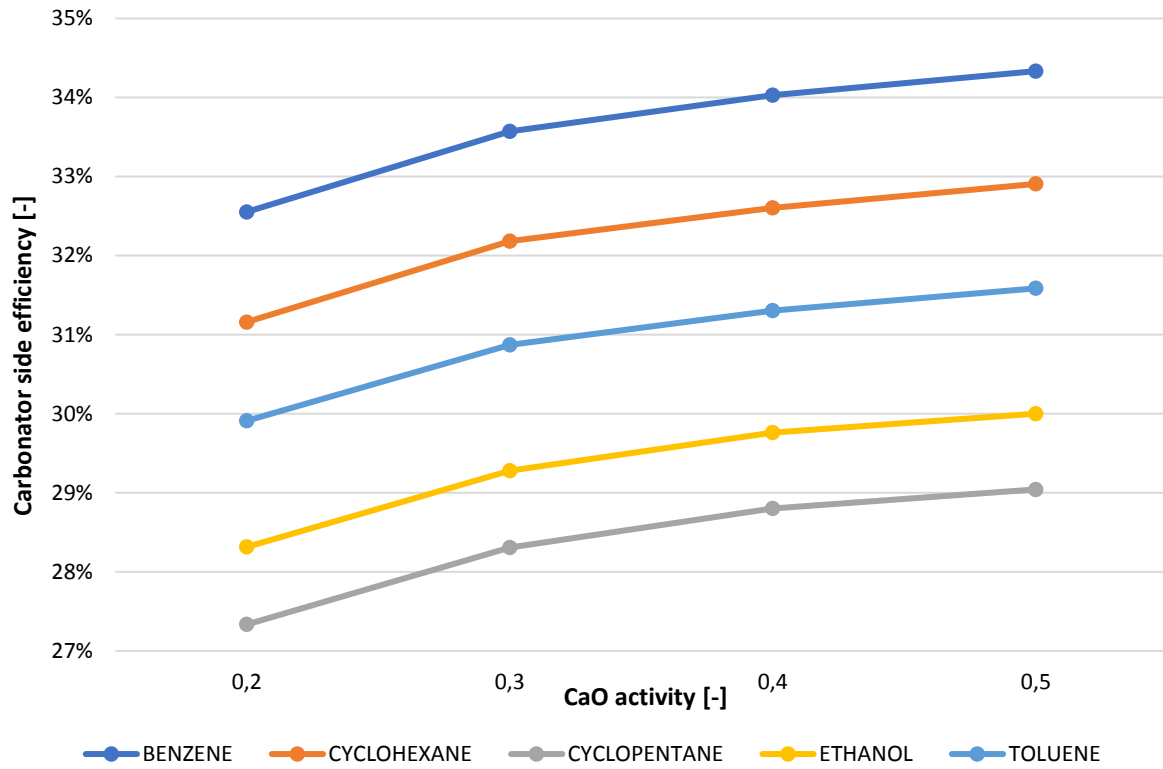


Figure 5.14 - Supercritical counter-pressure cycles integration results

Another interesting aspect to evaluate is the comparison between the integration efficiencies obtained with subcritical and supercritical counter pressure cycles.

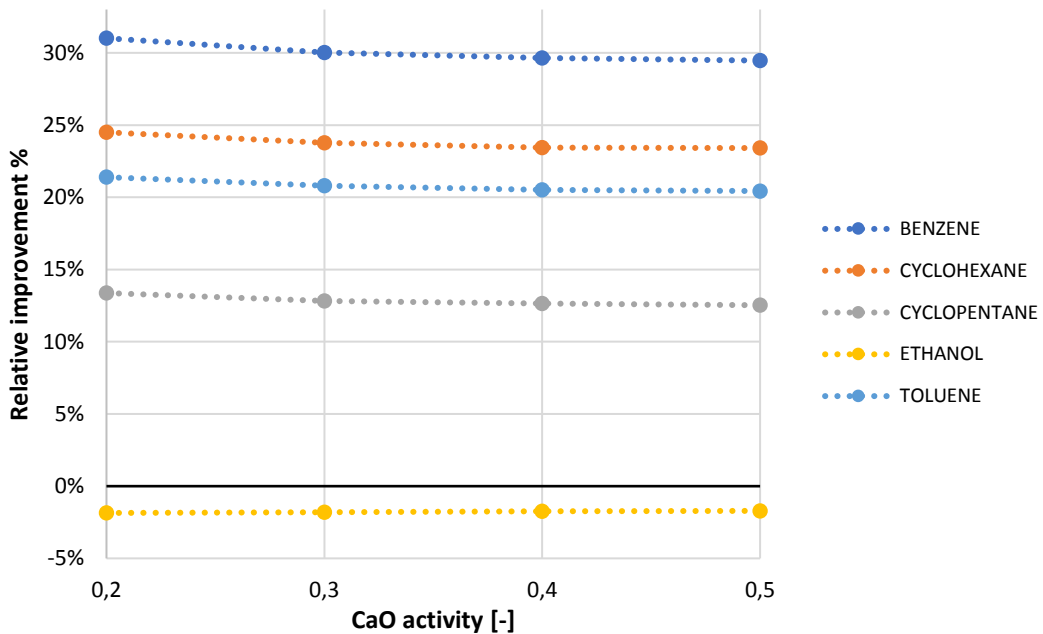


Figure 5.15 – Integration efficiency gain for the transition from subcritical to supercritical counter pressure cycles

Reaching supercritical conditions is generally quite convenient, except for the case of the ethanol, where, surprisingly, it's reported a little performance decrease. One possible explanation for these results it's the fact that a change in the power fluid temperature range and mass streams may cause a worst heat recovery from the carbonator hot products and, furthermore, a variation of the evaporation pressure can change the fluid properties (i.e. the specific heat capacity) such that the heat exchange is penalized.

	X [-]	Storage turbine power [kW _s]	Compressor power [kW _s]	Conveying power [kW _e]	Rejection power [kW _e]	Total auxiliaries consumption [kW _e]	Total plant net power [kW _e]
BENZENE	0,2	371	0,08	127	14,8	142	1218
	0,3	368	9,17	87	15,1	102	1246
	0,4	367	16,66	67	15,5	83	1257
	0,5	365	21,12	55	15,9	71	1262
CYCLOHEXANE	0,2	391	0,09	134	17,1	151	1228
	0,3	388	9,48	92	17,2	109	1258
	0,4	387	17,42	71	18,1	89	1269
	0,5	384	22,38	58	18,4	77	1274
CYCLOPENTANE	0,2	459	0,1	157	22,2	179	1266
	0,3	456	9,52	108	22,4	130	1303
	0,4	456	16,68	84	23,2	107	1319
	0,5	453	21,94	69	23,2	92	1326
ETHANOL	0,2	440	0,1	151	19,1	170	1257
	0,3	437	10,44	103	20,4	124	1290
	0,4	436	18,35	80	20,9	101	1304
	0,5	433	23,11	66	21,0	87	1311
TOLUENE	0,2	419	0,1	144	4,8	142	1265
	0,3	416	11,73	98	4,5	98	1294
	0,4	414	21,59	76	4,5	76	1305
	0,5	411	27,41	62	5,1	62	1310

Table 5.17 - Shaft and electrical powers obtained from the indirect integration optimization process of supercritical ORCs with counterpressure condensation

	INDEPENDENT VARIABLES						DEPENDENT VARIABLES				FLOWRATES					
	X [-]	T _{carb} [°C]	T _{CaO,in} [°C]	T _{CO2,in} [°C]	TIT [°C]	CIT [°C]	COT [°C]	TOT [°C]	T _{co2,mix} [°C]	Excess index [-]	\dot{m}_{CaO} [kg/s]	$\dot{m}_{CO_2,stoic}$ [kg/s]	$\dot{m}_{CO_2,rec}$ [kg/s]	$\dot{m}_{CaO,unr}$ [kg/s]	\dot{m}_{CaCO_3} [kg/s]	η_{carb} [%]
BENZENE	0,2	875	368	174	650	168	182	294	293	1,007	5,89	0,92	0,006	4,71	2,1	32,55
	0,3	875	310	104	650	114	127	294	218	1,836	3,89	0,92	0,767	2,73	2,09	33,57
	0,4	875	310	125	650	113	126	294	192	2,526	2,91	0,92	1,397	1,75	2,08	34,03
	0,5	875	310	143	650	104	116	294	176	2,995	2,31	0,91	1,814	1,16	2,07	34,33
CYCLOHEXANE	0,2	875	368	174	650	156	170	294	293	1,007	6,20	0,97	0,007	4,96	2,21	31,16
	0,3	875	310	104	650	106	119	294	214	1,837	4,10	0,97	0,809	2,87	2,2	32,18
	0,4	875	310	132	650	105	117	294	187	2,548	3,07	0,96	1,492	1,84	2,19	32,60
	0,5	875	310	145	650	104	117	294	176	3,004	2,44	0,96	1,918	1,22	2,18	32,91
CYCLOPENTANE	0,2	875	368	175	650	136	149	294	293	1,007	7,29	1,14	0,008	5,83	2,6	27,33
	0,3	875	310	70	650	77	89	294	205	1,773	4,83	1,14	0,880	3,38	2,59	28,31
	0,4	875	310	70	650	70	82	294	171	2,385	3,61	1,14	1,573	2,17	2,58	28,80
	0,5	875	310	74	650	80	92	294	165	2,783	2,87	1,13	2,012	1,43	2,56	29,04
ETHANOL	0,2	875	368	174	650	180	194	294	293	1,007	6,98	1,10	0,007	5,58	2,49	28,32
	0,3	875	311	100	650	100	112	294	211	1,832	4,62	1,09	0,906	3,23	2,47	29,28
	0,4	875	311	100	650	101	114	294	187	2,462	3,46	1,09	1,588	2,07	2,47	29,76
	0,5	875	311	100	650	100	112	294	176	2,859	2,75	1,08	2,007	1,37	2,45	30,00
TOLUENE	0,2	875	368	174	650	169	183	294	293	1,007	6,65	1,05	0,007	5,32	2,38	29,91
	0,3	875	310	134	650	134	148	294	225	1,899	4,40	1,04	0,931	3,08	2,36	30,87
	0,4	875	310	170	650	135	148	294	203	2,660	3,29	1,03	1,715	1,97	2,35	31,30
	0,5	875	310	178	650	134	148	294	194	3,122	2,61	1,03	2,177	1,30	2,33	31,59

Table 5.18 - Pressures, temperatures and flowrates obtained from the indirect integration optimization process of supercritical ORCs with counterpressure condensation

Condensation cycle

In this case the assumptions made for this kind of ORC cycles are the same already seen for the subcritical condensation case, therefore they won't be repeated.

Thermodynamic cycles optimization (first step):

Also concerning the cycles optimization strategy there aren't any remarkable differences, and even the sensitivity analysis brings to an analogue outcome, so, only the final results are reported.

	BENZENE		CYCLOHEXANE		CYCLOPENTANE		ETHANOL		TOLUENE	
	P [bar]	T [°C]								
1	0,198	35	0,2009	35	0,619	35	0,138	35	0,1	45,25
2	112,25	40,20	112,25	40,93	59	38,23	112,25	38,9	112,25	50,39
3	110	428	110	365	57,82	270	110	370	110	420
4	0,202	223,8	0,205	201,4	0,631	116,6	0,14	98,8	0,102	216,2
\dot{m}_{ORC}	3,724 [kg/s]		4,614 [kg/s]		6,466 [kg/s]		2,404 [kg/s]		4,268 [kg/s]	
η_{cycle}	27,46%		24,19%		22,81%		28,91%		25,86%	
$\dot{W}_{s,turb}$	1095 [kW]		1121 [kW]		1100 [kW]		1077 [kW]		1107 [kW]	
$\dot{W}_{s,pump}$	64,5 [kW]		90,2 [kW]		68,9 [kW]		46,3 [kW]		75,6 [kW]	
Gain %	9,05%		5,04%		4,78%		3,29%		5,04%	

Table 5.19 - Optimization results of supercritical condensation ORC cycles (the relative gain is referred to the analogous subcritical case)

As already seen in the supercritical condensation cycles, the benzene is the fluid that receive the higher benefit by the passage from subcritical to supercritical operating conditions; anyway, the highest efficiency is again reported for the ethanol cycle.

Indirect integration optimization (second step):

Also the indirect integration results are similar to the last case, but this time the toluene efficiency overcome the one obtained with the cyclohexane.

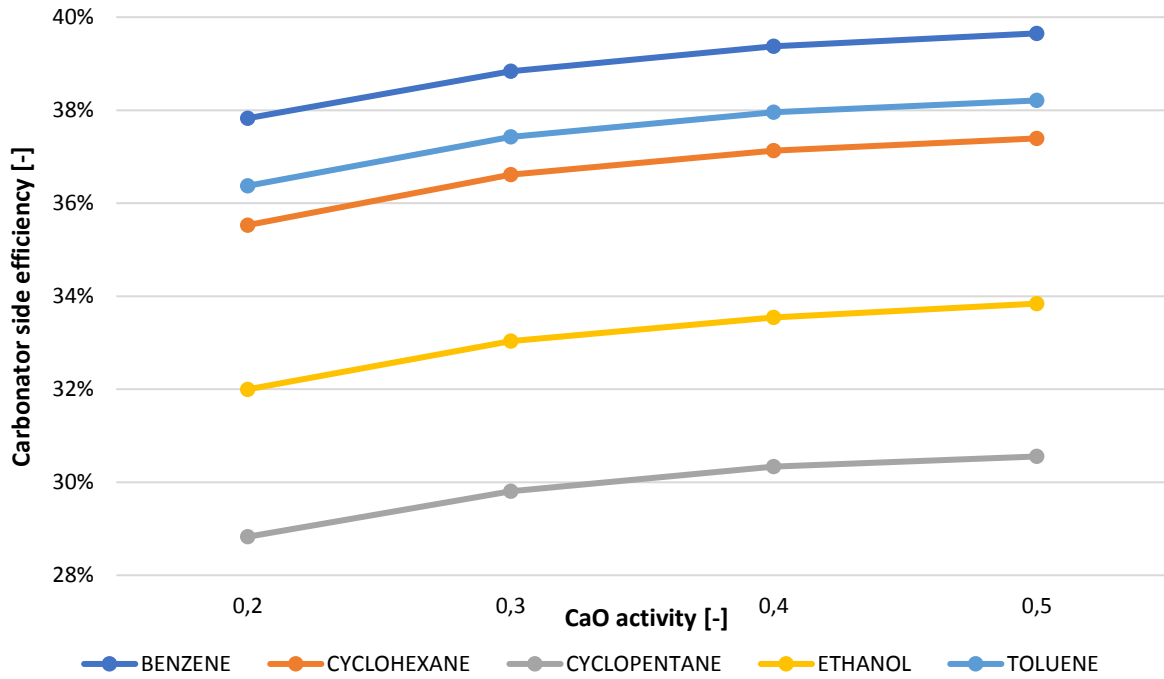


Figure 5.16 - Efficiency results for the supercritical condensation cycles indirect integration

Finally, are showed two graphs in order to observe how the integration efficiency changes both with respect to the subcritical case and the supercritical counter-pressure case. These last results are in line with the ones already seen from the other paragraphs, in fact it seems that condensing at lower pressures always determine an improvement, but reaching supercritical conditions becomes deleterious for the case of the ethanol (while for the other fluids is actually convenient).

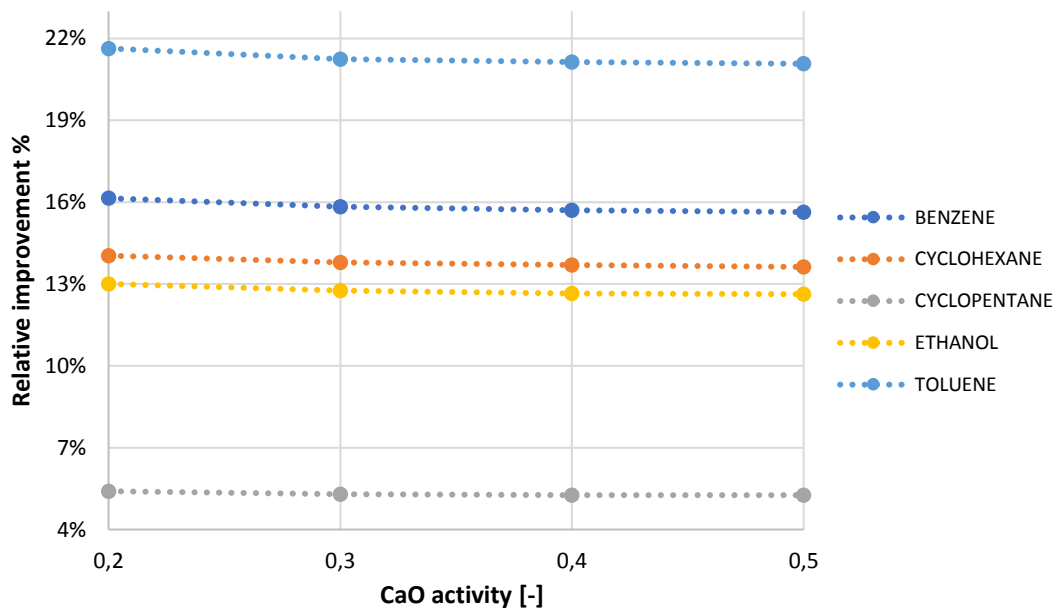


Figure 5.17 - Integration efficiency gain for the transition from counterpressure to condensation supercritical cycles

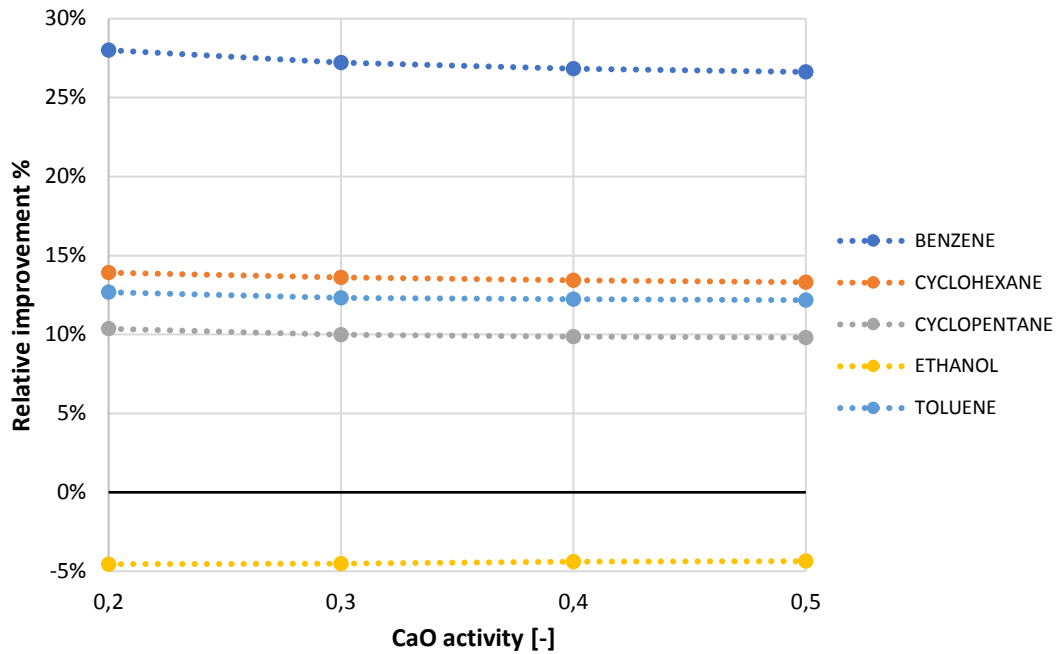


Figure 5.18 - Integration efficiency gain for the transition from subcritical to supercritical counterpressure cycles

	X [-]	Storage turbine power [kW _s]	Compressor power [kW _s]	Conveying power [kW _e]	Rejection power [kW _e]	Total auxiliaries consumption [kW _e]	Total plant net power [kW _e]
BENZENE	0,2	309	0,45	106	12,8	119	1181
	0,3	308	7,51	73	13,3	86	1205
	0,4	307	12,61	56	13,2	70	1216
	0,5	305	16,48	46	12,6	59	1221
CYCLOHEXANE	0,2	333	0,08	114	15,0	129	1194
	0,3	331	7,86	78	14,9	93	1220
	0,4	330	13,81	61	15,1	76	1231
	0,5	328	16,61	50	14,5	64	1238
CYCLOPENTANE	0,2	430	0,12	147	20,6	168	1249
	0,3	427	9,09	101	21,3	122	1283
	0,4	427	14,52	78	21,4	100	1300
	0,5	424	18,5	64	21,1	85	1308
ETHANOL	0,2	378	0,1	129	17,2	147	1220
	0,3	375	8,43	89	18,0	107	1249
	0,4	375	13,76	69	17,4	86	1264
	0,5	373	16,72	57	17,8	74	1271
TOLUENE	0,2	325	0,08	111	13,7	125	1190
	0,3	322	7,88	76	13,6	90	1215
	0,4	321	13,91	59	13,2	72	1226
	0,5	320	17,09	49	13,8	62	1231

Table 5.20 - Shaft and electrical powers obtained from the indirect integration optimization process of supercritical ORCs with vacuum condensation

	INDEPENDENT VARIABLES						DEPENDENT VARIABLES				FLOWRATES					
	X [-]	T _{carb} [°C]	T _{CaO,in} [°C]	T _{CO₂,in} [°C]	TIT [°C]	CIT [°C]	COT [°C]	TOT [°C]	T _{co₂,mix} [°C]	Excess index [-]	\dot{m}_{CaO} [kg/s]	$\dot{m}_{CO_2,stoic}$ [kg/s]	$\dot{m}_{CO_2,rec}$ [kg/s]	$\dot{m}_{CaO,unr}$ [kg/s]	\dot{m}_{CaCO_3} [kg/s]	η_{carb} [%]
BENZENE	0,2	875	397	44	649	47	58	293	280	1,059	4,91	0,77	0,046	3,93	1,75	37,83
	0,3	875	310	47	650	158	172	294	242	1,735	3,25	0,77	0,564	2,28	1,74	38,84
	0,4	875	310	49	650	126	139	294	205	2,338	2,44	0,77	1,024	1,46	1,74	39,37
	0,5	875	310	81	650	116	129	294	188	2,803	1,94	0,76	1,371	0,97	1,73	39,65
CYCLOHEXANE	0,2	875	368	174	650	183	197	294	293	1,007	5,29	0,83	0,006	4,23	1,89	35,53
	0,3	875	310	57	650	138	151	294	233	1,751	3,49	0,82	0,619	2,45	1,87	36,61
	0,4	875	310	62	650	125	138	294	204	2,367	2,62	0,82	1,124	1,57	1,87	37,13
	0,5	875	310	98	650	82	94	294	164	2,851	2,08	0,82	1,514	1,04	1,86	37,39
CYCLOPENTANE	0,2	875	368	176	650	146	159	294	293	1,009	6,82	1,07	0,009	5,45	2,43	28,83
	0,3	875	311	51	650	99	112	294	216	1,743	4,51	1,06	0,791	3,16	2,42	29,81
	0,4	875	311	51	650	56	68	294	164	2,344	3,38	1,06	1,429	2,03	2,42	30,34
	0,5	875	310	53	650	55	67	294	150	2,726	2,69	1,06	1,825	1,34	2,4	30,55
ETHANOL	0,2	875	368	176	650	137	150	294	292	1,009	6,00	0,94	0,008	4,80	2,14	32,00
	0,3	875	311	47	650	122	135	294	226	1,738	3,96	0,94	0,690	2,78	2,13	33,04
	0,4	875	311	47	650	84	96	294	181	2,336	2,97	0,93	1,248	1,79	2,12	33,54
	0,5	875	311	47	650	67	79	294	158	2,712	2,36	0,93	1,591	1,18	2,11	33,84
TOLUENE	0,2	875	368	174	650	184	199	294	293	1,007	5,15	0,81	0,005	4,12	1,84	36,37
	0,3	875	310	65	650	142	156	294	234	1,765	3,40	0,80	0,614	2,39	1,82	37,42
	0,4	875	310	97	650	114	127	294	195	2,452	2,55	0,80	1,163	1,53	1,82	37,95
	0,5	875	310	118	650	90	102	294	168	2,912	2,03	0,80	1,523	1,01	1,81	38,21

Table 5.21 - Pressures, temperatures and flowrates obtained from the indirect integration optimization process of supercritical ORCs with vacuum condensation

Comments and comparisons

The results obtained for the different configurations have some interesting aspects in common. One of those is the fact that the optimization algorithm converges always to the highest achievable value of the carbonator operating temperature, such that the thermal power recovery is performed on a source of high quality heat.

Unfortunately, it's a little more difficult to justify the temperatures obtained for the two carbonator feed streams, which tend to reach low or minimum values. Anyway, one possible explanation consists in the fact that, as observed in simulations conducted separately, higher values assumed by these two parameters would make necessary to operate with a consistent CO₂ excess, which worsen the heat recovery and increase the requirement of external cooling, leading therefore to waste a higher amount of the heat produced by the carbonation reaction. This phenomenon is monotonic (at least in the investigated range) for the CaO stream but not for the CO₂ flow, so this is because the calcium oxide feed stream reaches its minimum acceptable inlet temperature, but the carbon dioxide does not.

However, when the CaO reactivity decrease, if the two streams entering the carbonator are at low temperature the chemical reaction becomes physically unfeasible, because the heat released by the exothermic reaction is insufficient to guarantee the operating temperature. This concept has been already explained and proved in the previous chapter (for the carbonator modelling and simulation) and it's the reason why the results obtained for an X equal to 0,2 of the CaO (and consequently also the CO₂) carbonator inlet temperature doesn't reach the same value obtained in the other cases.

Another thing that is very easy to notice is the fact that also the heating temperature of the stoichiometric carbon dioxide extracted from the pressurized storage (TIT) reaches always its acceptable maximum. This can be explained considering the temperatures achieved by the other cold fluids, which are quite small if compared to the temperature at which are available the two hot streams exiting the carbonator.

Therefore, heating the stoichiometric CO₂ up to a relatively high temperature allows both to make the two composite curves to approach each others (at least at their ends) and to obtain a very effective expansion, producing a consistent amount of electrical power from a fluid that is at high pressure (75 bar).

The last independent variable, the compressor inlet temperature (CIT), generally tends to decrease for higher values of the calcium oxide, although the trend depends on the specific case analysed. In fact, being the pressure increment equal to only 0,1 bar, to reach a low inlet temperature in order to minimize the compression power is not fundamental, since in absolute terms this absorbed electrical power is nearly negligible when compared to the other powers involved.

Concerning the turbomachinery shaft and electrical powers, the results obtained are overall reasonable and easy to motivate: the storage turbine power production slightly decreases when the CaO reactivity increases because the amount of calcium oxide actively participating to the exothermic reaction tends to shrink, as could be expected after having observed the carbonator side efficiency charts. The compressor power is directly dependent on X and this is due to the fact that a higher value of the CO₂ excess means a higher flowrate for the recirculated carbon dioxide and therefore will be required more shaft power to compensate the pressure losses that take place in the carbon dioxide circuit.

Moreover, as already noticed in the direct integration analysis, the rejection power is quite small and, in absolute terms, its variations are considerable as negligible, while the conveying power is inversely proportional to the CaO activity because lowering the amount of inert matter obviously determines a reduction of the total solid mass that must be transported.

Finally, it worth to compare the hot and cold composite curves for the most convenient cases between the different investigated alternatives for every configuration analysed (subcritical/supercritical/condensation/counterpressure). All of these charts are therefore referred to simulations performed assuming a value of X equal to 0,5 while the fluid considered is the one that achieves the highest integration efficiency.

From the point of view of the composite curves, the difference between the configurations with the condenser operating in vacuum conditions or at the atmospheric pressure is simply limited to the fact that the isothermal step due to the phase change is shifted to lower temperatures. The change that happens when passing from a subcritical power block to a supercritical one is instead more significant because with the evaporation stage disappearance the entire cold composite curve becomes straighter, also because of the different temperature dependence of the specific heat capacity at high pressures.

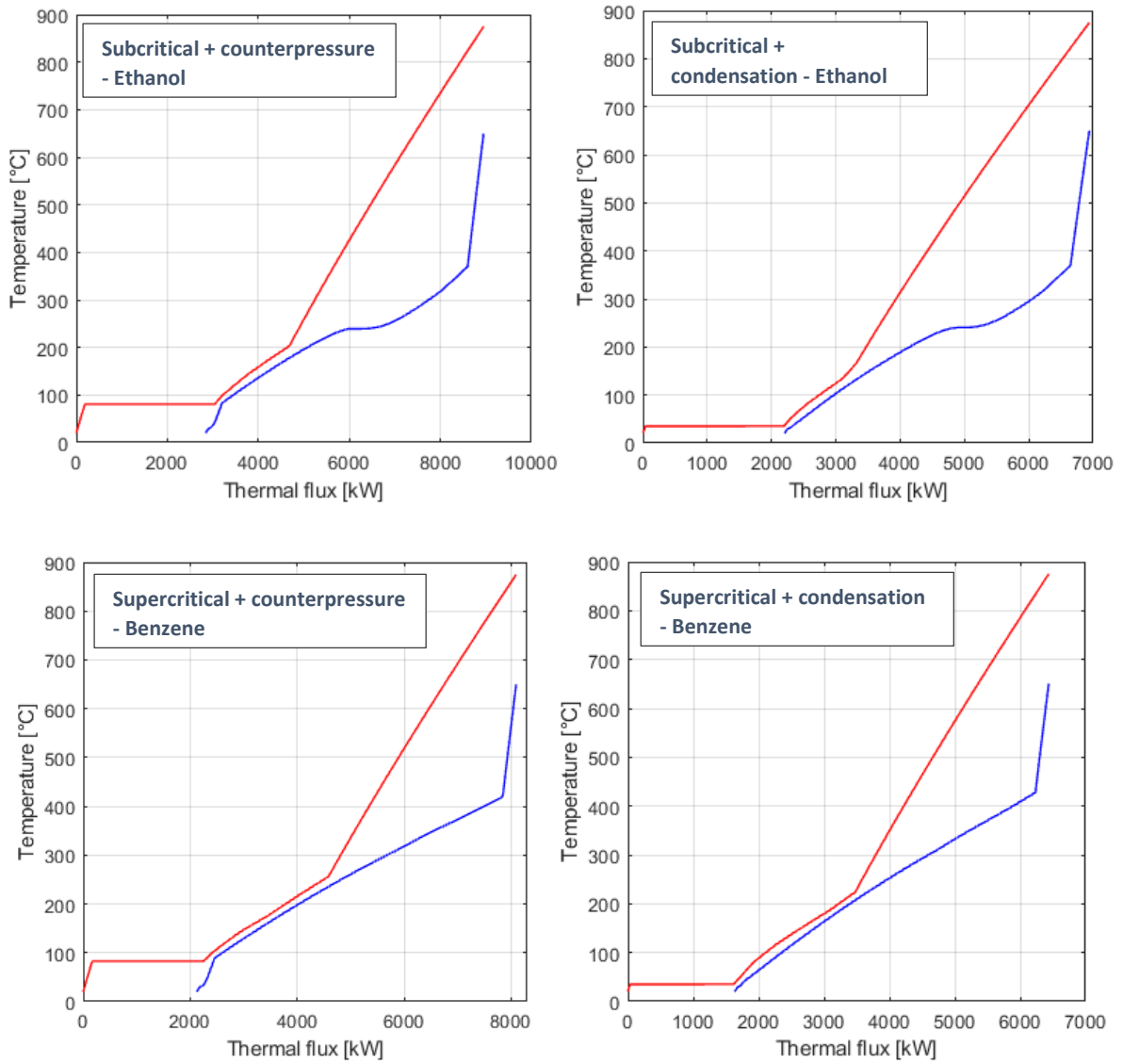


Figure 5.19 - Composite curves for the best alternative in every configuration investigated

Finally, one last comparison will be made at the end of these chapters dedicated to the integration alternatives results, and for the case of the ORCs will be chosen the supercritical power block condensing under vacuum conditions with benzene as working fluid, which is the most performing configuration.

SRC indirect integration

The second investigated typology of power cycle consist in the classic water steam Rankine cycle (SRC). At the state of the art, this is one of the two most common technologies utilized to produce electrical power from a heat input (the other one is the Brayton-Joule cycle), and it's adopted in many different context, from the nuclear plants to the coal plants.

Concerning the technical aspects, the cycle operating conditions are strictly related to the power plant size and, obviously, the bigger are the machineries, the higher are the sustainable temperatures and pressure, simply because the consistent work load and the higher cost of the components justify an in-depth research on the materials and an effective performance optimization (scaling effect).

For these reasons it's currently unfeasible the realization of a supercritical water steam cycle having a rated power of 1 MW_e [23] and therefore all the simulated cycles operate under subcritical conditions.

According to the analysed layouts, the vapor expansion can be executed in a single turbine or in two turbines in series; therefore, the turbomachinery size can be quite different depending on the specific case. To make an evaluation as coherent as possible, have been chosen two different turbines as reference: the first one is the Siemens SST-050 and it is adopted in case of double-step expansion, while the second one is the Siemens SST-060 (already used for the ORC fluids, but it's also compatible with water) and it is adopted in case of single-step expansion (although its datasheet values have been arbitrary decreased because its rated power is higher than the needed).

Furthermore, for all the SRC simulations performed, when the power block is integrated in the carbonator side and it's executed the pinch analysis, it must be evaluated the possible exclusion of the stream exiting the turbine and passing through the condenser from the hot fluids. In fact, differently from the ORC cases, when the vapor exit from the (last) turbine it is or in saturated condition or very close to it; therefore, it's probable that a heat recovery at such a low temperature isn't very interesting and it would only determine a complexity increase in the heat exchanger system.

Anyway, as a proof of concept, from some simulations (conducted separately) in which the water condensation was included, it has been possible to observe an integration efficiency

increment up to the 1,5% in comparison with the case without condensation, which is actually a poor advantage if are considered the drawbacks already exposed.

So, the results showed in the following paragraphs are referred to simulations performed avoiding taking into account the condensing stream between the hot fluids and therefore all the latent heat is rejected in the atmosphere with dry-coolers.

DATA

One-step expansion			Double-step expansion		
Parameter		Reference	Parameter		Reference
TIP_{max}	110 bar	[24]*	TIP_{max}	101 bar	[24]
TIT_{max}	510°C		TIT_{max}	500°C	
TOP_{min}	0,1 bar		TOP_{min}	0,1 bar	
TOP_{max}	15 bar		TOP_{max}	11 bar	

Parameter	Reference
$\eta_{is,turb}$	0,85
$\eta_{is,pump}$	0,75
η_{el}	0,97
$\Delta P_{cooling}$	$2\% \cdot TOP$
$\Delta P_{heating}$	$2\% \cdot POP$

CONSTRAINTS

Parameter	Parameter	Reference
$T_{cond,min}$	$T_{amb} + \Delta T_{pinch} = 35^{\circ}C$	[22]
$P_{el,net}$	1 MW	
$\dot{Q}_{heat,need}$	0 MW	

Tables 5.22, 5.23, 5.24 – Assumptions and constraints for the steam Rankine cycle's components
(* data arbitrary decreased)

Finally, differently from the ORC report, the cycles optimizations are exposed singularly and separately from the integrations results, where the outcomes are showed all together in order to make a more effective comparison.

Basic power block layout

The first investigated power cycle's layout is the simplest as possible, with one turbine, one pump and two steps for the heat exchange. Its optimization is very trivial because, as well known, the best performances are obtained when both the turbine inlet temperature and the evaporation pressure are the higher as possible, while for the condensing pressure the proportionality is inverse.



	Pressure [bar]	Temperature [°C]
1	0,1	45,8
2	112,24	47,1
3	110	510
4	0,102	46,2
VF_4	0,873	
\dot{m}_{water}	0,943 [kg/s]	
$\dot{W}_{s,turb}$	1045 [kW]	
$\dot{W}_{s,pump}$	14,2 [kW]	
η_{cycle}	33,33%	

Figure 5.20 and Table 5.25 - SRC basic layout for the pinch analysis and cycle's operating conditions

Single bleeding power block layout

The second investigated layout is basically equal to the first one but has the addition of a turbine bleeding. This stream is mixed with the liquid coming from the condenser and compressed up to the bleeding pressure, in order to avoid sudden pressure drops; therefore, two pumps are needed.

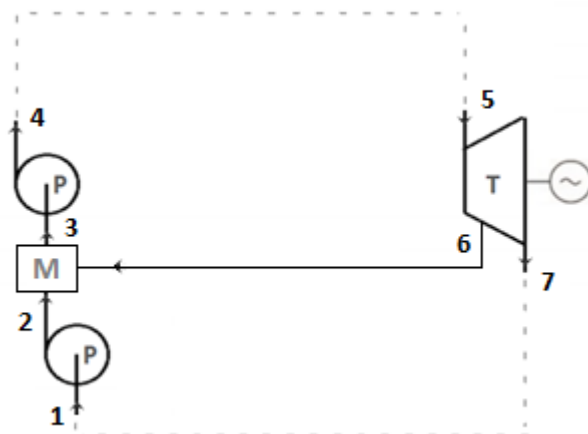


Figure 5.21 - SRC single bleeding layout for the pinch analysis

Besides the constraints already seen, another requirement to satisfy in this configuration is the fact that at the mixer outlet the saturated liquid conditions must be reached. Therefore,

the only variable to optimize is the bleeding pressure; its sensitivity analysis is showed in the following graph.

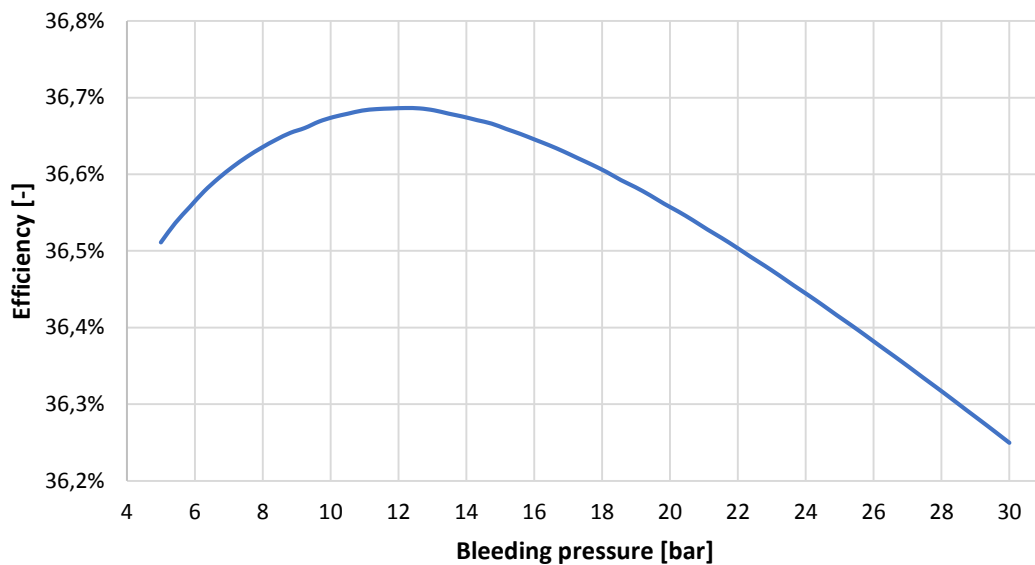


Figure 5.22 - Bleeding pressure sensitivity analysis

Finally, the operating conditions of the optimized case are summed up in the next table.

	1	2	3	4	5	6	7
Pressure [bar]	0,1	12,5	12,5	112,24	110	12,5	0,102
Temperature [°C]	45,8	46	189,8	192,2	510	236,9	45,8
VF₇	0,872	$\dot{W}_{s,turb}$	1048,4 [kW]	Bleeding%	22,63		
\dot{m}_{water}	1,062 [kg/s]	$\dot{W}_{s,pumps}$	17,5 [kW]	η_{cycle}	36,69%		

Table 5.26 - Optimized SRC simple bleeding operating conditions

Single reheat power block layout

In the next layout is performed a reheat that divides the vapor expansion in two steps; as well known, the thermodynamic efficiency has a direct dependence on the temperature at the end of the reheat stage,

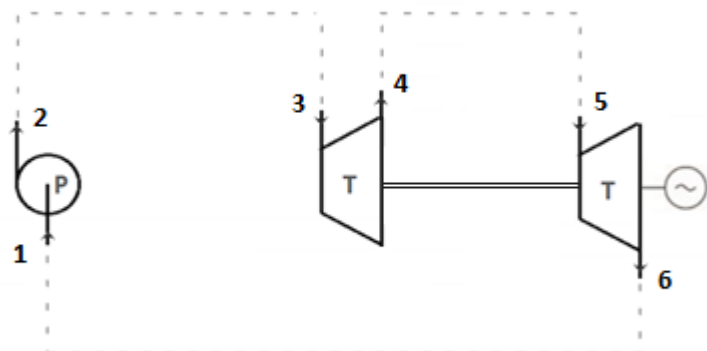


Figure 5.23 - SRC single reheat layout for the pinch analysis

therefore this temperature is set to its maximum available value, which is actually equal to the one at the first turbine inlet.

So, the only parameter to optimize is the intermediate pressure at which is made the reheat.

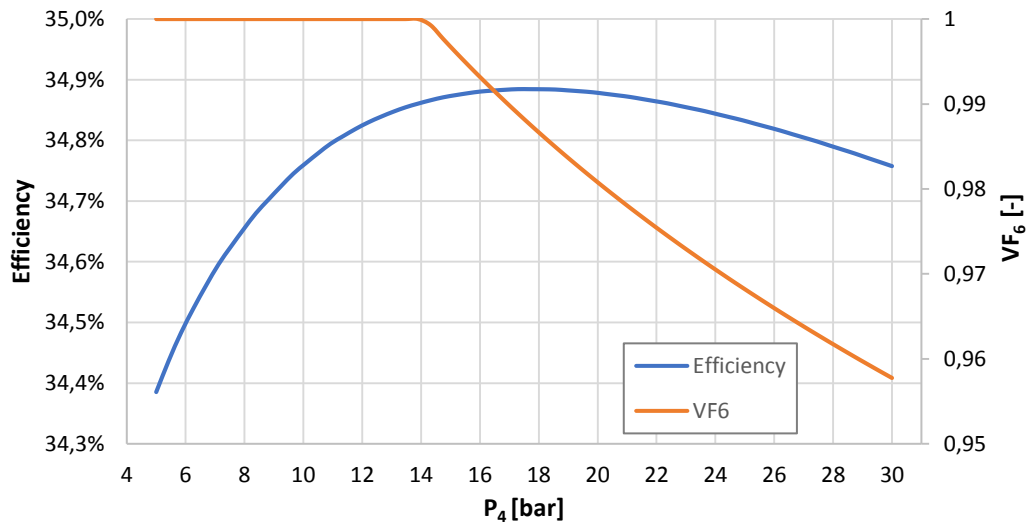


Figure 5.24 - Sensitivity analysis for the reheat pressure

Now, the maximum of the efficiency is reached near the 18 bar, but, according to the assumptions made for the turbine, the highest achievable outlet pressure is equal to 11 bar, which is the value actually assumed in order to respect this technical constraint. Furthermore, for these operating conditions, traces of condensate at the second turbine outlet are completely absent, which is always a good thing for the machinery's functioning.

	1	2	3	4	5	6
Pressure [bar]	0,1	103,1	101	11	10,78	0,102
Temperature [°C]	45,8	47	500	226,5	500	57,6
\dot{m}_{water}	0,766 [kg/s]	$\dot{W}_{s,turb,1}$	373,8 [kW]	η_{cycle}	34,71%	
$\dot{W}_{s,pumps}$	10,6 [kW]	$\dot{W}_{s,turb,2}$	667,8 [kW]			

Table 5.27 - Optimized SRC single reheat operating conditions

Regeneration and reheat power block layout

The last steam Rankine cycle configuration analysed is basically the union of the last two layouts, although there's the difference that it isn't performed a turbine bleeding, but a simple stream split. Also in this case are imposed saturated conditions at the mixer outlet and the bleeding fraction is consequently

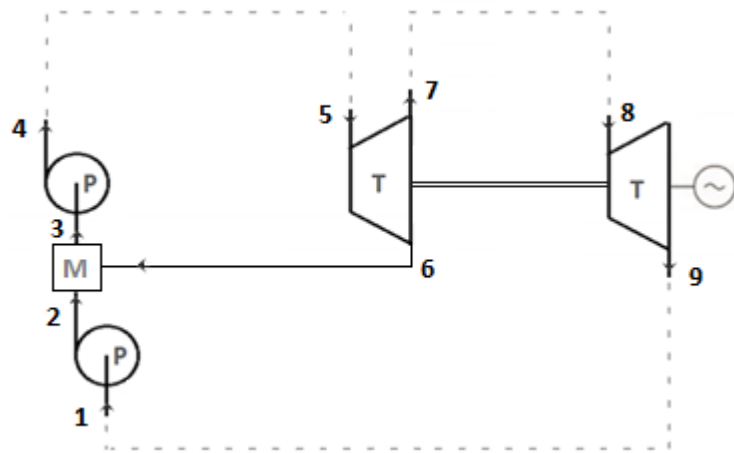


Figure 5.25 - Regeneration + reheat cycle layout for the pinch analysis

computed to satisfy this constraint, while the reheat temperature is again set to the same value reached at the first turbine inlet.

The optimization is therefore executed on the reheat pressure, exactly as for the last investigated layout.

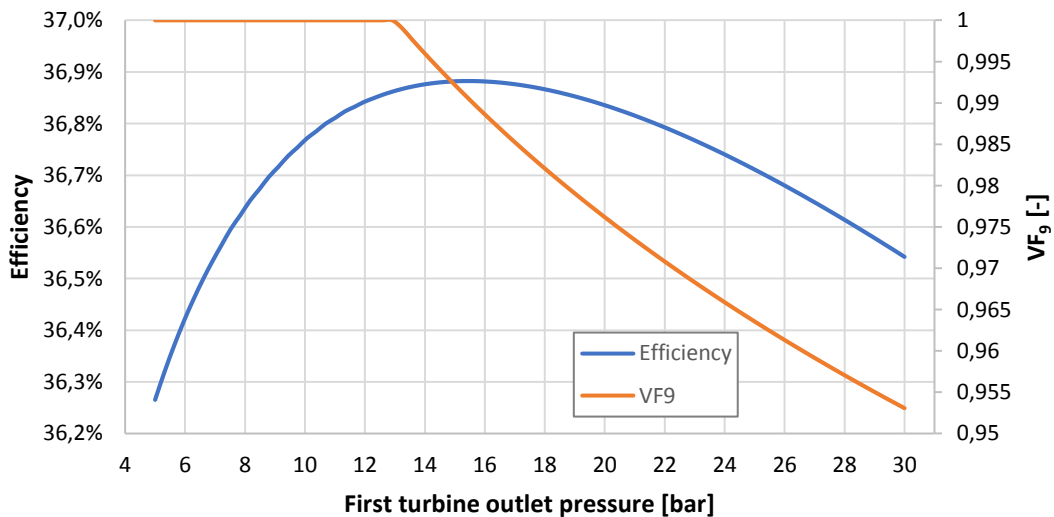


Figure 5.26 - Sensitivity analysis for the reheat pressure

This last graph is qualitatively identical to the one already seen in the previous layout and even its comment will be the same, since the maximum of the efficiency is located near 15 bar which is over the technical constraint for the higher achievable backpressure and therefore it's again necessary to choose 11 bar as outlet pressure for the first turbine.

	1	2	3	4	5	6=7	8	9
Pressure [bar]	0,1	11	11	103,1	101	11	10,78	0,102
Temperature [°C]	45,8	46	184,1	186,2	500	226,5	500	57,6
$\dot{W}_{s,turb,1}$	435,8 [kW]		$\dot{W}_{s,turb,2}$	608,6 [kW]		Bleeding %	21,83%	
\dot{m}_{water}	0,893 [kg/s]		$\dot{W}_{s,pumps}$	13,4 [kW]		η_{cycle}	36,81%	

Table 5.28 - Optimization results for the regeneration + reheat layout

Results, comments and comparisons

Before to show the integration results it can be interesting to make a brief comparison between the thermodynamic efficiencies obtained for the configurations analysed.

	Basic	Single bleeding	Single reheat	Regeneration + reheat
Efficiency	33,33%	36,69%	34,71%	36,81%

Table 5.29 - Thermodynamic efficiency comparison for the SRCs

It's interesting to notice that, although the cycle with the regeneration and reheat has the higher absolute value of efficiency, its performance is very close to the one achieved with a single bleeding. In fact, despite the improvements adopted, both the cases of single reheat and regeneration with reheat have a double-step expansion, which means that must be used two smaller turbines whose rated functioning conditions are less competitive than the ones achieved with a single turbine; this fact penalizes their efficiency.

Now, regarding the integration results, the outcomes of the second optimization step are showed together in the following graphs and tables, in order to simplify the comparison.

For the steam Rankine cycles investigated, the integration efficiency follows very closely the thermodynamic cycle efficiency; therefore, the best alternatives are again the single bleeding and the regeneration with reheat.

In absolute terms, the results obtained are quite similar to the ones coming from the ORC simulations, although there are non-negligible variations depending on the specific fluid and power block configuration. Any other comment is left for the final comparison, once that all the simulations outcomes have been collected.

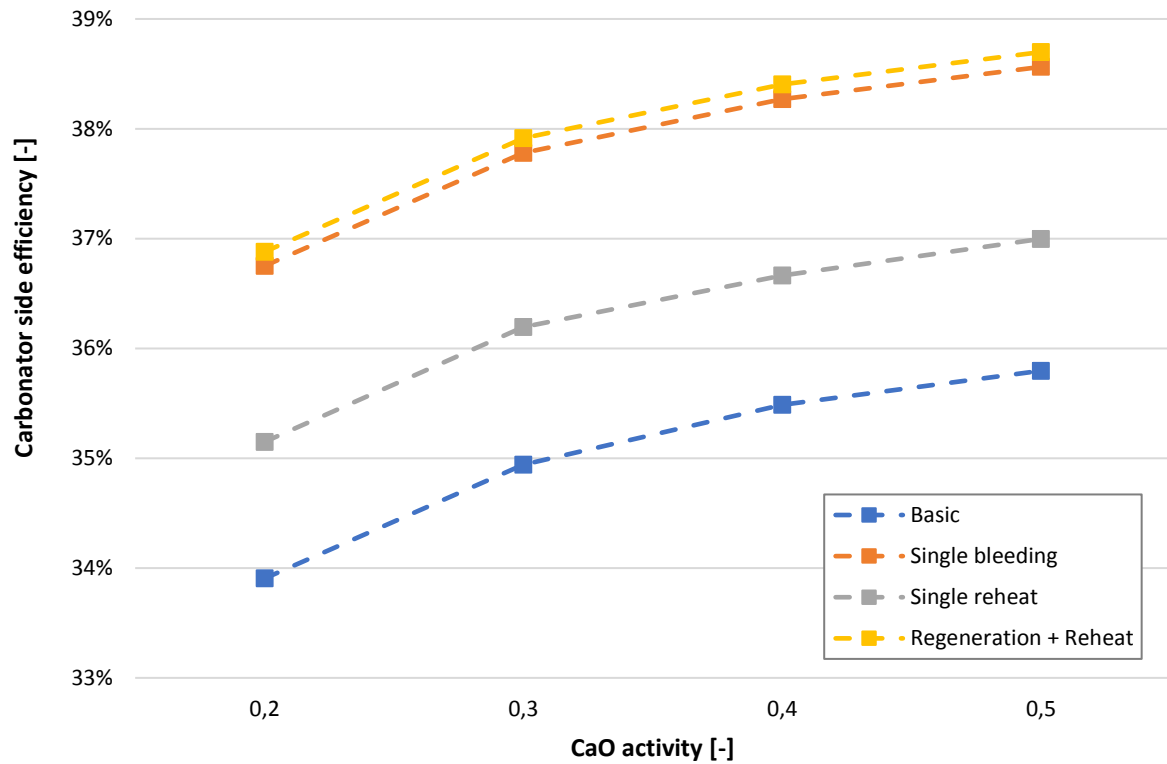


Figure 5.27 - SRCs integration results

	X [-]	Storage turbine power [kW _s]	Compressor power [kW _s]	Conveying power [kW _e]	Rejection power [kW _e]	Total auxiliaries consumption [kW _e]	Total plant net power [kW _e]
BASIC	0,2	353	0,17	121	15,7	136	1205
	0,3	350	8,24	83	15,7	98	1233
	0,4	350	11,32	64	15,7	80	1246
	0,5	348	14,41	53	15,7	69	1255
SIMPLE BLEEDING	0,2	320	0,12	110	13,6	123	1187
	0,3	317	10,29	75	13,6	89	1209
	0,4	316	18,38	58	13,6	72	1217
	0,5	314	21,92	48	13,6	61	1222
SIMPLE REHEAT	0,2	338	0,09	116	14,7	130	1197
	0,3	335	7,80	79	14,7	94	1224
	0,4	335	10,81	61	14,7	76	1238
	0,5	333	16,04	51	14,7	65	1242
REGENERATION + REHEAT	0,2	319	0,09	109	13,5	123	1187
	0,3	316	9,94	75	13,5	88	1209
	0,4	315	17,52	58	13,5	71	1217
	0,5	313	21,27	48	13,5	61	1222

Table 5.30 - Shaft and electrical powers obtained from the indirect integration optimization process of different SRC layouts

Concerning the values of the independent variables to whom the optimization converged and the obtained turbomachinery powers, all the comments and considerations already made for the indirect integration of the organic Rankine cycles are still valid, as could be expected since the two thermodynamic cycles are actually quite similar.

	INDEPENDENT VARIABLES						DEPENDENT VARIABLES				FLOWRATES					
	X [-]	T _{carb} [°C]	T _{CaO,in} [°C]	T _{CO₂,in} [°C]	TIT [°C]	CIT [°C]	COT [°C]	TOT [°C]	T _{CO₂,mix} [°C]	Excess index [-]	\dot{m}_{CaO} [kg/s]	$\dot{m}_{CO_2,stoic}$ [kg/s]	$\dot{m}_{CO_2,rec}$ [kg/s]	$\dot{m}_{CaO,unr}$ [kg/s]	\dot{m}_{CaCO_3} [kg/s]	η_{carb} [%]
BASIC	0,2	875	368	177	650	114	127	294	291	1,016	5,59	0,88	0,014	4,47	2,00	33,91
	0,3	875	312	52	650	134	148	294	231	1,751	3,70	0,87	0,655	2,59	1,98	34,94
	0,4	875	310	38	650	47	58	294	160	2,314	2,77	0,87	1,145	1,66	1,98	35,48
	0,5	875	310	36	650	47	58	294	146	2,682	2,21	0,87	1,458	1,10	1,97	35,80
SIMPLE BLEEDING	0,2	875	368	175	650	213	228	294	293	1,010	5,08	0,80	0,008	4,07	1,82	36,75
	0,3	875	312	145	650	179	193	294	245	1,932	3,36	0,79	0,737	2,35	1,80	37,78
	0,4	875	312	170	650	179	193	294	231	2,668	2,51	0,79	1,315	1,51	1,79	38,27
	0,5	875	310	197	650	139	152	294	197	3,196	1,99	0,78	1,721	1,00	1,78	38,56
SIMPLE REHEAT	0,2	875	368	176	650	144	158	294	293	1,008	5,36	0,84	0,007	4,29	1,91	35,15
	0,3	875	311	35	650	148	162	294	239	1,717	3,55	0,84	0,599	2,48	1,90	36,19
	0,4	875	310	36	650	47	58	294	160	2,310	2,66	0,83	1,093	1,59	1,90	36,66
	0,5	875	310	52	650	90	102	294	173	2,723	2,11	0,83	1,430	1,06	1,89	37,00
REGENERATION + REHEAT	0,2	875	368	175	650	250	266	294	293	1,007	5,06	0,80	0,006	4,05	1,81	36,88
	0,3	875	310	132	650	183	197	294	248	1,895	3,34	0,79	0,706	2,34	1,79	37,91
	0,4	875	310	172	650	159	172	294	218	2,671	2,50	0,79	1,313	1,50	1,79	38,41
	0,5	875	310	192	650	132	145	294	192	3,178	1,99	0,78	1,700	0,99	1,77	38,70

Table 5.31 - Pressures, temperatures and flowrates obtained from the indirect integration optimization process of different SRC layouts

Finally, also for this power block typology is chosen one particularly interesting configuration that will be reported in the final comparison between the different integration alternatives; in this case has been chosen the simple bleeding layout. Its efficiency is actually a little bit smaller than the configuration with both regeneration and reheat, but its higher layout simplicity makes it a more interesting alternative. The relative grand composite and the hot and cold composite curves are showed in the following charts (again, they are referred to a value of CaO activity equal to 0,5).

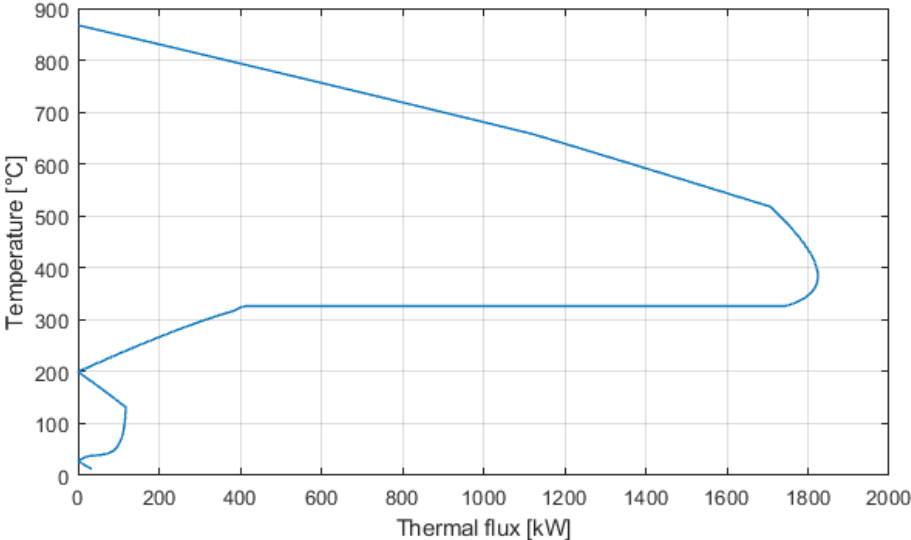


Figure 5.28 - Grand composite curve for the single bleeding SRC layout (X=0,5)

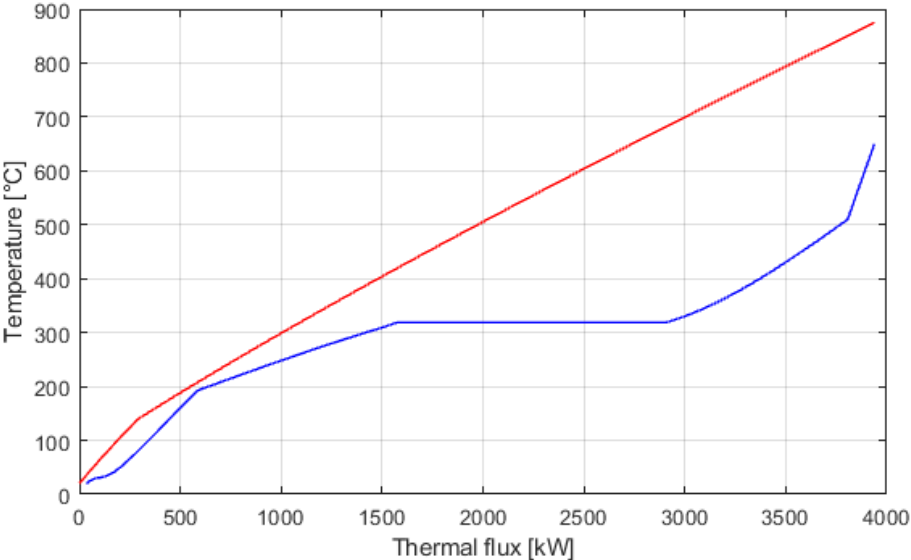


Figure 5.29 - Hot and cold composite curves for the single bleeding SRC layout (X=0,5)

As already happened in the direct integration, the thermal flux in the grand composite curve becomes zero for three times, which means that during the heat recovery the minimum temperature difference will be reached twice.

Furthermore, it must be remembered that, as previously justified, the condensing water hasn't been considered between the hot fluids and obviously this is why, differently from the ORC seen in the previous chapter, the hot composite curve doesn't show an isothermal stage at low temperatures.

Finally, as could be expected in consequence to the high latent heat of the water, it's easy to notice that the evaporation step constitutes a relevant part in the total heat exchange process, especially if compared to the results obtained in the previous chapter.

SCO₂ indirect integration

Another typology of power block to integrate in the carbonator side consists in the Brayton-Joule cycle. As well known, this cycle involves a power fluid always kept under the conditions of vapor or gas, avoiding any process of phase change.

As already seen for the ORCs, also in this case there are many alternatives for the power fluid choice; anyway, according to the research works found in the scientific literature, the most commonly adopted substance is the carbon dioxide. This is due to several reasons, since it has very good thermal properties, its critical pressure (73,77 bar) is relatively easy to achieve and the machineries size can be up to twenty times smaller than the ones used in the Rankine cycle [25]. Furthermore, thanks to the high pressures and temperatures that can be reached, the thermodynamic cycle efficiency can theoretically overcome the 50%.

Actually, it must be said that at the state of the art this type of power cycle is not very commonly used and its current main field of application is represented by the nuclear technology. Anyway, with the consistent improvements of the concentrated solar power plants happened during the last years, some industries have started to develop new dedicated turbomachinery. This is the case of the U.S. Department of Energy's SunShot Initiative, in which General Electrics is building a 10 MW turbine and recently has been successfully tested a prototype of size equal to 1 MW, whose operating conditions are assumed for the simulations performed in this work.

All the assumptions made for the components operating conditions are reported in the following tables.

ASSUMPTIONS

Parameter		Reference	Parameter		Reference
TIP_{max}	250 bar	[26]	ΔT_{hex}	15°C	[-]
TIT_{max}	715°C		η_{is,turb}	0,9	[27]
ΔP_{LP}	1% · P _{in}	[1]	η_{is,comp}	0,87	
ΔP_{HP}	0,5% · P _{in}		η_{el}	0,97	[-]

CONSTRAINTS

$P_{el,net}$	1 MW
$\dot{Q}_{heat,need}$	0 MW
$T_{cooler,min}$	$T_{amb} + \Delta T_{pinch} = 35^{\circ}C$
$P_{min,abs}$	74 bar

Tables 5.32, 5.33 - Assumptions and constraints for the SCO₂ cycles simulations

Reaching very high pressures in absolute terms, it's important to optimize the stream fluid dynamic between the compressor outlet and the turbine inlet in order to reduce the penalization due to the pressure losses, which are instead less important for the low-pressure side of the layout. This is why it has been assumed two different percentages for the pressure drops, introducing the difference between the high-pressure side (HP) and low-pressure side (LP). Furthermore, during the cycles optimization it has been set a minimum for the achievable operating pressure with the aim of avoid the possibility of reach subcritical pressures.

In the successive paragraphs the two investigated configurations of supercritical carbon dioxide power cycles with their relative optimization are presented. The integration results are again reported at the end.

Single intercooling power block layout

The first power block configuration consists in a series of two compressors with one intercooling stage, a turbine and two other steps for the heat exchange. The reason for which has been assumed no more than one intercooling is due to the attempt to avoid an excessive plant complexity, especially if it's considered the power block size.

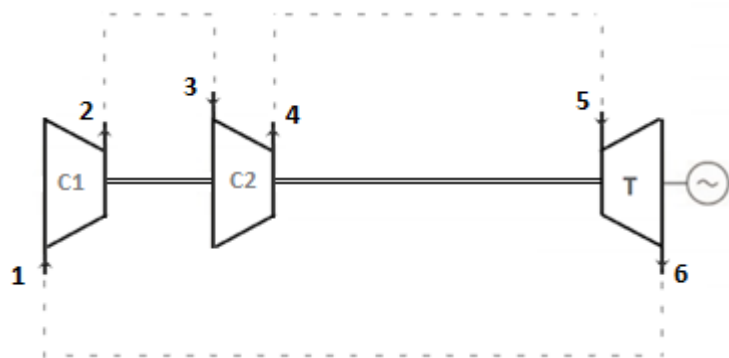


Figure 5.30 - Single intercooling layout

As well known, a low temperature at the inlet of both the compressors helps to increase the efficiency, and for this reason it is set to its lower achievable value, equal to the sum of the ambient temperature and the minimum temperature difference adopted in the pinch analysis. Moreover, the turbine inlet temperature is fixed to its maximum value because, since the simulation of the thermodynamic cycle doesn't consider any heat recovery, if this parameter would be considered as variable the optimization would provide a misleading result. So, the parameters assumed as independent variables for the power block optimization are three: the turbine inlet pressure, the turbine outlet pressure and the intercooling pressure (more precisely, the first compressor outlet pressure).

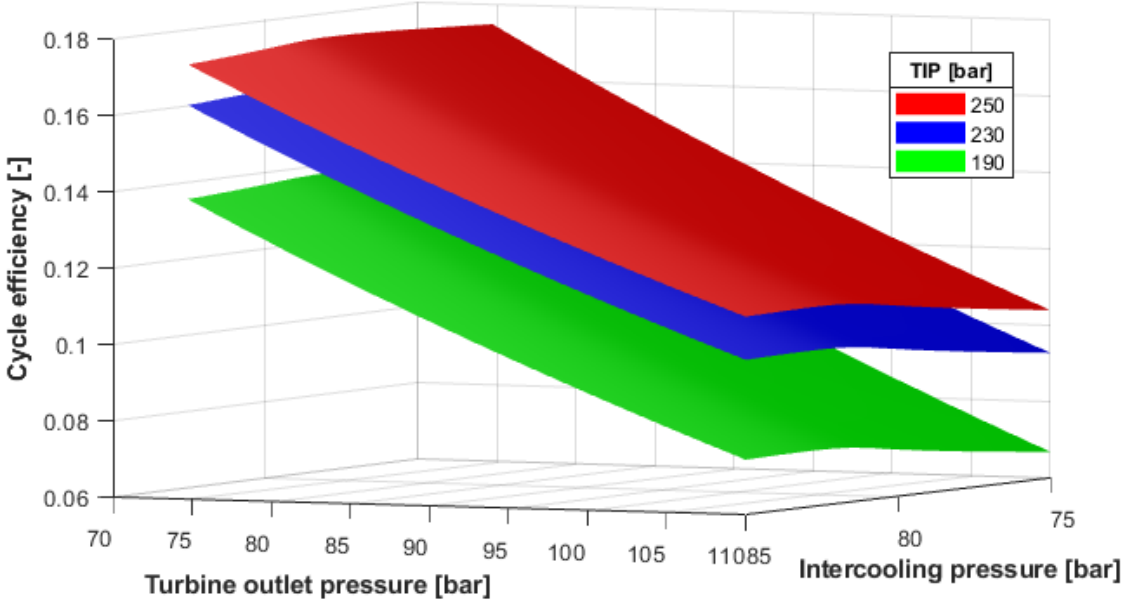


Figure 5.31 - Sensitivity analysis for the single intercooling layout

From this last graph is easy to evaluate the efficiency dependence on the three considered parameters. In fact, an increase of the turbine inlet pressure or a decrease of the turbine outlet pressure is always able to determine an improvement of the cycle performance (at least in the analysed variation field); instead, the pressure at which is performed the intercooling stage has a non-monotonic influence on the efficiency, although the variations caused by this last parameter are quite small.

The operating conditions of the optimized layout are reported in the table below.

		1	2	3	4	5	6
Pressure [bar]		74	80,3	79,5	251,3	250	74,7
Temperature [°C]		35	40,7	35	97,6	715	555,1
$\dot{W}_{s,turb}$	1313,3 [kW]	$\dot{W}_{s,comp,1}$		18,8 [kW]	η_{cycle}		17,13%
\dot{m}_{CO_2}	6,931 [kg/s]	$\dot{W}_{s,comp,2}$		263,6 [kW]			

Table 5.34 - Optimized single intercooling layout operating conditions

As is easy to notice from the last chart and the table, the result of the cycle efficiency is quite low, but this is due to the fact that, differently from the following case, the hot flow exiting the turbine is not used to preheat the turbine inlet stream because every heat exchange will be performed with the pinch analysis in the second step of the optimization.

Recompression power block layout

The other investigated layout represents (according to the scientific literature) one of the best alternatives between the possible configurations for the supercritical CO₂ power plants. It is based on two parallel compressors that operate with two feed streams at approximately the same inlet pressure but different temperatures. This is due to the particular heat recovery strategy

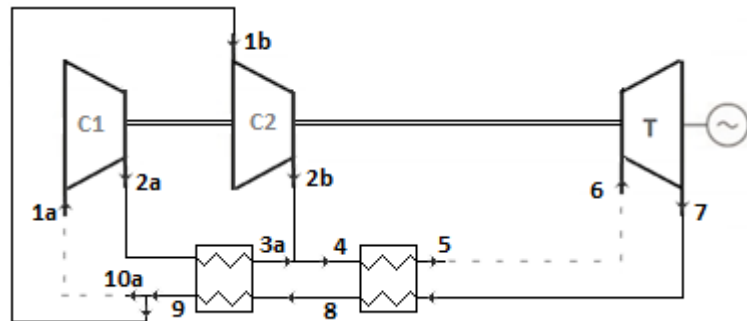


Figure 5.32 - Recompression layout for the SCO₂ power cycle

performed at the turbine outlet, which has the aim of exploit the consistent heat capacity difference between the high-pressure side and the low-pressure side. The hot stream crossing the two exchangers is the same, but the cold stream has different flowrates, depending on that it is the low-temperature exchanger or the high-temperature exchanger.

This is the only case analysed in which the heat recovery in the power block is (partially) performed before the second optimization step. Furthermore, since it's involved an exchange of thermal power, the cycle optimization should include the pinch analysis but, as already said,

the tools available to perform this thesis doesn't allow a similar execution; so, the heat exchangers are set to operate until the minimum temperature difference between hot and cold fluid is reached.

As already done for the previous layout, the turbine inlet temperature is set to its maximum sustainable value, while the first compressor inlet temperature (T_{1a}) is set to the minimum value achievable performing a dry cooling (35°C). So, the remaining parameters to optimize are the turbine inlet pressure, the turbine outlet pressure and the split fraction of the hot stream exiting from the low-temperature heat exchanger.

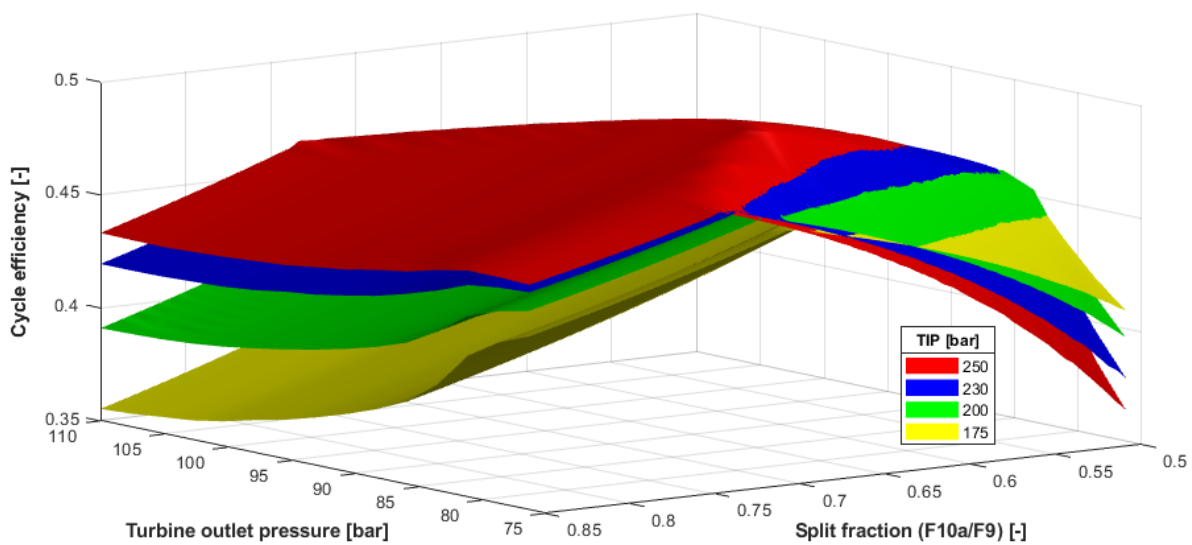


Figure 5.33 - Sensitivity analysis for the recompression layout

The graph above shows a more complex situation with respect to the previous layout. The efficiency dependence on the parameters analysed has never a monotonic trend, although it's possible to say that increasing the turbine inlet pressure generally determines an improvement of the performances (except for a small corner of the investigated variable field).

	1a	1b≡9≡10a	2a	2b	3a	4	5	6	7	8
Pressure [bar]	82,7	83,7	253,8	252,5	252,5	252,5	251,3	250	85,4	84,6
Temperature	35	89,7	74,7	199,2	197,5	198,1	522	715	571	213
$\dot{W}_{s,turb}$	1419,4 [kW]		$\dot{W}_{s,comp,1}$		159,8 [kW]		\dot{m}_{10a}/\dot{m}_9		0,6492	
$\dot{m}_{CO_2,tot}$	8,315 [kg/s]		$\dot{W}_{s,comp,2}$		228,8 [kW]		η_{cycle}		49,25%	

Table 5.35 - Optimization results of the recompression layout

The cycle efficiency result is the higher obtained between the power blocks analysed and this is easily explainable looking at the very high operating temperatures and pressures, besides the execution of heat recovery before the second step of the optimization. Anyway, only with the complete integration optimization will be possible to evaluate in absolute terms its convenience.

Results, comments and comparisons

From the integration results is interesting to observe not only the differences on the performances but also the variation of the relative convenience of a layout with respect to the other one, as showed in the following chart.

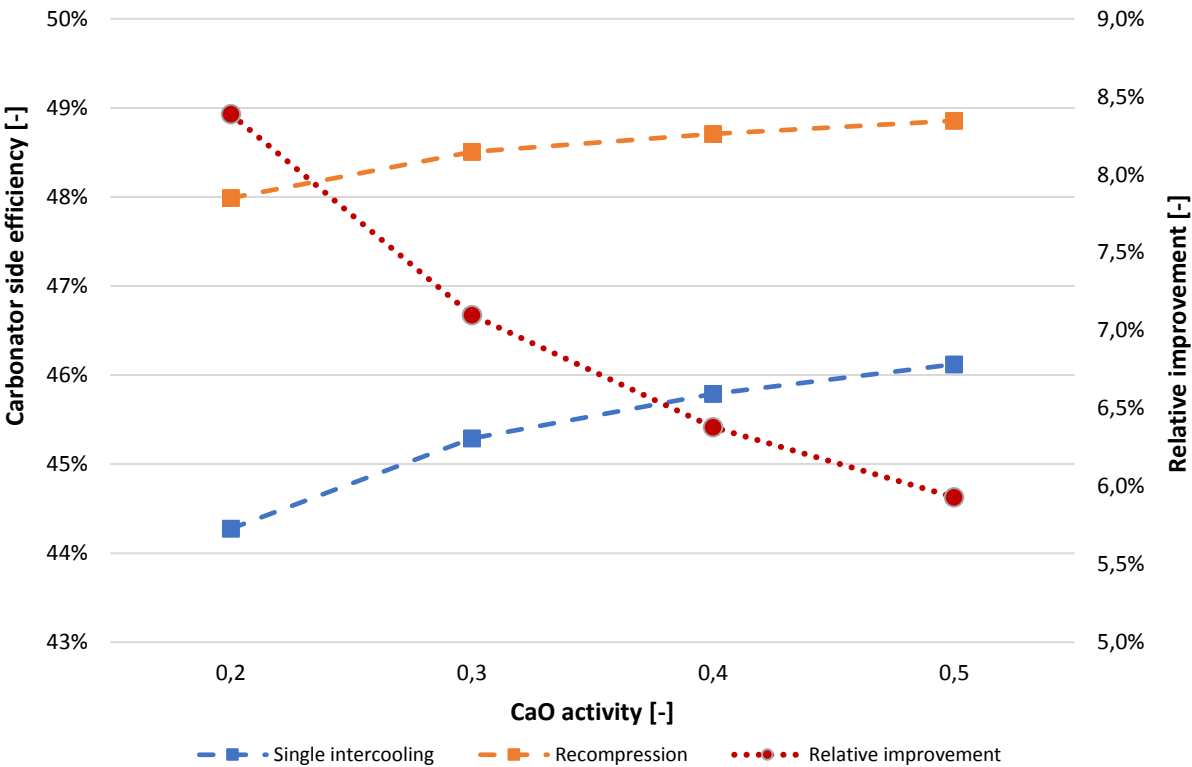


Figure 5.34 - Integration results of the two SCO2 power plants

Between the variation range of the analysed parameters, the recompression layout is always better performing, although its relative improvement (with respect to the single intercooling layout) decreases with the increase of the calcium oxide reactivity.

The low efficiency variations observed for the recompression layout can reasonably be attributed to the fact that this one is the only thermodynamic cycle (between the ones

investigated) in which a partial heat recovery is already performed before the pinch analysis-based optimization and therefore the effectiveness of this second step of the optimization process is reduced. However, the recompression layout is the alternative chosen to represent the supercritical carbon dioxide cycles in the following chapter, dedicated to the comparison of the integration typologies.

Any other result obtained from the optimization process is reported in the following tables. Regarding the shaft and electrical power fluxes, all the considerations already done for the other indirect integration alternatives previously analysed are still valid, while it is worthwhile to comment the outcomes of the independent variables to the whom the algorithm converged. In fact, if compared to the results obtained for the ORC and SRC simulations, the carbonator feed stream temperatures are much higher (especially for the recompression layout), determining the necessity of consistent CO₂ excesses and therefore increasing the compressor power consumption.

Furthermore, for the recompression layout are reported some cases where the storage turbine inlet temperature (TIT) doesn't converge to its maximum achievable value (650°C), which had never happened before.

There are actually many reasonable explanations to justify these phenomenon, and one of these consists in the fact that, being the carbon dioxide both the working fluid (in the power block) and one of the carbonator outlet streams, providing heat to the thermodynamic cycle with a CO₂ flowrate as high as possible (with respect to the CaCO₃ and the unreacted CaO flowrates) can improve the thermal recovery.

Another reason for the high carbonator inlet temperatures observed in the recompression layout integration can be due to the fact that the cold fluid of the power block (exiting the high-temperature exchanger and entering the turbine) requires only heat at high temperature (522°C – 715°C) and therefore heating up these other two streams allows to recover the thermal power at mid-low temperature. Moreover, this last consideration can also justify the fact that the storage turbine inlet temperature (TIT) doesn't always reach its acceptable maximum.

Finally, always concerning the recompression layout, another very uncommon aspect that can be observed is related to the particularly high values obtained for the compressor inlet

temperature (CIT); however, the cause of this trend will be much easier to understand once that the charts on the pinch analysis are exposed and therefore this is because this clarification is explained further on.

	X [-]	Storage turbine power [kW _s]	Compressor power [kW _s]	Conveying power [kW _e]	Rejection power [kW _e]	Total auxiliaries consumption [kW _e]	Total plant net power [kW _e]
SINGLE INTERCOOLING	0,2	258	1,5	88	8,3	97	1152
	0,3	255	14,7	60	8,6	69	1164
	0,4	254	20,6	47	8,8	55	1171
	0,5	252	24,6	38	8,9	47	1174
RECOMPRESSION	0,2	228	32,4	78	6,8	85	1105
	0,3	215	54,7	53	7,1	60	1095
	0,4	212	67,6	41	7,2	48	1092
	0,5	204	73,9	33	7,3	41	1085

Table 5.36 - Shaft and electrical powers obtained from the indirect integration optimization process of different SCO₂ layouts

	INDEPENDENT VARIABLES						DEPENDENT VARIABLES				FLOWRATES					
	X [-]	T _{carb} [°C]	T _{CaO,in} [°C]	T _{CO₂,in} [°C]	TIT [°C]	CIT [°C]	COT [°C]	TOT [°C]	T _{CO₂,mix} [°C]	Excess index [-]	\dot{m}_{CaO} [kg/s]	$\dot{m}_{CO_2,stoic}$ [kg/s]	$\dot{m}_{CO_2,rec}$ [kg/s]	$\dot{m}_{CaO,unr}$ [kg/s]	\dot{m}_{CaCO_3} [kg/s]	η_{carb} [%]
SINGLE INTERCOOLING	0,2	875	387	179	650	215	230	294	285	1,157	4,09	0,64	0,101	3,28	1,46	44,27
	0,3	875	446	241	650	125	138	294	192	2,886	2,70	0,64	1,198	1,89	1,44	45,29
	0,4	875	433	303	650	113	126	294	171	3,725	2,02	0,63	1,728	1,21	1,44	45,79
	0,5	875	493	291	650	114	127	294	166	4,269	1,60	0,63	2,057	0,80	1,43	46,12
RECOMPRESSION	0,2	875	516	504	650	401	419	293	386	3,731	3,62	0,57	1,554	2,90	1,29	47,99
	0,3	875	514	514	616	438	458	270	424	5,458	2,37	0,56	2,488	1,66	1,27	48,50
	0,4	875	506	521	612	468	488	267	453	6,308	1,77	0,56	2,950	1,06	1,26	48,71
	0,5	875	511	518	589	472	492	251	457	6,847	1,40	0,55	3,211	0,70	1,25	48,86

Table 5.37 - Pressures, temperatures and flowrates obtained from the indirect integration optimization process of different SCO₂ layouts

In conclusion of the chapter are showed the hot and cold composite curves for both the SCO_2 power block layouts (as always, they are referred to a value of CaO activity equal to 0,5).

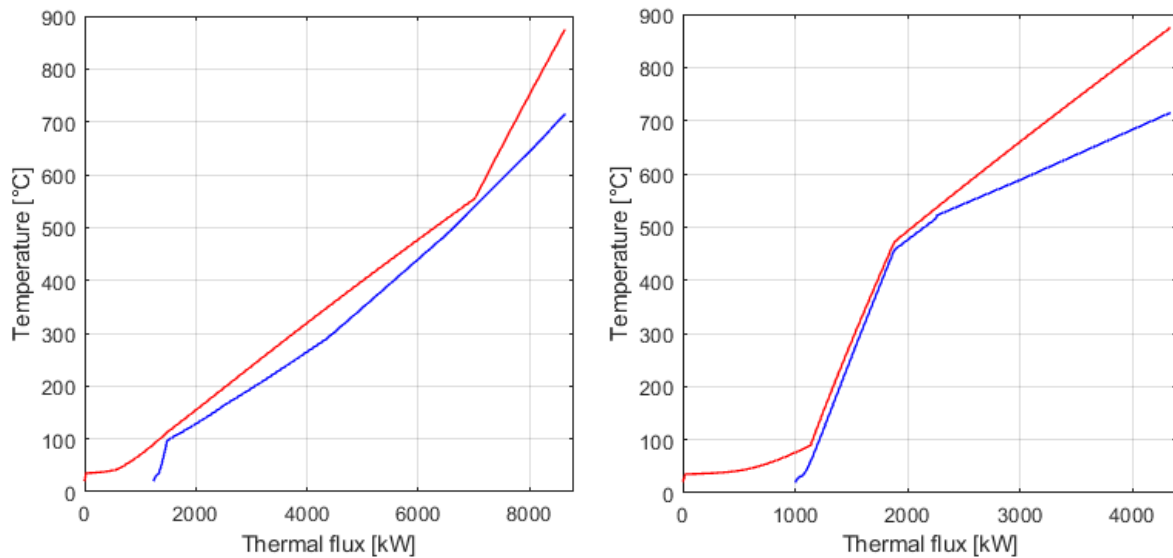


Figure 5.35 - Hot and cold composite curves for the single intercooling layout (left) and the recompression layout (right)

Regarding the single intercooling case, the hot composite change of slope at high temperature is caused by the addition between the hot streams of the carbon dioxide exiting the power block turbine, which makes available a consistent amount of thermal power.

The chart obtained for the recompression layout is instead very different, since for both the curves is observed a substantial slope change around 500°C; this behaviour is determined by the fact that the power block requires heat only at high temperatures and provides a thermal power at relatively low temperature.

The optimization algorithm converges therefore to a configuration in which the recirculated carbon dioxide (the most important hot stream) is not subject to a complete cooling, such that the mixer outlet stream is already at high temperature and needs just a very little heating. In this way the two curves manage to approach each other and the plant reaches a very good performance.

Finally, it is worth to notice that for both the layouts the hot composite curve becomes nearly horizontal at low temperatures. This is simply due to the strong variations of the carbon dioxide specific heat capacity when the critical point conditions are approached, thing that happens when the CO_2 stream is cooled down before to enter the power block compressor, but actually has always been present even for the other integration alternatives previously

investigated, since it takes place also during the heating of the stoichiometric carbon dioxide extracted from its pressurized storage.

This phenomenon is clearly showed in the following image.

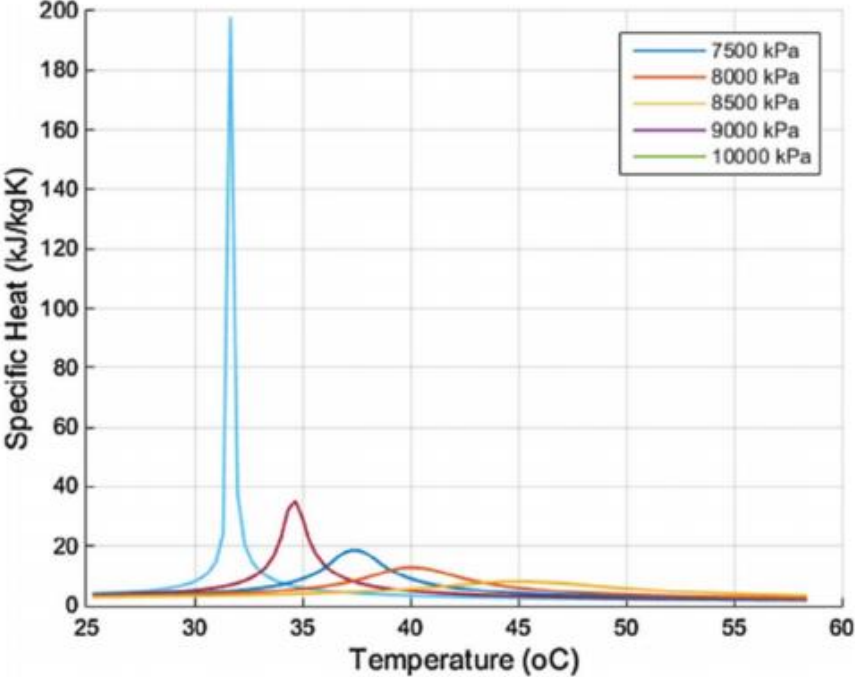


Figure 3.36 - Carbon dioxide specific heat dependence on pressure and temperature near the critical conditions [28]

Final comparison

Now that the integration alternatives have been separately evaluated, it may be interesting to make a brief comparison between the different typologies based on the integration efficiencies obtained. A single representative layout has been selected for every category and the choice has been done considering both the performance and the power block layout complexity.

Integration typology	Chosen layout
Direct integration	-
Indirect integration - ORC	Supercritical Benzene + vacuum condensation
Indirect integration - SRC	Single bleeding
Indirect integration - SCO ₂	Recompression

Table 4.1 - Summary of the most significant configurations for the different integration alternatives

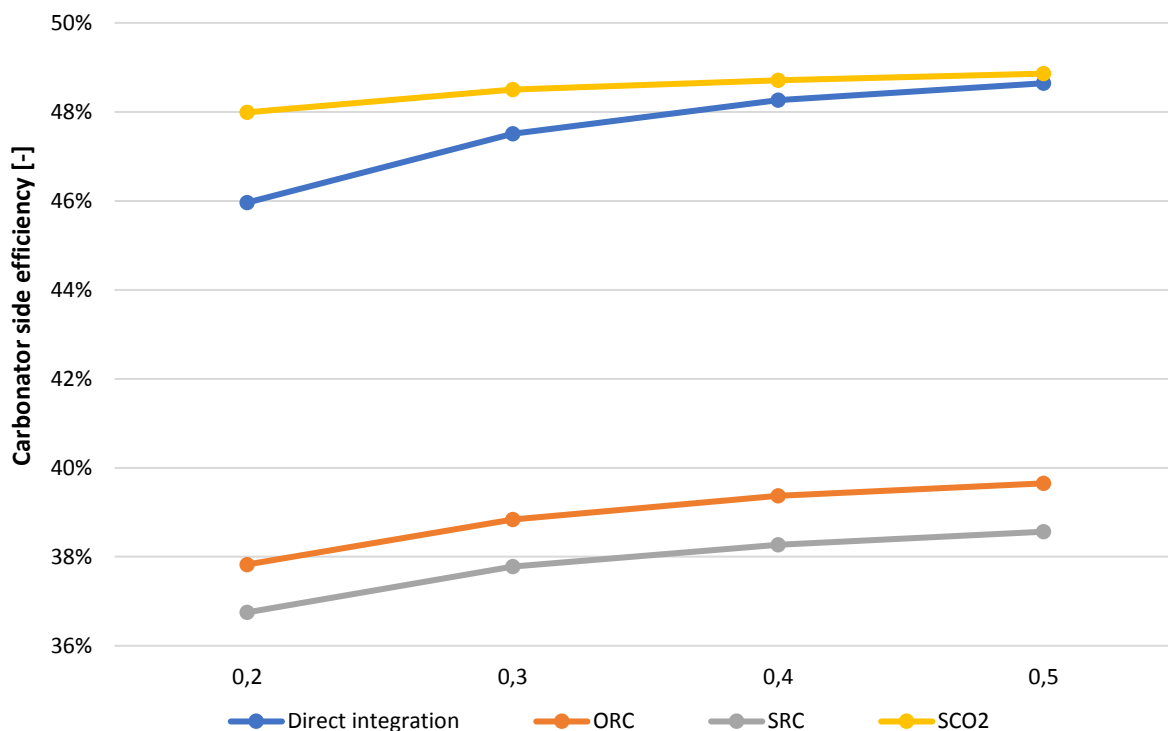


Figure 6.1 - Performance comparison as a function of the calcium oxide activity

As could be expected, the ORC and the SRC are the less convenient alternatives and this can be explained considering both their thermodynamic cycle efficiencies and the intrinsic penalties in the heat exchange process due to the evaporation and condensation steps.

The other two integrations, both based on the carbon dioxide as working fluid, show a consistent gain in terms of efficiency, although their plant configuration is very different. Furthermore, it's very interesting to notice that the advantage of the SCO_2 indirect integration on the direct integration layout decreases with the increase of the calcium oxide reactivity, such that when X reaches a value of 0,5 the two alternatives are practically equally performing. The reason of this behaviour can be probably explained looking at the justification for the efficiency trend of the recompression layout provided in the previous chapter: the heat recovery performed on the single power cycle before the second step of the optimization process seems to be slightly deleterious in case of high values of the calcium oxide activity.

So, for the umpteenth time, these results prove the very strong performances dependence on the thermo-physical properties of the CaO solid grains, underlying the importance of the choice of its most suitable precursor and the necessity to guarantee the right operating conditions (especially at the calciner).

Conclusions

Reached the final point of this work, it worth to sum up the main steps through which has been possible to perform this analysis. For first, it has been exposed the context in which the SOCRATCES project will take place, providing an essential description of its functioning and of the different components involved in the process.

Then it has been made a choice between the integration alternatives for the power production of 1 MWe; in case of indirect cycle, before the optimization with the genetic algorithm (evaluating an objection function based on the pinch analysis), it has been necessary to make separately an optimization only on the thermodynamic cycle. One important constraint imposed was that the plant wouldn't had the need of power sources different from the solar radiation. In this way have been obtained the results of the integration efficiency for the optimized operating conditions and it has been tried to provide some reasonable justifications regarding their meaning.

Although these outcomes aren't actually the total plant efficiencies (since the calciner side hasn't been simulated), they have been at least sufficient to make a comparison between the investigated alternatives. Form this comparison emerged that the most performing typologies are the indirect integration with a supercritical carbon dioxide cycle and the direct integration.

Now, it is actually non-trivial to establish in absolute terms which of these two is the best choice, because there are many other features not considered in this work (such as the economic aspect) that may consistently influence the decision.

However, regarding the economic factor, it can be tried to make some qualitative comments. In fact, although the direct integration has the disadvantage of having larger size turbomachinery (which contributes to make it more expensive), on the other hand the operating pressures reached in the SCO_2 plant (250 bar) represent a criticality for the power block components (whose price will be increased by the high-quality materials adopted). Anyway, it must be also remembered that the physical dimensions of the machines involved in this cycle are actually quite small. Furthermore, it is reasonable to imagine that the practical functioning of the supercritical CO_2 power plant will be more complex with respect to the case of the direct integration, where the maximum pressure achieved is about 3,5 bar.

So, without taking into account the economical aspect (for which would be required a detailed analysis) and considering only the integration efficiencies and the simplicity of operation, it's possible to say that in case of high values of the calcium oxide activity the direct integration can be the most convenient choice, providing both very good performances and a not particularly demanding functioning. On the other hand, when X becomes smaller, the higher integration efficiency could be worthwhile the increased operation complexity determined by a supercritical carbon dioxide indirect integration.

References

- [1] C. Ortiz, R. Chacartegui, J. Valverde, A. Alovio and J. Becerra, "Power cycles integration in concentrated solar power plants with energy", *Energy Conversion and Management*, pp. 815-829, Oct. 2017.
- [2] -, "SOCRATCES project presentation".
- [3] A. Alovio, "Process integration of a thermochemical energy storage system based on Calcium Looping incorporating air/CO₂ cycles in CSP power plants", Jul. 2015.
- [4] R. Chacartegui, A. Alovio, C. Ortiz, J. Valverde, V. Verda and J. Becerra, "Thermochemical energy storage of concentrated solar power by integration of the calcium looping process and a CO₂ power cycle", *Applied Energy*, vol. 173, pp. 589-605, Jul. 2016.
- [5] M. Benitez-Guerrero, J. M. Valverde, P. E. Sanchez-Jimenez, A. Perejon and L. A. Perez-Maqueda, "Multicycle activity of natural CaCO₃ minerals for thermochemical energy storage in Concentrated Solar Power plants", *Solar Energy*, vol. 153, pp. 188-199, Sept. 2017.
- [6] J. Sever, "Calix Calciner: A Green Application in the Production of Magnesium", *Drying, Roasting, and Calcining of Minerals*, pp. 121-126, 2015.
- [7] Y. Fu-Chen and F. Liang-Shih, "Kinetic study of high-pressure carbonation reaction of calcium-based sorbents in the Calcium Looping process (CLP)", *Industrial & Engineering Chemistry Research*, vol. 50, pp. 11528-11536, Sept. 2011.
- [8] "Fox venturi products", [Online]. Available: www.foxvalve.com. [Accessed Oct. 2018].
- [9] "IEDCO", [Online]. Available: <https://iedco.com/>. [Accessed Oct. 2018].
- [10] I. Alabi, K. Olaiya and A. Oluwasanmi, "Parametric and Quantitative Analysis on the Development of Shell and Tube Heat Exchanger", Jun. 2018.
- [11] "National Energy Technology Laboratory", [Online]. Available: <https://www.netl.doe.gov/>. [Accessed Oct. 2018].
- [12] J. Khorshidi and S. Heidari, "Design and Construction of a Spiral Heat Exchanger", *Advances in Chemical Engineering and Science*, vol. 6, pp. 201-208, Jan. 2016.
- [13] A. Shimizu, T. Yokomine and T. Nagafuchi, "Development of gas–solid direct contact heat exchanger by use of axial flow cyclone", *International Journal of Heat and Mass Transfer*, vol. 47, pp. 4601-4614, Oct. 2004.

- [14] “Solex thermal science”, [Online]. Available: www.solexthermal.com. [Accessed Oct. 2018].
- [15] C. Ortiz, M. Romano, J. Valverde, M. Binotti and M. Chacartegui, “Process integration of Calcium-Looping thermochemical energy storage system in concentrating solar power plants”, *Energy*, vol. 155, pp. 535-551, Jul. 2018.
- [16] A. Alovio, R. Chacartegui, C. Ortiz, J. Valverde and V. Verda, “Optimizing the CSP-Calcium Looping integration for Thermochemical Energy Storage”, *Energy Conversion and Management*, vol. 136, pp. 85-98, Mar. 2017.
- [17] W. Stein and R. Buck, “Advanced power cycles for concentrated solar power”, *Solar Energy*, vol. 152, pp. 91-105, Aug. 2017.
- [18] J. Facão and A. C. Oliveira, “Analysis of Energetic, Design and Operational Criteria When Choosing an Adequate Working Fluid for Small ORC Systems”, *ASME 2009 International Mechanical Engineering Congress and Exposition*, vol. 6, pp. 175-180, Nov. 2009.
- [19] Siemens Energy, “Siemens Organic Rankine Cycle Waste Heat Recovery with ORC”, Mar. 2014.
- [20] J. Bonafin, M. Del Carria, M. Gaia and A. Duvia, “Turboden Geothermal References in Bavaria: Technology, Drivers and Operation”, *Proceedings World Geothermal Congress 2015*, Apr. 2015.
- [21] M. Astolfi, S. Lasala and E. Macchi, “Selection Maps For ORC And CO2 Systems For Low-Medium”, *Energy Procedia*, pp. 971-978, Sept. 2017.
- [22] J. Milewski and J. Krasuck, “Comparison of ORC and Kalina cycles for waste heat recovery in the steel industry”, *Journal of Power Technologies*, vol. 97, p. 302–307, 2017.
- [23] W. Stein and R. Buck, “Advanced power cycles for concentrated solar power”, *Solar Energy*, vol. 152, pp. 91-105, Aug. 2017.
- [24] Siemens Energy, “Pre-designed Steam Turbines”, 2012.
- [25] G. E. Rochau, J. J. Pasch, G. Cannon, M. Carlson, D. Fleming, A. Kruizenga, R. Sharpe and M. Wilson, “Supercritical CO2 Brayton Cycles”, *NP-NE Workshop #2*, Aug. 2014.
- [26] J. Moore, S. Cich, M. Day, T. Allison, J. Wade and D. Hofer, “Commissioning of a 1 MWe Supercritical CO2 Test Loop”, *The 6th International Supercritical CO2 Power Cycles Symposium*, Mar. 2018.
- [27] J. D. Osorio, R. Hovsopian and J. C. Ordonez, “Dynamic analysis of concentrated solar supercritical CO2-based power”, *Applied Thermal Engineering*, vol. 93, p. 920–934, Jan. 2016.

- [28] S. Seongmin, H. Jin Young and L. Jeong Ik, "Prediction of inner pinch for supercritical CO₂ heat exchanger using Artificial Neural Network and evaluation of its impact on cycle design", *Energy Conversion and Management*, vol. 163, pp. 66-73, May 2018.
- [29] S. E. Edwards and V. Materic', "Calcium looping in solar power generation plants", *Solar Energy*, vol. 86, pp. 2494-2503, Sept. 2012.
- [30] M. Benitez-Guerrero, J. M. Valverde, P. E. Sanchez-Jimenez, A. Perejon and L. A. Perez-Maqueda, "Calcium-Looping performance of mechanically modified Al₂O₃-CaO composites for energy storage and CO₂ capture", *Chemical Engineering Journal*, vol. 334, pp. 2343-2355, Feb. 2018.